2020

Identification of Previously Unknown Interactions Between G Protein-Coupled Receptors and Receptor Activity-Modifying Proteins

Emily Margaretha Lorenzen

IDENTIFICATION OF PREVIOUSLY UNKNOWN INTERACTIONS BETWEEN G PROTEIN-COUPLED RECEPTORS AND RECEPTOR ACTIVITY-MODIFYING PROTEINS

A Thesis Presented to the Faculty of

The Rockefeller University

in Partial Fulfillment of the Requirements for

the degree of Doctor of Philosophy

by

Emily Margaretha Lorenzen

June 2020

IDENTIFICATION OF PREVIOUSLY UNKNOWN INTERACTIONS BETWEEN G PROTEIN-COUPLED RECEPTORS AND RECEPTOR ACTIVITY-MODIFYING PROTEINS

Emily Margaretha Lorenzen, Ph.D.

The Rockefeller University 2020

G protein-coupled receptors (GPCRs) are known to interact with several other classes of integral membrane proteins. However, the extent of these interactions and their role in regulating GPCR-mediated transmembrane signaling is not well understood. For example, receptor activity-modifying proteins (RAMPs), a family of single transmembrane proteins with only three members, are ubiquitously expressed and have been shown to interact with several different GPCRs. Most research to date has focused on the ability of RAMPs to modulate the function of several GPCRs in the secretin-like GPCR family. GPCR-RAMP interactions were shown to affect the ligand binding affinity of two different secretin-like GPCRs, causing the functional diversity of the GPCRs to be driven by an interacting protein. Yet, potential direct interactions among the three known RAMPs and hundreds of non-olfactory GPCR has never been investigated and whether RAMP-GPCR interactions are widespread remains an open question.

To determine the breadth of GPCR-RAMP interactions, we first investigated the global coexpression and coevolution between GPCRs and RAMPs. On the one hand, if many GPCRs interact with RAMPs we would except to see statistically significant coexpression and coevolution in comparison to random gene pairs. On the other hand, if GPCR-RAMP interactions are limited to a small number of genes, then averaged coexpression and coevolution would be similar to that expected by chance. To calculate coexpression, we analyzed an RNA-Seq database of human transcriptomes across 53 different tissues and found that coexpression

between non-olfactory GPCRs and RAMPs is significantly higher than random gene pairs. We also analyzed genomic data from all currently available sequenced organisms to calculate the coevolution between non-olfactory GPCRs and RAMPs. We discovered that GPCRs and RAMPs have a significant percentage of shared species and significantly correlated phylogenetic trees. Our results support the hypothesis that GPCRs interact globally with RAMPs.

Only a handful of GPCR-RAMP interactions have been reported to date, but our coexpression and coevolution analysis suggested that additional GPCRs interact with RAMPs. To begin to address the potential for direct interactions among the three known RAMPs and hundreds of GPCRs, we developed a highly multiplexed immunoassay using a suspension bead array (SBA) assay designed to detect RAMP-GPCR complexes. We engineered three epitope-tagged RAMPs and 23 epitope-tagged GPCRs, including all members of the secretin-like family of GPCRs, as well as eight other GPCRs. We then used 64 antibodies raised against native RAMPs and GPCRs, along with four antibodies targeting the epitope tags, to multiplex the SBA assay to detect and measure all possible combinations of interaction among the 23 GPCRs and three RAMPs from detergent-solubilized lysates. We also used the epitope-tagged constructs to verify a collection of antibodies that target native GPCRs and RAMPs. We validated nearly all previously reported secretin-like GPCR-RAMP interactions, and also found previously unidentified RAMP interactions with additional secretin-like GPCRs, chemokine receptors, and orphan receptors. Using in situ proximity ligation assay, we verified a subset of these novel GPCR-RAMP interactions in cell membranes. The results of the SBA assay provide a complete interactome of secretin-like GPCRs with RAMPs. GPCR-RAMP interactions are more common than previously appreciated, and the SBA strategy will be useful to search for additional GPCR-RAMP complexes and other interacting membrane protein pairs in cell lines and tissues.

Dedicated to my late mother, Marcia Lorenzen. May I always make you proud.

ACKNOWLEDGMENTS

Dr. Thomas P. Sakmar has been a fantastic adviser and mentor. Tom entrusted me to pursue a completely new project and was an ardent supporter. I am grateful to him for making my PhD fulfilling, engaging, and enjoyable. I admire Tom for his ability to lead through inspiration, and I hope to implement his technique in my future career.

The Sakmar Lab has been a supportive and wonderful place to work for the past five years. My friendship with Manija Kazmi has been vital to my development, both as a scientist and overall as a person. Dr. Thomas Huber has always been there with brilliant scientific ideas. The other PhD students of the Sakmar Lab, Dr. Jennifer Peeler, Dr. He Tian, Dr. Carlos Rico, Mizuho Horioka, Jordan Mattheisen, and Ilana Kotliar have been great comrades. Ilana Kotliar dedicated her time to this project as a rotation student and produced the proximity ligation assay results (Chapter 4). Other members of the lab, Dr. Vallen Graham, Dr. Alessandra Bonito-Oliva, and Dr. Emilie Ceraudo, Dr. Yamina Berchiche, Dr. Shahar Barbash, and Dr. Minyoung Park have been valuable sources of support and advice. Dr. Shahar Barbash performed several bioinformatics analyses presented in this thesis (Chapter 3). The IP1 and adenylate cyclase assays were performed by Dr. Emilie Ceraudo and Dr. Yamina Berchiche (Appendix). I am appreciative of the funders of my PhD work – the Women in Science Program at Rockefeller and the David Rockefeller Graduate Fellowship.

I was able to work at the Science for Life Laboratory in Stockholm, Sweden for nearly a year of my PhD thanks to the generosity of the Nicholson Short-Term Exchange, the Albert Cass Fellowship, and the Alexander Mauro Fellowship. I am grateful to Dr. Jochen Schwenk for being a wonderful scientific host, Dr. Elisa Pin for training me, and Tea Dodig-Crnković for the data analysis support.

Finally, I thank my parents, Henry Lorenzen and Marcia Lorenzen, and my sister, Jessica Lorenzen, for their unconditional love and support. I am also greatly appreciative of all my friends – in New York, Portland and Stockholm – for being there for me and providing diversions from the lab.

TABLE OF CONTENTS

LIST OF FIGURES

LIST OF TABLES

CHAPTER 1. Introduction

1.1 G protein-coupled receptor (GPCR) structure and signaling

Cells within organisms have evolved intricate systems to sense and respond to their local environments and to communicate intercellularly and intracellularly. Cell signaling occurs over a range of distances - within an individual cell, between nearby cells and over long distances in the body. Many secreted intercellular signaling molecules, which are key to physiological responses, are unable to penetrate through the plasma membrane, and instead mediate effects by binding to specific cell surface receptors on target cells. The largest family of these plasma membrane receptors are G protein-coupled receptors (GPCRs), termed for their ability to activate intracellular heterotrimeric G proteins. The first two GPCRs to be biochemically characterized and sequenced were rhodopsin, a light-sensing receptor that binds an 11-*cis*-retinylidene chromophore, and the β_2-adrenergic receptor, which mediates the effects of the potent stress hormones adrenalin and noradrenaline *(1–4)*. Despite their disparate ligands and physiological responses, both receptors were predicted to have a similar topological structure, with seven transmembrane spans. The molecular cloning of the β_2-adrenergic in 1986 facilitated the cloning of several additional GPCRs over the next several years *(5–7)*. Yet the GPCRs cloned prior to the release of the human genome sequence represented just a small fraction of the total number of GPCRs. By analyzing the human genome, Fredriksson et al. and Takeda et al. identified approximately 800 genes that were thought to encode GPCRs *(8, 9)*. The extensive repertoire of GPCR genes is mirrored by the diverse array of ligands that activate GPCRs, including but not limited to photons, odorants, hormones, histamine and dopamine.

GPCRs are the most ubiquitous plasma membrane receptors, expressed in every tissue and cell type and regulating nearly all known physiological functions. GPCRs function as signal transducers by changing conformation in response to the binding of an extracellular agonist ligand. The conformational change of the GPCR opens up a pocket on the intracellular side to allow binding and activation of the G protein, thereby transferring information from the extracellular to the intracellular side. The G protein is a heterotrimeric protein consisting of a Gα subunit in complex with Gβγ subunits. The GPCR activates the G protein by catalyzing the exchange of GDP for GTP within Gα, allowing the dissociation of the G protein heterotrimer into constituent Gα and Gβγ components (Figure 1-1). The Gα protein subtypes include G_s, $G_{i/o}$, $G_{q/11}$, and $G_{12/13}$. Depending on the particular G protein subtype and its cellular context, either Gα or Gβγ, can mediate downstream effector activity through activation or inhibition of enzymes or channels.

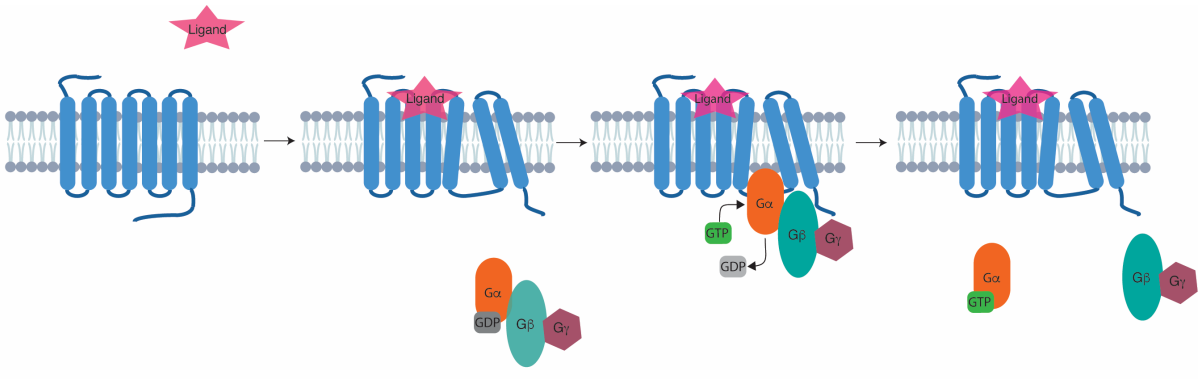

Figure 1-1. GPCR signaling through heterotrimeric G proteins. An agonist ligand binds to the GPCR causing a conformational change. In response, the heterotrimeric G protein, composed of Gα, Gβ, and Gγ, binds to the GPCR and GDP is exchanged for GTP within the Gα subunit. The heterotrimeric G protein then dissociates into Gα and Gβγ to activate or inactivate various enzymes and channels.

Following activation, the receptors must be desensitized to maintain cellular homeostasis and prepare to respond to new stimuli. Desensitization of the GPCR is accomplished through phosphorylation of Ser/Thr residues on the cytoplasmic C-terminal tail by GPCR kinases (GRKs). Phosphorylation of the GPCR mediates β-arrestin recruitment, blocking further G protein coupling. β-arrestin then facilitates receptor sequestration or internalization in addition to activating noncanonical signaling systems such as mitogen-activated protein kinase pathways *(10)*. The internalized receptor is either recycled back to the cell membrane or degraded.

Historically, GPCR signaling was believed to involve sequential activation of a single type of Gα protein class followed by β-arrestin-dependent activation of noncanonical signal pathways. Activation was believed to be binary, with a receptor acting somewhat like a molecular switch that would adopt either an active or inactive structure. It has now been established that GPCR activation and signaling is a much more complex process. There are multiple states along the energetic pathway from the inactive to active conformation of a GPCR, as well as probably several active state conformations *(11)*. The multi-faceted conformational states allow activation of several different downstream signaling pathways. For example, many GPCRs couple to and signal through multiple G protein classes in response to an activating ligand. Also, GPCR agonists demonstrate signaling bias towards either G protein or β-arrestin pathways *(12)*. Signaling bias has also been shown to occur at the level of different G protein subclasses, where certain ligands would activate one G protein subclass and other ligands would activate another subclass *(13)*.

1.2 Classifications of GPCRs

The GPCR signaling paradigm is fairly limited within the "Tree of Life", being utilized by eukaryotic organisms, with the exception of plants *(14)*. Virally-encoded GPCRs have also been described *(15)*. Yeast, one of the simplest eukaryotic organisms, has only two GPCRs *(16)*. In humans, the evolutionary processes of gene duplication and subsequent mutations led to a large expansion in the number of GPCR subtypes *(17, 18)*. While all GPCRs display the canonical seven transmembrane structure, they have substantial differences in lengths of the N-terminal tails, C-terminal tails, and extracellular loops, as well as various post-translation modifications. Based on phylogenetic analysis, human GPCRs are grouped into five primary receptor families – rhodopsin, glutamate, adhesion, frizzled/TAS2, and secretin – and are differentiated by structural features and molecular composition of ligands *(19)* (Figure 1-2). The rhodopsin-like GPCR family constitutes by far the largest number of GPCRs, with a total of ~700 members, and are characterized by relatively short N-terminal tails. Within rhodopsin-like GPCR family, the majority of receptor types respond to odorant molecules and are termed olfactory GPCRs. Non-olfactory, rhodopsin-like GPCRs respond to a chemically diverse set of ligands including amines, purines, lipids, peptides, and large glycoproteins. Glutamate-like receptors bind to small molecule ligands via a distinctive N-terminal Venus-flytrap domain. The secretin-like family is composed of 15 GPCRs that share a conserved N-terminal hormone-docking/binding domain, which plays a pivotal role in the binding of large peptide, hormone ligands. The adhesion-like family of GPCRs is characterized by a very long N-terminal tail (200-2800 amino acids) with multiple O- and S-glycosylation sites, as well as epidermal growth factor and GPCR proteolytic domains that are important for their ability to facility cellular adhesion. Finally, the frizzled

receptors respond to secreted glycoproteins named WNTs, which are instrumental in embryonic development. The term WNT is a portmanteau coined from Wingless-related integration site *(20)*.

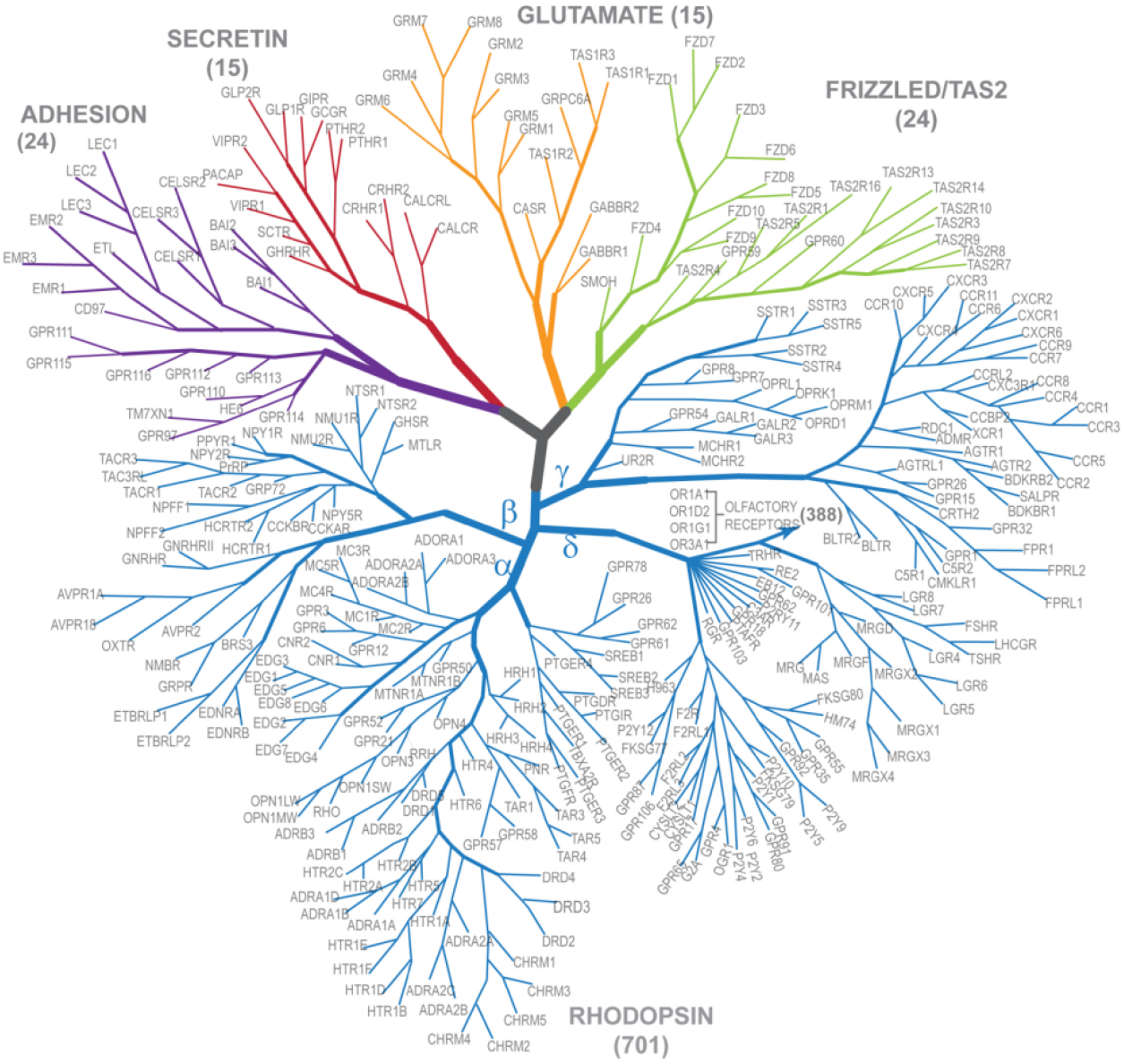

Figure 1-2. Phylogenetic relationship between GPCRs in the human genome. There are approximately 800 GPCRs that can be categorized into five major families based on sequence similarity: adhesion, secretin, glutamate, frizzled/TAS2, and rhodopsin. Numbers in parentheses indicate the number of GPCRs in the family. The phylogenetic tree was adapted from *(19, 21)*

1.3 GPCRs in drug discovery

GPCRs are tractable pharmaceutical targets because of their ubiquitous expression, "druggable" ligand-binding pockets, and access to the extracellular milieu. Highlighting the clinical importance of GPCRs, 457 approved drugs (~36% of all approved drugs) have been developed that target 134 specific GPCRs *(22)*. However, although drugs that target GPCRs are over-represented in the pharmacopeia of FDA-approved drugs, only about one-third of non-olfactory GPCRs have been targeted to date, and 401 GPCR-targeted drugs, or ~70%, act through the 35 aminergic receptor. The aminergic receptors include adrenoreceptors, muscarinic acetylcholine receptors and receptors for serotonin, dopamine and histamine. Approximately 140 of the non-olfactory GPCRs remain "orphans," whose endogenous physiological agonist is unknown *(23)*. Thus, there remain many potential opportunities for the development of more GPCR-targeted pharmaceuticals. Current clinical trials have begun to address novel GPCR targets. Amongst the 321 drugs in clinical trials that target GPCRs, about 20% target 66 GPCRs that have yet to be therapeutically exploited (Figure 1-3). Rapidly increasing numbers of crystal structures, new agent types, such as monoclonal antibodies, and new targets will greatly assist future GPCR-targeted drug development *(24, 25)*.

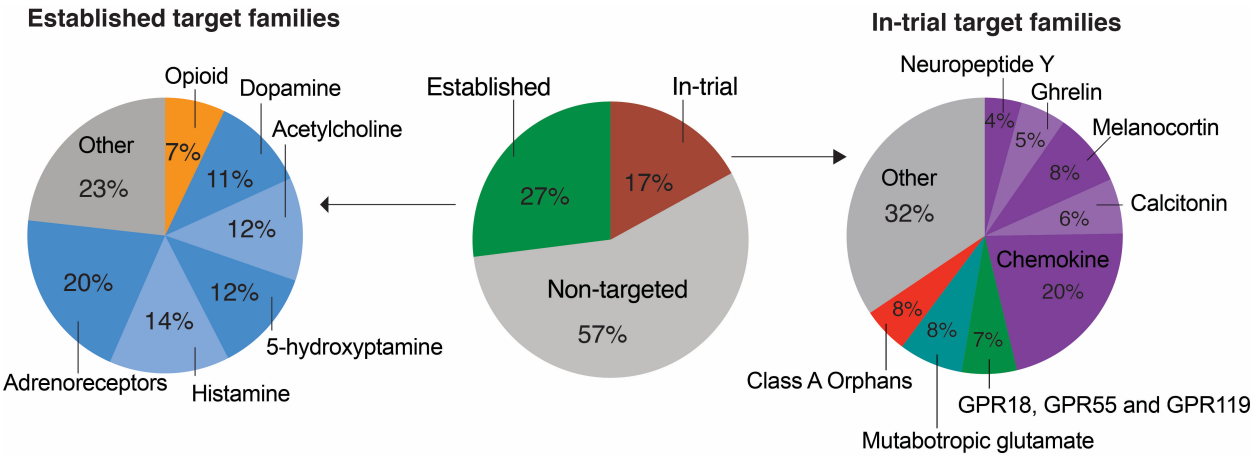

Figure 1-3. GPCRs targeted by drugs that are approved and in clinical trials. Of the non-olfactory GPCRs, 108 have drugs approved (green), 66 have agents in clinical trial (red), and 224 have not been targeted (middle panel). The 108 established GPCR drug targets (left panel) are primarily aminergic receptors (blue). The 66 currently untargeted GPCRs with agents in clinical trial (right panel) are primarily peptide and protein receptors (purple). Figure adapted from *(22)*

As additional GPCRs are investigated as therapeutic targets, the number of disease indications for potential GPCR-targeting drugs has also expanded. Some disease indications targeted by approved GPCR-targeting drugs address dysfunctions of the central nervous system (CNS) disorders highlighting the critical role of GPCRs in neurotransmission. These drugs target a variety of GPCRs, including 5-hydroxytryptamine (serotonin), dopamine, opioid, and cannabinoid receptors for the treatment of mood disorders, pain, epilepsy, and psychosis *(26)*. New CNS disorder indications with GPCR-targeted drugs in clinical trials address additional CNS dysfunctions, including multiple sclerosis, Alzheimer's disease, and Huntington's disease. GPCRs also play a pivotal role in energy homeostasis, and the development of medications for type 2 diabetes and obesity has increasingly focused on GPCRs, with approved drugs targeting glucagon-like receptor 1 (GLP1R) *(27)*. In addition, more GPCRs have been implicated in cancer development and the establishment of the tumor microenvironment. Aberrant expression of

GPCRs is found in a variety of cancers, and both inactivating and activating mutations in GPCRs drive cancer formation and progression *(28, 29)*. For example, a mutation in cysteinyl leukotriene receptor 2 causes the receptor to be constitutively active and is responsible for 5% of uveal melanoma cases *(30)*. As more research has revealed the roles of different GPCRs in cancer, oncological therapeutics has become increasingly focused on GPCRs *(28)*.

1.4 GPCR interactions with transmembrane proteins

Traditionally, GPCRs were believed to exist and function as monomers. It is now appreciated that many GPCRs form homo- and hetero- oligomers. The potential to target oligomeric forms of GPCRs remains an untapped area for GPCR drug discovery. The GPCR interaction network database, GPCR-HetNet [http://www.gpcr-hetnet.com] indicates a total of 537 interactions between GPCRs, encompassing 183 GPCRs *(31)*. The functional role of these interactions depends on the particular GPCRs involved. Members of the glutamate GPCR family function and exist as stable homodimers. For other GPCRs, the role of oligomerization is less clear since several rhodopsin-like GPCRs function as monomers *(32–35)*. However, receptor oligomerization affects ligand binding affinity for some GPCRs *(36)*. Some GPCR oligomers are disease specific and provide attractive targets for L-DOPA-induced dyskinesia, morphine tolerance, and alcohol-induced liver fibrosis *(37, 38)*. In addition, GPCR oligomers provide the opportunity for development of more selective drugs with less chance of side effects.

While the number of known GPCR-GPCR interactions continues to expand, less appreciated is the potential for GPCRs to interact with other transmembrane proteins. The number of transmembrane proteins known to interact with GPCRs is currently limited and

includes receptor transport proteins (RTPs), receptor expression-enhancing protein (REEP), melanocortin receptor accessory proteins (MRAP), M10 major histocompatibility protein (MHC), and receptor activity-modifying proteins (RAMPs). Each of these single transmembrane proteins has been shown to chaperone particular GPCRs to the cell surface *(39)*. Despite the limited knowledge about transmembrane proteins that interact with GPCRs, a GPCR-RAMP complex is the only GPCR oligomers targeted by FDA-approved drugs *(40)*. More information on GPCR-membrane protein interactions will contribute to further GPCR-targeted drug discovery and development.

1.5 Discovery of receptor-activity modifying proteins (RAMPs)

The family of RAMP proteins were initially discovered in the search for the receptor for calcitonin gene-related peptide (CGRP). CALCRL was recognized to be a likely candidate, due to its homology to the calcitonin receptor (CALCR). However, expression of CALCRL alone caused only a subset of tested cell lines to be responsive to CGRP, suggesting that another protein expressed in the sensitive cell lines was required to form a functional receptor for CGRP. Using an expression cloning approach, McLatchie et al. discovered that RAMP1 was the additional component required for CALCRL functionality and that CALCRL required to RAMP1 to be transported to the cell membrane *(41)*. Database searches for homologous proteins revealed two additional proteins belonging to the RAMP family, RAMP2 and RAMP3, with 31% homology. Surprisingly, coexpression of CALCRL with RAMP2 or RAMP3 leads to a receptor responsive to a different peptide hormone, adrenomedullin *(41–43)*.

The change in ligand binding affinity as a consequence of RAMP association was also observed with another receptor closely related to CALCRL, calcitonin receptor (CALCR). CALCR binds with a high affinity to calcitonin in the absence of RAMP association, but becomes an amylin receptor in the presence of any of the three RAMPs *(44, 45)*. In contrast to CALCRL, CALCR does not require RAMP expression for localization to the cell membrane. These initial studies on RAMP interactions with the calcitonin subfamily of GPCRs created a paradigm shift in the GPCR field by revealing that the functional diversity of GPCRs can be driven by interacting proteins.

1.6 Functional domains and structural features of RAMPs

The three members of the RAMP family have a similar secondary structure, although they share only ~30% sequence identity. Each RAMP has a long extracellular N-terminal tail of ~90-100 amino acids, which contributes to determining ligand specificity *(46)*. The N-terminus of RAMP2 contains one N-linked glycosylation site, and RAMP3 has four N-linked glycosylation sites. Although both RAMP2 and RAMP3 are linked to adrenomedullin pharmacology, the glycosylation sites do not determine the ligand binding specificity *(43)*. The C-terminal tails of RAMPs are relatively short, being only 9 amino acids long. Within the C-terminal tail of each RAMP is an endoplasmic reticulum (ER) retention signal that prevents RAMP translocation to the cell surface in the absence of an interacting GPCR. The C-terminus of RAMP3 also contains a type 1 PDZ recognition site that contributes to the modulation of receptor trafficking.

Structural studies of RAMP interaction with CALCRL indicate that the molecular mechanism by which RAMPs influence ligand binding to CALCRL are subtle. Studies with chimeric, extracellular domain (ECD) proteins show that both RAMP1 and RAMP2 have ECDs with a three-helix bundle fold and similar interaction with CALCRL. Because RAMPs make only minimal contacts to the agonist, the molecular mechanism by which RAMPs affect ligand binding to CALCRL is mostly through allosteric shaping of CALCRL *(46–48)*. Although the ECD-ECD contacts between RAMPs and CALCRL are important in ligand binding, RAMPs also interact with GPCRs through the transmembrane domain to form stable complexes. Recently, a cryogenic electron microscopy structure of a complex including RAMP1, CALCRL, CGRP, and a G_s protein heterotrimer defined the interaction of the transmembrane domains and confirmed findings from previous crystal structures of the ECDs *(49)*. RAMP1 forms extensive contacts with CALCRL, causing 23% of the RAMP1 surface to be buried. The TM domain of RAMP1 nestles into an interface between TM helices 3, 4 and 5 of CALCRL, and the ECD of RAMP1 interacts with the extracellular loop 2 (ECL2) of CALCRL. As seen in the crystal structures, there are minimal contacts between RAMP1 and the agonist CGRP (Figure 1-4).

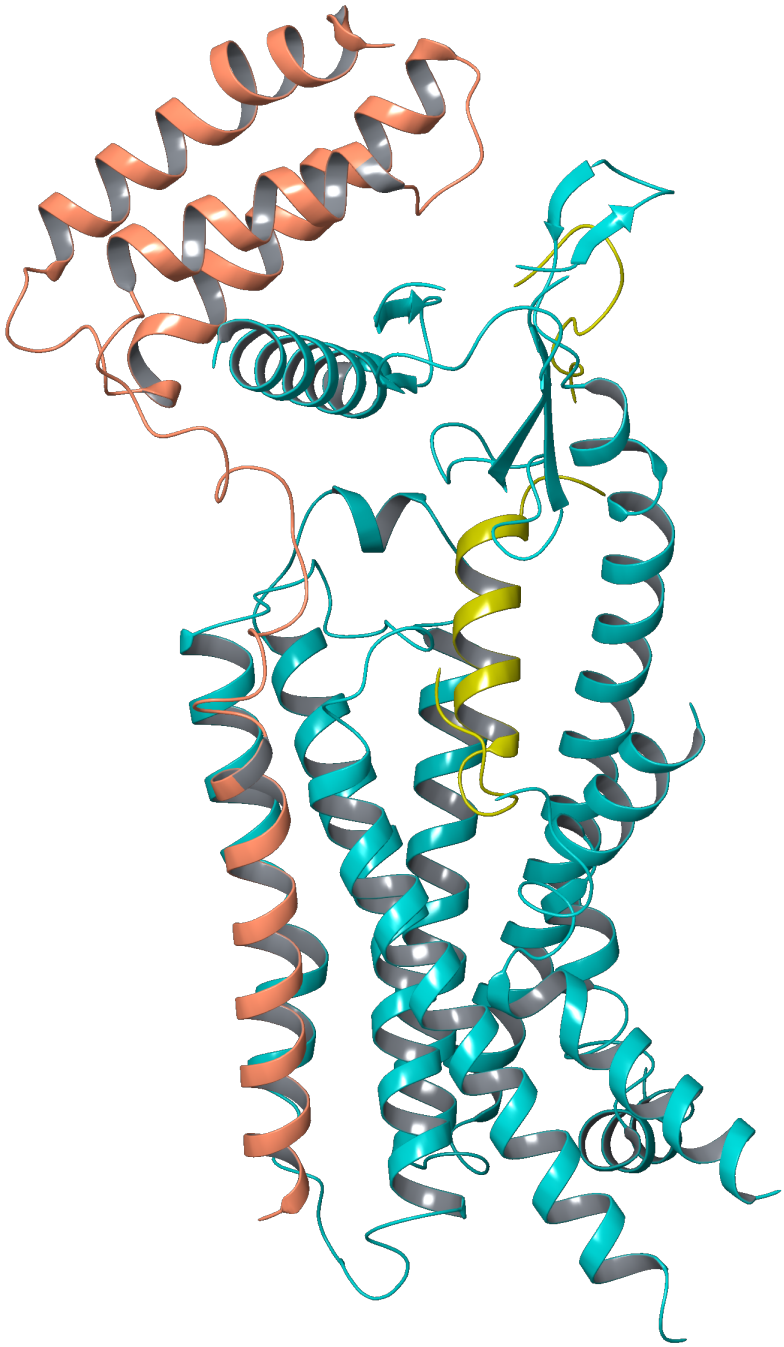

Figure 1-4. Structure of the RAMP1, CALCRL, and CGRP complex. Salmon, RAMP1; cyan, CALCRL; mustard, CGRP. Adapted from *(49)*, PDB code: 6E3Y.

1.7 Consequences of RAMP interaction with GPCRs

While CALCRL and CALCR have been the most studied RAMP-interacting GPCRs, several additional secretin-like receptors, as well as a rhodopsin-like and glutamate-like receptor also interact with RAMPs (Table 1-1). Due to their endoplasmic reticulum retention signal, RAMPs are generally poorly expressed on the cell membrane in the absence of an interacting GPCR. Thus, additional GPCR-RAMP interactions were determined by assessing RAMP cell surface localization upon coexpression of the putative interacting GPCR. These studies established that GPCRs demonstrate selectivity for certain RAMPs and that RAMP interaction was not universal for secretin-like receptors. However, the consequences of many of these interactions have not been investigated. Notably, the handful of studies addressing the function of RAMP association with GPCRs have failed to reveal the distinctive switch in ligand affinity seen with CALCRL and CALCR. Instead, the glucagon receptor (GCGR) may lose its ability to bind GLP-1 with RAMP2 coexpression, but studies have shown conflicting results *(50, 51)*. RAMPs instead have effects on GPCRs beyond ligand binding affinity. Investigations on the consequence of RAMP interaction with GPCRs have demonstrated that RAMPs alter GPCR trafficking and G-protein signaling in a receptor-, agonist-, and pathway-dependent manner.

Table 1-1. GPCRs reported to interact with RAMPs. Listed are the abbreviation of the GPCRs, GPCR family, RAMP interaction(s), and references.

GPCR	Abbreviation	GPCR family	RAMP interaction
Calcitonin receptor-like receptor	CALCRL	Secretin	RAMP1, 2 and 3 *(41)*
Calcitonin receptor	CALCR	Secretin	RAMP1, 2 and 3 *(44, 45)*
Corticotropin-releasing hormone receptor 1	CRHR1	Secretin	RAMP2 *(52, 53)*
Glucagon receptor	GCGR	Secretin	RAMP2 *(50, 51, 54)*
Growth hormone-releasing hormone	GHRHR	Secretin	None *(54)*
Glucagon-like receptor 1	GLP1R	Secretin	None *(50, 54, 55)*
Glucagon-like receptor 2	GLP2R	Secretin	None *(54)*
Parathyroid hormone receptor 1	PTH1R	Secretin	RAMP2 *(54)*
Parathyroid hormone receptor 2	PTH2R	Secretin	RAMP3 *(54)*
Secretin receptor	SCTR	Secretin	RAMP3 *(56)*
VIP and PACAP receptor 1	VIPR1	Secretin	RAMP1, 2 and 3 *(54)*
VIP and PACAP receptor 2	VIPR2	Secretin	RAMP1, 2, and 3 *(55)*
G protein-coupled estrogen receptor 1	GPER1/ GPR30	Rhodopsin	RAMP3 *(9)*
Calcium-sensing receptor	CaSR	Glutamate	RAMP1 and 3 *(57–59)*

One of the first functions ascribed to RAMPs was their chaperoning role with CALCRL *(41)*. In the absence of RAMPs, CALCRL is poorly localized to the cell membrane. RAMPs also act as a chaperone for several additional GPCRs – CRHR1, SCTR, GPER1 and CaSR *(9, 53, 55–57)*. But RAMPs may also have the opposite effect on GPCR trafficking. GCGR demonstrates reduced cell surface expression upon coexpression of RAMP2 when assayed in CHO cells, but not in HEK293S cells *(50, 51)*.

RAMPs also modulate and participate in receptor internalization and post-internalization trafficking. For CALCRL, RAMPs and CALCRL remain complexed during the internalization process. The PDZ binding domain on RAMP3 can interact with N-ethylmaleimide-sensitive factor *(60)* or Na^+/H^+ exchange regulatory factor-1 to promote CALCRL recycling or inhibit receptor internalization, respectively *(61)*. Agonist-induced β-arrestin recruitment to GCGR is completely inhibited upon RAMP2 coexpression, although the effects of on receptor internalization have not been explored *(51)*.

The effects of RAMPs on GPCR downstream signaling pathways are pleiotropic, and thus far, no clear patterns have emerged. However, it is important to note that unlike CALCRL, other RAMP-interacting GPCRs traffic to the cell surface in the absence of RAMP coexpression. Thus, both RAMP-free and RAMP-associated GPCRs are present on the cell surface, potentially masking pharmacological effects. The effects of RAMP association on receptor pharmacology has only been investigated for CALCR, CaSR, CRHR1, GCGR, and VIPR1. Depending on the receptor, RAMPs can either augment or inhibit GPCR signaling through different downstream signaling pathways *(50, 51, 55, 58, 62)*. However, outside of the chaperoning function of RAMPs for some interacting GPCRs, it remains unclear how RAMPs modulate G protein signaling. Structural studies do not demonstrate direct contacts between RAMP1 and G protein, suggesting that changes in signaling is likely accomplished through allosteric modulation of the receptor structure *(49)*.

1.8 Role of RAMPs in physiology

To date, physiological studies have focused on the interaction between RAMPs and just a subset of interacting GPCRs, largely CALCRL. RAMP knockout mice show expected abnormalities in blood pressure regulation and cardioprotection that are linked to actions of the two peptides that signal through CALCRL-RAMP complexes, CGRP and adrenomedullin. However, the different RAMP transgenic mouse models demonstrate distinctive phenotypes. It is important to note that other GPCRs may also be involved in the phenotypes of RAMP transgenic mice.

CGRP signals through the CALCRL-RAMP1 complex and has clinical importance in migraines. *Ramp1*$^{-/-}$ mice are viable but show dysfunction in the vascular system as well as an alteration in inflammatory responses *(63–65)*. In mice with neural overexpression of RAMP1, increased sensitivity to CGRP causes increased neurogenic inflammation *(66)*. Excess CGRP induces migraines by causing vasodilation, and thus, monoclonal antibodies (mAbs) have been developed to block the interaction between CGRP and CALCRL-RAMP1. These antagonizing mAbs are the first RAMP-targeted therapeutics to be FDA-approved *(67, 68)*.

Although both RAMP2 and RAMP3 complex with CALCRL to form a receptor for adrenomedullin, knockout mice of RAMP2 and RAMP3 have revealed distinct roles of these two RAMP isoforms. Genetic loss of RAMP2 causes embryonic lethality due to defects in vascular development and cardiac mitochondrial dysregulation *(69)*. Consistent with the role of RAMP2 in vasculature, endothelial restoration of RAMP2 expression rescues *Ramp2*$^{-/-}$ lethality, but mice still exhibit cardiomyopathy *(70, 71)*. Haplosufficient RAMP2 mice survive to birth but demonstrate increased vascular permeability *(72, 73)*. In contrast to RAMP2, *RAMP3*$^{-/-}$ mice

have no major abnormalities, but exhibit higher blood pressure, and reduced lymphatic vessel function *(65, 72, 74, 75)*. The phenotypes described above are recapitulated by genetic loss of *Calcrl*, *Adrenomedullin*, or *Cgrp (76)*.

More research is needed to uncover the physiological role of RAMP interactions with other GPCRs. Only a handful of studies have begun to show that the physiological role of RAMPs is not limited to the modulation of CALCRL. Yet several of the phenotypes that RAMP knockout mice display are distinct from *Calcrl*, *Adrenomedullin,* or *Cgrp* knockout mice. With regards to the CALCR-RAMP1 complex, neuronal overexpression of RAMP1 in mice leads to sensitization of amylin, leading to increased energy expenditure *(66)*. Alteration of RAMP2 expression also leads to changes in expression of GPCRs other than CALCRL and CALCR, including *Gcgr and Pth1r*. For PTH1R, reduced expression causes an attenuated response to parathyroid hormone, resulting in improper placental development *(70, 77)*. Reduction in RAMP2 expression also attenuates the ability of CRF1 to induce stimulation of adrenal corticotropin hormone, a vital hormone in the stress response *(55)*. RAMP3 acts as a chaperone and serves as an essential regulator of GPER30 function. Genetic loss of RAMP3 eliminated the cardioprotective effects of GPR30 activation in chronic hypertension and cardiac hypertrophy mouse model *(9)*. These and other GPCR-RAMP complexes beyond CALCRL are potential therapeutic targets for the treatment of heart failure, infertility, and anxiety.

1.9 Identification of previously unknown GPCR-RAMP interactions

The breadth of GPCR-RAMP interactions remains unclear and warrants further investigation. Several lines of evidence suggest that more GPCR-RAMP interactions remain to be discovered. RAMPs are ubiquitously expressed throughout human tissues, indicating a broad role in human physiology *(41)*. RAMP transgenic mice have unexpected phenotypes, such as infertility, that cannot be linked to the well-established RAMP-CALCRL complexes *(77, 78)*.

Only 15, or ~4%, of all non-olfactory GPCRs have been studied for interactions with GPCRs. The vast majority of the GPCRs investigated for RAMP interaction have focused on the secretin-like GPCRs. Yet, both a rhodopsin-like and a glutamate-like GPCR interact with RAMPs *(9, 57)*. This opens up the possibility that more GPCRs outside the secretin-like family are also modulated by RAMP interaction. Compellingly, CXCR7/ACKR3, a rhodopsin-like GPCR, binds to adrenomedullin, the agonist for the CALCRL-RAMP2 and CALCRL-RAMP3 complexes *(79)*.

Even the previously identified secretin-like GPCRs that have been determined to interact with RAMPs require further study. Except for a few, these GPCR-RAMP interactions have not been confirmed by direct methods or are reported in only one publication. In some cases, the literature provides conflicting information as to whether a GPCR interacts with RAMPs or not. To date, a complete secretin-like GPCR-RAMP interactome has not been described.

Thus, I was interested in developing methods to identify previously undescribed GPCR-RAMP interactions. With nearly 340 non-olfactory GPCRs, pairwise investigation of GPCR-RAMP interactions would be prohibitive. Thus, I took two approaches to address GPCR-RAMP interactions in a high-throughput and scalable fashion. First, I implemented computational

approaches to investigate the possibility of global interactions between RAMPs and GPCRs. If RAMPs interact with many GPCRs, as opposed to the few that are reported in the literature, we expected to observe significant coevolution and coexpression. I then developed a multiplexed immunoassay to screen for direct interaction between RAMPs and all secretin-like GPCRs, as well as several other GPCRs. This method, which utilized the suspension bead array and Luminex technologies, is highly scalable and can be used to screen for all GPCR-RAMP interactions as well as GPCR-membrane protein interactions more generally.

CHAPTER 2. Materials and Methods

2.1 Bioinformatics analysis

2.1.1 Percent of shared species

Orthologs of human RAMPs and GPCRs were identified using the OMA database *(80)*. To calculate percent shared species among gene pairs, we first constructed lists of species for each gene, in which one can find orthologs. Percent of shared species for a pair of genes a and b (PSS(a,b)) was calculated by the intersection of species lists for gene a (Sa) and gene b (Sb), divided by their union, multiplied by 100:

$$PSS(a,b) = \frac{Sa \cap Sb}{Sa \cup Sb} \times 100$$

Intersection and union are operations from set theory.

2.1.2 Phylogenetic comparison

For species that contained both a GPCR and a RAMP ortholog we first aligned orthologous sequences using the BLOSUM50 scoring matrix, which is based on local alignments *(98)*. Then a matrix of pairwise sequence distance, or the evolutionary rate of change between two gene pairs, was calculated using the Jukes-Cantor algorithm to build the phylogenetic trees *(99)* (MatLab, Bioinformatics Toolbox, seqlinkage). We compared phylogenetic trees using two methods. First, we compared trees by calculating the correlation between two genes based on pair-wise distances among species. The second method we used is an established phylogeny

comparison algorithm *(81)*. This algorithm is based on pruning tree branches and comparing the resulting species partitions. The full algorithm can be found in the above citation. Briefly, given a pair of phylogenetic trees, the algorithm arbitrarily chooses one tree, goes through each of the edges (*i.e.*, branches) and prunes the tree in this spot. This pruning produces two subtrees which determine a specific partition of the leaf nodes (this is the first partition for the first tree). Similarly, all the possible partitions produced by edge pruning of the second tree are generated and compared with the first partition of the first tree. A score representing the similarity of each partition pairs is calculated. The same procedure is performed for all the other edges of the first tree. Next, the optimal match between branch pruning-derived partitions of the two trees is attained with the Munkres algorithm (also known as the Hungarian algorithm). Lastly, a global similarity score based on the optimal branches match is calculated.

2.1.3 'Tree of life' normalization

When comparing phylogenetic patterns of two genes across species of varying classifications, the primary determinant of the comparison is the global phylogenetic distance between the species. To reduce the global phylogenetic distance effect and directly compare the phylogenetic patterns of specific gene pairs, it is necessary to normalize the trees by the general 'tree of life' *(82)*. We compared phylogenetic patterns between genes using matrices of amino acid sequence distance and normalized by the 18S rRNA matrix. Normalizing distance matrices by the 18S rRNA matrix introduces a higher correlation among the compared genes than the non-normalized matrices. In addition, the normalization procedure reduced the global phylogenetic distance by mixing the inter- and intra-species clusters. Hence, normalization to the

'tree of life' corrects for the inter-species basal distances and enables the specific protein pair to govern the correlation strength.

2.1.4 Coexpression analysis

RNA-seq data from 53 tissues provided by 544 donors, with a total of 8555 samples, were downloaded from gtexportal.org (GTEx_Analysis_v6p_RNA-seq_RNA-SeQCv1.1.8_gene_rpkm.gct.gz). Downloaded data was provided as reads per kilobase per million mapped reads (RPKM). Only samples passing quality control were included in the dataset. Read counts, and RPKM values were produced with RNA-SeQC; importantly, reads were mapped to a single gene (see gtexportal.org documentation for more information). For transcripts per kilobase million (TPM) normalization, the RPKM of each gene was divided by the total RPKM for the sample and multiplied by 10^6. For rank normalization, each gene in each sample was ranked in descending order (highest RPKM having the highest numeric rank). For quantile normalization, gene expression across an individual sample was fit to the averaged distribution observed across samples. Before implementing the Spearman correlation analysis, the median normalized expression (RPKM, TPM, rank, or quantile) per tissue was calculated to account for differences in the number of samples per tissue type. Spearman correlation coefficient was calculated for each RAMP-non-olfactory GPCR pair as well as ligand-receptor, receptor subunit and random gene pairs. For coexpression analysis by GPCR cluster, GPCR clusters were assigned as per Fredriksson et al. *(19)*.

2.2 DNA constructs

2.2.1 RAMP constructs

Epitope-tagged human RAMP DNA constructs were encoded in a pcDNA3.1(+) mammalian expression vector. The human RAMP1, RAMP2, and RAMP3 cDNAs encoded an N-terminal FLAG tag (DYKDDDDK) following the signal peptide (amino acids 1-26, 1-42 and 1-27 for RAMP1, RAMP2 and RAMP3 respectively) and a C-terminal OLLAS tag (SGFANELGPRLMGK). The RAMP DNA constructs were codon-optimized for expression in human cell lines.

2.2.2 Secretin-like and ADGRF5 GPCR constructs

Epitope-tagged human secretin-like GPCR DNA constructs were encoded in a pcDNA3.1(+) mammalian expression vector. The human secretin-like GPCR and ADGRF5 cDNAs encoded a 5-hydroxytryptamine receptor 3a receptor (5-HT3a) signal sequence (MRLCIPQVLLALFLSMLTGPGEG) in place of the native signal sequence, as determined by SignalP 4.1 (Table 2-1) *(83)*. Also, an N-terminal hemagglutinin (HA) tag (YPYDVPDYA) followed the 5-HT3a signal sequence, and the C-terminus encoded a 1D4 tag (TETSQVAPA). The secretin-like GPCR and ADGRF5 DNA constructs were codon-optimized for expression in human cell lines.

Table 2-1. Signal sequence of each secretin-like GPCR. Signal sequences were determined by SignalP4.1 *(83)*.

GPCR	Signal Peptide
ADCYAP1R1	1-23
ADGRF5	1-21
CALCRL	1-22
CALCR	1-42
CRHR1	1-23
CRHR2	1-19
GIPR	1-25
GCGR	1-26
GLP1R	1-23
GLP2R	None
GHRHR	1-22
PTH1R	1-28
PTH2R	1-24
SCTR	1-27
VIPR1	1-30
VIPR2	1-20

2.2.3 Chemokine and orphan GPCR constructs

Epitope-tagged human GPCR DNA constructs were encoded in a pcDNA3.1(+) mammalian expression vector. Expression constructs of human GPR182, GPR4, and CXCR3 cDNAs encoded an N-terminal HA tag (cDNA.org). The human CCR5, CCR7, CXCR4, and ACKR3/CXCR7 cDNA encoded a C-terminal 1D4 epitope tag.

2.2.4 Immunoblot validation of RAMP and GPCR constructs

Solubilized lysates were combined with NuPAGE loading buffer with 100 mM DTT and resolved by SDS-PAGE using NuPAGE 4-12% Bis-Tris gel (Thermo Fisher). Proteins were transferred to an Immobilon PVDF membrane-Fl (Sigma-Aldrich) using a semi-dry transfer apparatus. The membranes were then blocked in Odyssey blocking buffer (LI-COR) for one hour at room temperature and incubated overnight at 4ºC with antibodies (Abs) diluted in blocking buffer with the addition of 0.2% Tween-20. The dilutions used for each Ab were 1:5000 for anti-1D4 mouse monoclonal, 1:2000 for anti-OLLAS rat monoclonal, 1:1000 for anti-FLAG rabbit polyclonal (Sigma-Aldrich), and 1:1000 anti-HA rabbit polyclonal (Cell Signaling). Membranes were washed 3 x 10 minutes in wash buffer (PBS + 0.1% Tween) and then incubated with goat anti-mouse IR 680 or goat anti-rabbit 800 CW (LI-COR) diluted to 1:10,000 in Odyssey blocking buffer supplemented with 0.2% Tween-20 for one hour at room temperature. Follow washing 3 x 10 min in wash buffer, protein bands were visualized using an Odyssey SA (LI-COR).

2.2.5 Cell surface expression validation of RAMP and GPCR constructs

Transfected HEK293 Freestyle cells (Thermo Fisher), approximately 1,000,000 in 0.5 mL media, were harvested and washed once in Hank's balanced salt solution (Thermo Fisher) with 20 mM HEPES (HBSS-H) + 0.5% bovine serum albumin (BSA) (Roche). PE anti-FLAG (BioLegend) diluted to 1:2000 in 100 µL HBSS-H + 0.5% BSA was added to the cells, and Ab binding occurred for 45 min at 4ºC. Following Ab incubation, cells were washed 2 times with 1

mL of HBSS-H + 0.5% BSA. The surface expression of each RAMP was quantified by flow cytometry using the Accuri C6 flow cytometer (BD Biosciences).

2.2.6 Adenylyl cyclase activity validation of RAMP and GPCR constructs

Production of cAMP production in response to adrenomedullin was monitored in HEK293T cells coexpressing epitope-tagged CALCRL and a RAMP2 construct (either RAMP2, FLAG-RAMP2, or FLAG-RAMP2-OLLAS). In addition, the reporter plasmid RLuc3-EPAC-GFP10 was also coexpressed and acts as a $BRET^2$ biosensor for cAMP levels as previously described *(84)*. For each well of a 96-well plate, HEK293T cells (100,000 in 0.1 mL) were transiently transfected with 12 ng of RLuc3-EPAC-GFP10, a $BRET^2$ cAMP sensor, with or without cotransfection of 100 ng of CALCRL and/or 100 ng of RAMP2. Total DNA was brought up to 212 ng with pcDNA3.1(+) when needed. Cells were transfected using Lipofectamine 2000 (Thermo Fisher) and plated at 100 µL/well in a 96-well plate previously coated with 0.01% (w/v) poly-D-Lysine (Sigma-Aldrich). Twenty-four hours post-transfection, media was replaced by BRET Buffer (phosphate buffer saline containing 0.5mM $MgCl_2$ and 0.1% BSA). Coelenterazine 400A (Biotum) was added to a final concentration of 5 µM, followed by a 10 min incubation at room temperature. Cells were then stimulated with increasing concentration of adrenomedullin (AnaSpec) for 15 min at room temperature or with 5 µM of forskolin (Sigma-Aldrich) to induce the maximal cAMP production response. Luminescence and fluorescence readings were collected using the Synergy NEO2 plate reader and Gen5 software (BioTek). $BRET^2$ readings between RLuc3 and GFP10 were collected by sequential integration of the signals detected in the 365- to 435- nm (RLuc3) and 505- to 525- nm (GFP10) windows.

$BRET^2$ ratios were calculated as previously described and are expressed as a percentage of forskolin-stimulated response *(84)*. Dose-response curves were derived with GraphPad Prism.

2.3 Suspension bead array (SBA) experiments

2.3.1 Cell culture and transfection

HEK293F cells were cultured in serum-free Freestyle 293 Expression media using 125 mL disposable culture flasks (Thermo Fisher). Cells were shaken constantly at 125 rpm at 37°C with 5% CO_2. The day prior to transfection, the HEK293 freestyle cells were diluted to 600,000 cells/mL and allowed to grow overnight. The next day 3 mL of cells were transferred to one well of a 6-well plate. Each well of cells was transfected with 0.5 µg indicated RAMP plasmid DNA, and/or 0.5 µg indicated GPCR plasmid DNA with 3 µL Freestyle MAX Reagent (Thermo Fisher). Total transfected plasmid DNA was kept constant at 3 µg by adding empty vector pcDNA3.1(+).

2.3.2 Lysate preparation

HEK293 Freestyle cells were solubilized with *n*-Dodecyl-β-D-maltoside (DM) detergent (Anatrace) to form micelles around membrane proteins and maintain GPCR and RAMP structure and complex formation. Twenty-four hours post-transfection, transfected HEK293F cells were harvested and washed once with cold phosphate-buffered saline (PBS). Cells were then incubated in solubilization buffer (50 mM HEPES, 1 mM EDTA, 150 mM NaCl, 5 mM $MgCl_2$,

pH 7.4) with 1% (w/v) DM and cOmplete protease inhibitor (Roche) for two hours at 4°C with nutation. Following solubilization, lysates were clarified by centrifugation at 22k x g for 20 min at 4ºC. Lysates were then transferred to a microcentrifuge tube, and total protein content was determined by Protein DC assay according to the manufacturer's specifications (Bio-Rad).

2.3.3 Generation of the SBA

The SBA was produced by covalently coupling Abs to MagPlex Beads (Luminex Corp), which are magnetic, bar-coded beads where each bar-code is defined by a unique combination of infrared and near red dyes. Each Ab was coupled to a unique bead identity, as previously described *(85)*. In brief, 1.6 µg of each Ab was diluted in MES buffer (100 mM 2-(N-morpholino)ethanesulfonic acid pH 5.0) (Sigma-Aldrich) to a final volume of 100 µL. The carboxylated surface of the magnetic beads was then activated with N-hydroxysuccinimide (Pierce) and 1-Ethyl-3-(3-dimethylaminopropyl)-carbodiimide (Proteochem). After twenty minutes incubation with the activation solution, the diluted Abs were added to the beads, and coupling occurred for two hours at room temperature. Beads were then washed and stored in blocking reagent for ELISA (BRE) (Roche), a protein-containing blocking buffer, with the addition of ProClin300 (Sigma-Aldrich). The coupling efficiency for each Ab was determined by incubating the beads with PE-conjugated anti-rabbit IgG or PE-conjugated anti-mouse IgG (Jackson ImmunoResearch).

2.3.4 SBA assay procedure

Lysates were incubated with an aliquot of the SBA. Protein associated with each bead in the SBA was detected with a phycoerythrin (PE)-conjugated Ab. Lysates were diluted to 50 µg/mL in solubilization buffer containing 0.1% (w/v) DM, to a total volume of 25 µL in a half-volume, 96-well plate (Grenier). An equal amount of 2x SBA assay buffer (PBS containing 1% (w/v) polyvinyl alcohol (PVA) (Sigma-Aldrich), 1.6% (w/v) polyvinylpyrrolidone (PVP) (Sigma-Aldrich), 0.2% (w/v) casein (Sigma-Aldrich), and 20% rabbit-IgG (Bethyl)) was added to the diluted lysates. Aliquots of the SBA, containing 50-100 beads for each bead ID, were added to the lysates in 50 µL of 1x SBA assay buffer (PBS containing 0.5% PVA (w/v), 0.8% PVP (w/v), 0.1% (w/v) casein, and 10% rabbit IgG). The lysates and beads were incubated overnight at 4°C. Then the beads were washed five times with 100 µL PBS containing 0.05% Tween-20 (PBST) using a EL406 washer (BioTek). Beads were then incubated with 50 µL of PE-conjugated detection Abs diluted in BRE containing 0.1% DM, 0.1% Tween-20, and 10% rabbit IgG. The final dilutions used for the detection Abs were 1:1000 for PE-conjugated anti-FLAG (BioLegend) and PE-conjugated anti-1D4, 1:500 for PE-conjugated anti-OLLAS, and 1:200 for PE-conjugated anti-HA (BioLegend). PE conjugation to 1D4 and OLLAS Abs was performed according to manufacturer's directions (Abcam). Following incubation at 4°C for one hour, the beads were washed three times with 100 µL PBST. After the final wash, 100 µL of PBST was added to the beads, and the fluorescence associated with each bead was measured in a FlexMap3D instrument (Luminex Corp).

2.3.5 SBA data analysis

For GPCR-RAMP interactions determined through capture and detection of epitope tags, an ordinary one-way ANOVA, with Dunnett's multiple comparisons test, was used to compare MFI from the lysates cotransfected with an epitope-tagged RAMP and epitope-tagged GPCR to MFI from the negative control, mock transfected cells (Prism 7, Graphad). MFIs from at least three experiments performed in duplicate were used in the statistical analysis (Fig 4-5). We then calculated a combined statistical measure. The p-values for the GPCR-RAMP complexes determined by each capture-detection Ab pair were then converted to 4 for $p \leq 0.0001$, a 3 for $p \leq 0.001$, a 2 for $p \leq 0.01$, a 1 for $p \leq 0.05$, or a 0 for $p > .05$. For each GPCR-RAMP complex the converted p-values were added up and divided by either eight (for dual-tagged GPCRs) or four (for single-tagged GPCRs).

A Kruskal-Wallis ANOVA was used to compare the MFI from lysates transfected with RAMP1, RAMP2 and RAMP3 for RAMP Ab validation, with at least 200 experiments performed in duplicate (R package) (Fig 4-6). Statistical significance of GPCR Ab validation was determined using a single-tail Z-test comparing the signal from all Abs for each lysate with at least three experiments performed in duplicate for each lysate (Excel, Microsoft) (Figure 4-7 and Figure 4-8). Statistical significance of GPCR-RAMP complex formation captured by GPCR Abs was also determined using a single-tail Z-test comparing the signal from all Abs for each cotransfected lysate, with at least three experiments performed in duplicate for each lysate (Excel, Microsoft) (Figure 4-9). For the single-tail Z-test, a z-score greater than 1.645 corresponds to a p-value less than 0.05. The alpha level used for each statistical test was 0.05.

2.3.6 Statistical comparison of SBA data sets

The data obtained using anti-GPCR capture Abs was compared to the data obtained using the epitope-tag capture methods. Based on the data set for GPCR-RAMP complexes derived from the epitope-tag capture Abs, a matrix of hypothetical outcomes for the data set derived from the anti-GPCR Ab capture strategy was constructed (Figure 4-10). We then compared the two matrices of results (epitope-tag Ab capture versus protein-specific Ab capture) by converting them to binary score matrices (0,1). A Z-score threshold of 1.645 was applied for the anti-GPCR Ab data set, which corresponds to a confidence interval of 95% for a single-tailed test (Figure 4-9). The threshold used to convert the summarized and normalized epitope tag data to binary form was increased by an interval of 0.125 (Table 4-4). The following metrics were plotted as a function of the threshold used to convert the epitope tag data to a binary matrix: (1) overall percent agreement (P_0), (2) the percent of hits from the epitope tag data that are also found in the anti-GPCR Ab data (sensitivity), (3) the percent of non-hits from the epitope tag data that are also non-hits in the anti-GPCR Ab data (specificity), (4) the probability of a positive result in the anti-GPCR Ab data also being a positive in the epitope tag data (positive predictive value), (5) the probability of a negative result in the anti-GPCR Ab data also being a negative in the epitope tag data (negative predictive value) and (6) the similarity of the two data sets (Jaccard Index).

Table 2-2. Formulas used to compare SBA data sets. TP, true positive; TN, true negative; FP, false positive; TP, true positive.

Metric	Formula	Information
P_0	(TP+TN)/(TP+TN+FP+FN)	Overall percent agreement
Sensitivity	TP/(TP+FN)	Percent of all positives from epitope beads that the anti-GPCR beads detect
Specificity	TN/(TN+FP)	Percent of all negatives from epitope beads that the anti-GPCR beads detect
Positive Predictive Value	TP/(TP+FP)	Probability of being a positive from epitope beads if anti-GPCR beads says positive
Negative Predictive Value	TN/(TN+FN)	Probability of being a negative from epitope beads if anti-GPCR beads says negative
Jaccard Index	TP/(TP+FP+FN)	Similarity of positives between the epitope beads and the anti-GPCR beads

2.4 Proximity ligation assay (PLA) experiments

2.4.1 Cell culture and transfection

HEK293T cells were maintained in DMEM-Q (Thermo Fisher) with 10% FBS (Atlanta Biologicals). Gelatin-coated coverslips were placed within the wells of a 6-well dish with one well per transfection condition. HEK293T cells were seeded at 100,000 cells/mL and allowed to grow for 24 hours before transfection. The cells were transfected with 0.4 μg (except in one experiment where 0.5 μg was used) of pcDNA3.1(+) vector encoding the GPCR and RAMP2 constructs. The total amount of DNA used for each transfection was brought to 2 μg with an empty pcDNA3.1(+) vector. For the mock transfection, 2 μg of empty pcDNA3.1(+) vector was used. Transfection was performed with 4 μL Lipofectamine 2000 per well of the 6-well dish. The total volume of media per well was maintained at 2 mL.

2.4.2 PLA procedure

After 24 hours, cells were washed twice in PBS, fixed and permeabilized with ice-cold methanol for 5 mins at -20°C and then washed three times with PBS. For the formaldehyde (FA) fixation, cells were fixed for 10 mins at room temperature with 4% (w/v) FA (Polysciences, Inc) in 1x PBS, final concentration. After fixation, cells were washed three times in PBS and then processed following manufacturer's instructions for DuoLink In Situ Detection Reagents Red Mouse/Rabbit (Sigma-Aldrich) using rabbit anti-HA (Cell Signaling Technology) and mouse anti-FLAG (Sigma-Aldrich) primary Abs. After PLA processing, cells were mounted in DuoLink mounting medium with DAPI (Sigma-Aldrich), allowed to incubate at room temperature, stored overnight at -20°C, and imaged the following day.

2.4.3 PLA image acquisition

Deconvoluted PLA images were acquired with a DeltaVision Image Restoration Inverted Olympus IX-71 Microscope using a 100x oil immersion objective. Excitation/emission wavelengths were 390/435nm for the blue channel (DAPI) and 575/632nm for the red channel (PLA puncta). Exposure times and transmittance percentages were held constant while imaging all samples within the same experiment. At least three Z-stack images (0.2 μm thickness per slice) of different fields of view were captured per coverslip for each control, and at least five Z-stack images were captured for all other samples. Images from the maximum projection of Z-stack images and Imaris spot analysis result snapshots are shown in Figure 4-13 and 4-14.

2.4.4 PLA image processing

Image processing was done in ImageJ (adding scale bars, generating maximum projections) and Imaris. Nuclei stained with DAPI were counted to obtain the total number of cells per image. The PLA puncta were counted in a 3D rendering of each Z-stack in Imaris using the Spot tool. The same Spot parameters (estimated puncta XY and Z diameter, threshold) were used for all samples in all experiments. The puncta count value for each Z-stack was divided by the total number of cells per image, and results were plotted in Prism 8 (Graphpad).

2.4.5 PLA data analysis

A one-way ANOVA followed by Dunnett's multiple comparisons test was used to compare the mean PLA puncta count of the positive condition (CALCRL-RAMP2, both primary Abs) to that of each of the controls, and to compare CXCR3-RAMP2 and mock to the other GPCR-RAMP2 pairs (Fig. 4-14) (Prism 8, Graphpad). Outliers from each GPCR-RAMP pair were determined in Prism via the ROUT method with Q=1%. Two outliers were removed from the PTH1R-RAMP2 data set and three from the CXCR3-RAMP2 data set (Fig. 4-14). A two-tailed P-test in Prism was used to compare the numbers of PLA puncta from methanol-fixed and FA-fixed cells (Figure 4-13). Significance was determined by $P<0.05$. The alpha level used for each test was 0.05.

CHAPTER 3. Global Coexpression and Coevolution of RAMPs with GPCRs.

3.1 Introduction

Whether RAMP interactions are frequent among GPCRs outside the secretin-like family remains an open question. With hundreds of non-olfactory GPCRs in the human genome, pairwise biochemical experiments to determine whether additional GPCRs interact with each RAMP would be both time and resource consuming. The standard high-throughput, biochemical methods to identify protein-protein interactions are not amenable to GPCR-RAMP complexes *(86)*. Thus, we decided to take a bioinformatics approach to test our hypothesis that RAMPs interact globally with GPCRs by using two complementary approaches, coexpression and coevolution.

One method to elucidate protein-protein interactions (PPIs) is to evaluate the coexpression of two gene pairs. Physiological PPIs are expected to exist in the same cells, also known as "guilt-by-association." Interacting proteins have a higher correlation of expression across tissues in comparison to random gene pairs *(87)*. In addition, coexpression is often used to validate results from high-throughput, biochemical experiments identifying novel PPIs to reduce the rate of false positives *(88)*.

Another approach to elucidate PPIs is to carry out a phylogenetic analysis of protein sequences (Figure 3-1A). In a phylogenetic analysis, the evolutionary history of protein pairs is compared according to the hypothesis that interacting proteins coevolve in nature. Two methods can be implemented to examine phylogenetic similarities. The first identifies orthologs of two proteins across species with the assumption that interacting proteins are expected to coexist in

genomes *(89)*. The second method compares the evolutionary history of each pair member while assuming similar phylogenetic trees (i.e., similar mutational rate) for interacting proteins. Phylogenetic tree similarities can be calculated by either pair-wise correlation or comparison of phylogenetic tree shape. Pair-wise correlation calculates the rate of mutations across species. Mutations in one interacting protein are expected to be coupled to mutations in the other interacting protein and thus, interacting proteins display a similar rate of mutations *(82)*. For comparison of phylogenetic tree shape, coevolution of gene pairs is calculated by how the nodes, or species, are partitioned on a phylogenetic. Trees will similar branching patterns, or shape, show high coevolution (5). Phylogenetic analysis of protein sequences has previously been shown to correspond to experimentally determined PPIs *(90)*. In all, we address four different questions using the coevolution and coexpression analyses (Table 3-1).

Table 3-1. Questions addressed by coexpression and coevolution measurements.

Question	Measurement
Are RAMPs and GPCRs found in the same tissues?	Coexpression
Are GPCRs and RAMPs found in the same species?	Percent of shared species
Do GPCRs and RAMPs demonstrate similar mutational rates between species?	Pair-wise correlation
Do GPCRs and RAMPs have similarly shaped phylogenetic trees?	Phylogeny comparison

If RAMPs interact globally with GPCRs, then we would expect to identify higher coexpression and coevolution between GPCR-RAMP gene pairs in comparison to random pairs of genes. To ensure that strong coexpression and coevolution is indicative of protein interactions, we also examined the coexpression and coevolution of known pairs of interacting proteins -

proteins in same receptor complex and receptor-ligand pairs *(91, 92)*. For most GPCR-RAMP interacting pairs, interaction is not a requirement for the GPCR to signal in response to agonist ligand. Thus, we expected that the coexpression and coevolution of RAMP-GPCR pairs would be less significant than receptor complex or receptor-ligand gene pairs (Figure 3-1B). Since olfactory GPCRs constitute the largest group of GPCRs and would thus dominate the outcome of the coevolution measurements, we excluded them in the analyses.

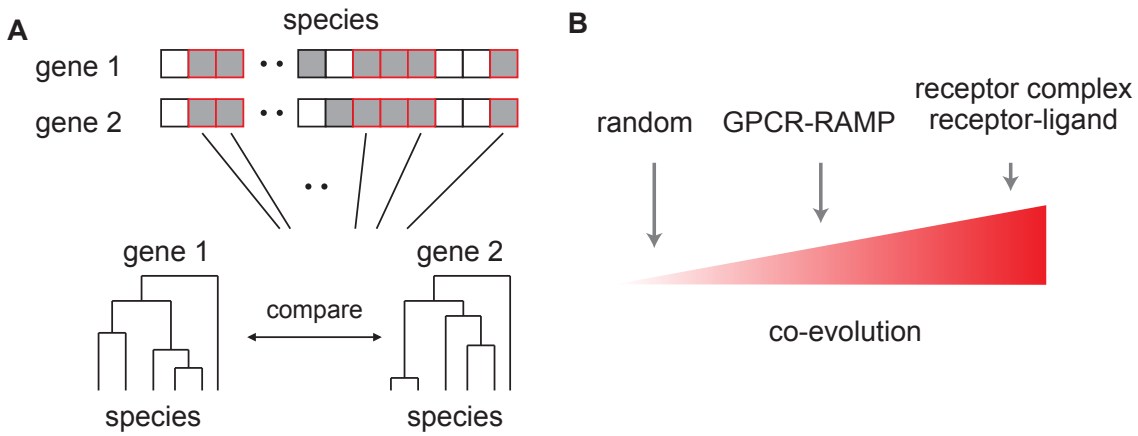

Figure 3-1. Estimates of coevolution and coexpression. (**A**) A method to calculate coevolution determines the number of species (grey shade) that two proteins share (red outline). Between species that share two proteins, the phylogenetic trees of gene pairs are compared by a phylogenetic comparison algorithm or by pair-wise correlation. (**B**) We hypothesized that RAMPs will show an intermediate level of coevolution and coexpression when compared to random gene pairs and known interacting gene pairs.

3.2 Coexpression analysis

3.2.1 Expression of RAMPs in human tissues

Northern blot analysis first showed that at least one RAMP isoform is expressed in seven different human and mouse tissues *(93)*. More recently, RNA-Seq databases have been developed to evaluate gene expression in a much wider variety of human tissues. To examine RAMP expression in human tissues, I accessed an RNA-Seq database of 53 distinct tissues from the Genotype-phenotype consortium (GTEx). The GTEx RNA-Seq database is comprised of 8,555 samples from 53 tissues provided by 544 human donors *(94)*. I found that RAMPs are ubiquitously expressed across human tissues, with the exceptions of whole blood, transformed fibroblasts and lymphocytes (Figure 3-2) *(41)*. In comparison to RAMP2 and RAMP3, RAMP1 mRNA is more abundantly found in brain tissues and both male and female reproductive organs. RAMP2 and RAMP3 show higher transcript levels in adipose tissues, lung, thyroid, and breast tissues than RAMP1. Overall, the mRNA expression levels of RAMPs in human tissues revealed that RAMP2 and RAMP3 show a more similar expression pattern than with RAMP1.

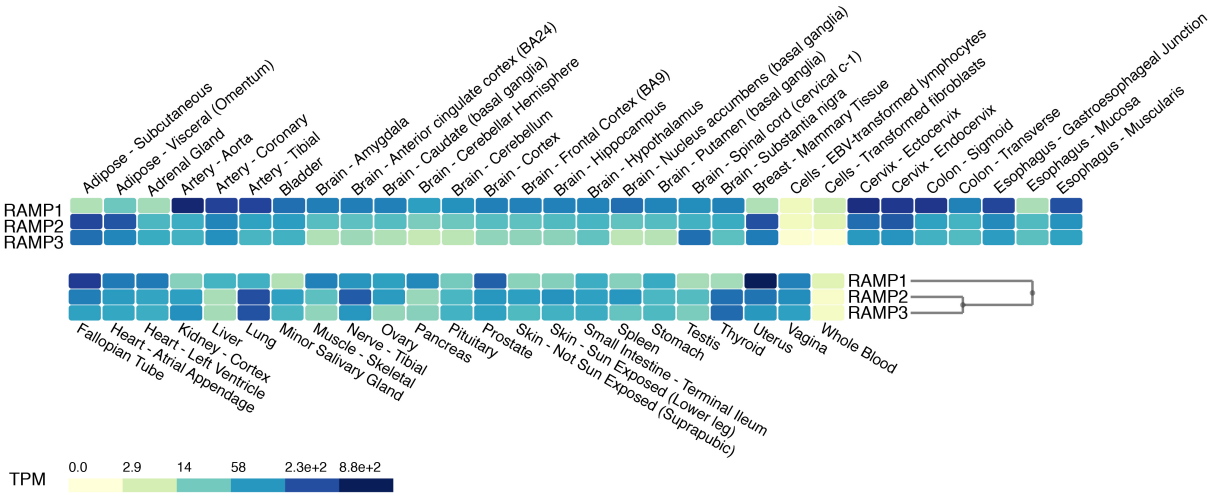

Figure 3-2. Expression of RAMP1, RAMP2, and RAMP3 in human tissues. Transcript levels reported as transcripts per kilobase million (TPM) from 53 human tissues are represented as a heatmap. RNA-Seq data were obtained from the GTEx Consortium *(94)*.

3.2.2 Normalization of RNA-Seq data sets

We hypothesized that transcripts of interacting proteins would tend to be coexpressed across human tissues. Thus, I calculated the coexpression for random, receptor-complex, and receptor-ligand gene pairs. To account for different statistical properties of the RNA-Seq datasets between each sample, I normalized the data sets by four commonly used methods - quantile normalization, rank, transcripts per kilobase million (TPM), and reads per kilobase million (RPKM) *(95)*. Following normalization, I found the median expression of each gene in each tissue to account for differences in the number of samples for each tissue type and then calculated the correlation coefficient by the Spearman method. For receptor-complex gene pairs, each normalization method showed significantly higher correlation than random gene pairs. However, receptor-ligand gene pairs showed significantly higher correlation only when quantile or rank normalization was used (Figure 3-3). Quantile normalization reduces unwanted technical variability from RNA-Seq data and was used for further analysis *(96)*.

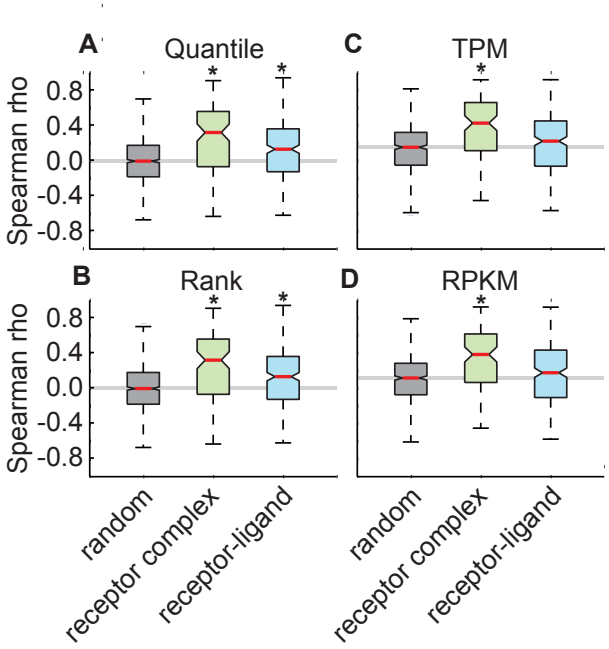

Figure 3-3. Normalization methods used prior to calculation of coexpression.
Boxplots of coexpression, measured as Spearman rho, across 8,555 samples derived from 53 tissues between protein pairs. Normalization methods used were (**A**) quantile, (**B**) rank order, (**C**) transcripts per kilobase million (TPM), and (**D**) reads per kilobase million (RPKM). These boxplots are shown for 500 randomly chosen gene pairs (grey), gene pairs that are members of the same receptor complex (green) or receptor-ligand gene pairs (blue). The boxplot shows the median (red line), 95% confidence interval (notch edge), 25th and 75th percentiles (box edges), two standard deviations (whiskers) and 95% confidence interval of the median for random gene pairs (grey bar). Data were obtained from the GTEx database *(94)*. Asterisks denote that the median differs from that of randomly chosen proteins pairs with P<0.05 (One-way ANOVA with Bonferroni correction).

3.2.3 Global coexpression between RAMPs and GPCRs

I next searched for evidence supporting global GPCR-RAMP interactions at the RNA expression level. I first calculated the coefficient of expression correlation (Spearman rho) between each RAMP and CALCRL, a well-validated interacting GPCR *(97)*. As expected, each RAMP had positive correlation with CALCRL (Figure 3-4A to C) with a Spearman rho of 0.21, 0.84 and 0.82 for RAMP1, RAMP2 and RAMP3 respectively. Next, the expression correlation was calculated for the following groups – random pairs, RAMP1-GPCR, RAMP2-GPCR, RAMP3-GPCR, receptor-ligand, and receptor-complex. Random gene pairs showed an averaged correlation coefficient close to zero, while receptor-complex and receptor-ligand gene pairs had an average Spearman rho of 0.12 and 0.26, respectively. Each RAMP also showed a significantly higher correlation coefficient with GPCRs than expected by chance, with a Spearman rho of 0.83, 0.85, and 0.83, for RAMP1, RAMP2 and RAMP3, respectively (Figure 3-4D).

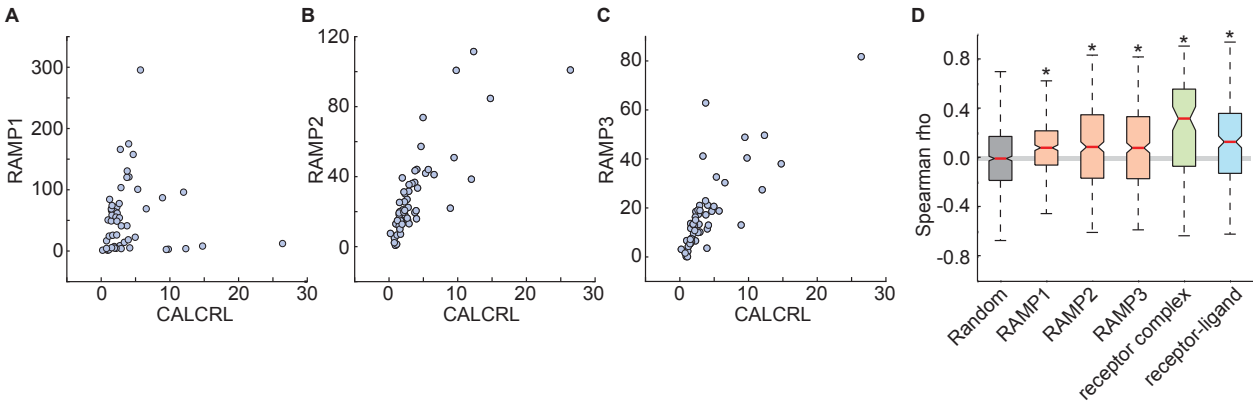

Figure 3-4. Coexpression between GPCRs and RAMPs across human tissues. Scatterplot of quantile normalized expression data for (**A**) RAMP1 (**B**) RAMP2 and (**C**) RAMP3 versus CALCRL. Spearman rhos are 0.21, 0.84, and 0.82 for A-C respectively. (**D**) Boxplot (as in Figure 3-3) of coexpression, measured as Spearman rho, across 8,555 samples derived from 53 tissues between protein pairs. This boxplot is shown for 500 randomly chosen gene pairs (grey), RAMP1, RAMP2 or RAMP3 against non-olfactory GPCRs (orange), gene pairs that are members of the same receptor complex (green) or receptor-ligand gene pairs (blue). Data were obtained from the GTEx database *(94)*. Asterisks denote that the median differs from that of randomly chosen proteins pairs, with $P<0.05$ (one-way ANOVA with Bonferroni correction).

GPCRs are subdivided into families (see Figure 1-2) and further subdivided into clusters that reflect the molecular composition of their activating ligands *(19)*. Specific clusters of GPCRs may drive the overall positive correlation between RAMPs and GPCRs. Thus, I calculated the expression correlation of RAMPs with each cluster of GPCRs and found that a select set of GPCR clusters showed significantly higher median expression correlation with RAMPs in comparison to RAMPs with all GPCRs. The melanin-concentrating hormone (MCH) GPCR cluster has the highest averaged coexpression with RAMP1, followed by the amine cluster. RAMP2 and RAMP3 have the highest coexpression with prostaglandin receptors, followed by chemokine and purine receptors (Figure 4-4). These receptor clusters respond to a

variety of agonists - small molecules (purine and amine GPCRs), lipids (prostaglandin GPCRs), and peptides (MCH and chemokine receptors). Although the secretin GPCR cluster has been the most well-studied in respect to RAMP interaction, the coexpression between secretin-like GPCRs and each RAMP was not more significant than between eacp RAMP and all GPCRs.

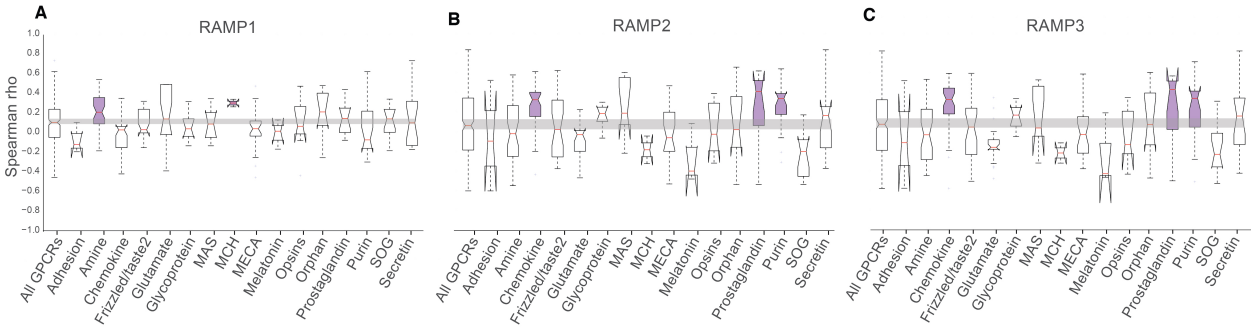

Figure 3-5. Coexpression between different GPCR clusters and RAMPs. Boxplot (as in Figure 3-3) of Spearman rhos across 53 human tissues between (**A**) RAMP1 (**B**) RAMP2 (**C**) RAMP3 and non-olfactory GPCRs. Data were obtained from the GTEx database *(94)*. Receptor clusters with significantly higher coexpression than all GPCRs are highlighted with purple. Abbreviations: MCH, melanin-concentrating hormone; MECA, melanocortin, endothelial differentiation, cannabinoid, and adenosine; SOG, somatostatin, opioid, and galanin.

3.2.4 Coexpression of RAMP2 and RAMP3 with similar GPCRs

I found that RAMP2 and RAMP3 are expressed in similar tissues and show high coexpression with the same clusters of GPCRs (Figure 3-2 and Figure 3-5). Thus, I was interested if RAMP2 and RAMP3 are coexpressed with similar GPCRs. As expected, RAMP2 and RAMP3 showed a similar pattern of coexpression with individual GPCRs and are thus coexpressed with similar sets of GPCRs. (Figure 3-6C). No clear pattern was observed between

the coexpression of RAMP1 with GPCRs and the coexpression of RAMP2 and RAMP3 with GPCRs (Figure 3-6A and B).

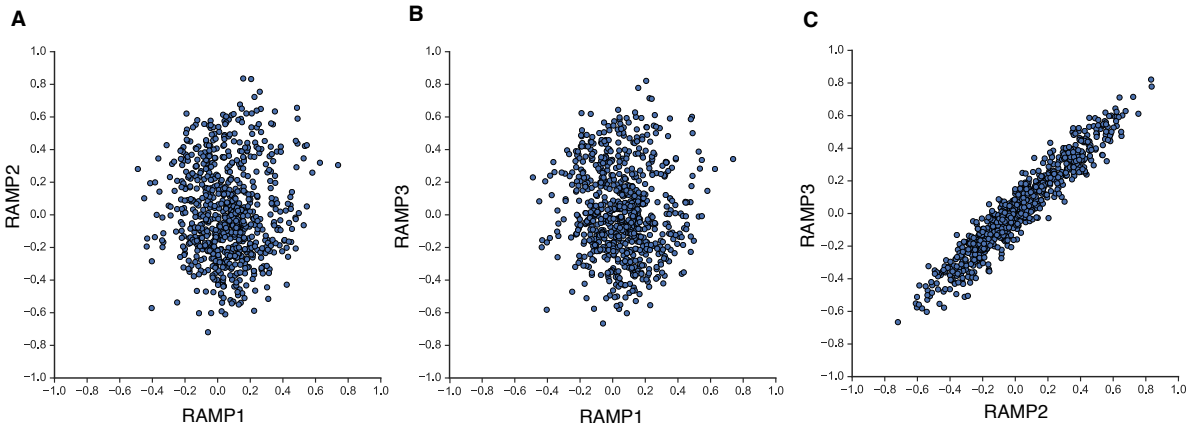

Figure 3-6. Similarity of coexpression between RAMPs with GPCRs. Scatterplots of Spearman rho values between (**A**) RAMP1 and each GPCR versus RAMP2 and each GPCR and similarly for (**B**) RAMP1 versus RAMP3 and (**C**) RAMP2 versus RAMP3. Each dot represents the Spearman rho value between the indicated RAMP and an individual GPCR. Data were obtained from the GTEx database *(94)*.

3.3 Coevolution of RAMPs with GPCRs

3.3.1 GPCR and RAMP orthologs across species

All eukaryotes express GPCRs, while a subset of eukaryotes, the chordates/vertebrates, express RAMPs. Thus, the orthologs of both genes are expected to be found exclusively in chordates. To determine in what species orthologs of RAMPs and GPCRs are found, we obtained

the OMA groups and genomic sequences from the OMA database, which includes genomes for 1970 organisms (18). OMA groups are sets of genes from various organisms which are bona fide orthologous to each other. These sets of genes that have been determined to relate by speciation events, and thus, there is at most one gene per species assigned to an OMA group. In the case of bony fish species, which encode two genes for RAMP1 and RAMP2, the most genetically distant RAMP is not included in the OMA group. In total, 44 of the 1970 species had OMA groups that included at least one ortholog of a human GPCR and an ortholog of a human RAMP. As expected, all species were members of the Chordata phylum. The Mammalia, Actinopteri and Aves classes constituted 79%, 9%, and 7%, respectively, of the species that had both a human GPCR and RAMP ortholog. However, more genomic data for more mammalian species were available in comparison to the Actinopteri and Aves classes.

3.3.2 Percent shared species between RAMPs and GPCRs

We next calculated the percent of shared species between groups of gene pairs as the fraction of the shared species from the joint list of species for both genes in the species pair. Percent shared species was calculated for each RAMP and all non-olfactory GPCR, 500 randomly chosen protein-coding gene pairs, and genes encoding known protein-protein interactions. As expected, the protein complex and ligand-receptor gene pairs showed significant signal, with 2.4- and 2.1- fold higher percentages of shared species than random gene pairs. The pairs of all three RAMPs with GPCRs showed significant, 1.6- to 1.8- fold higher percentage of shared species than expected by chance (Figure 3-7A).

3.3.3 Comparison of phylogenetic trees between RAMPs and GPCRs

We next calculated the estimated gene pair coevolution by comparing the phylogenetic trees of gene pairs across organisms that have orthologs for both examined genes. The average number of examined organisms that we built and compared the phylogenetic trees was 16.5, with a standard deviation of 7.5. For each GPCR-RAMP pair, we only compared phylogenetic trees that that shared more than five species (96% of pairs). The orthologous amino acid sequences across species were first aligned using the BLOSUM50 scoring matrix, which is based on local alignments *(98)*. Then a matrix of pairwise sequence distance, or the evolutionary rate of change between two gene pairs, was calculated using the Jukes-Cantor algorithm *(99)*. Two methods for comparing phylogenetic trees were then used. The first method compares the manner in which each tree partitions its nodes (species), or how many branches have a similar topology *(81)*. Species are partitioned within a gene's phylogenetic tree based on the number of amino acid differences between gene orthologs. The output of this method is a percent similarity score, or phylo-comparison score. We found that the phylogenetic correlation coefficient for each RAMP with GPCRs, receptor-complex gene pairs, and receptor-ligand gene pairs was significantly higher than random pairs (Figure 3-7B).

The second method, pair-wise correlation, calculates the Pearson correlation between distance matrices, or a correlation of the mutational rate of two gene pairs between shared species. Before calculating the pair-wise correlation, we normalized mutational rates to the "tree of life" with the 18S ribosomal RNA (rRNA). Normalization to the 18S rRNA gene reduces the "background" similarity resulting from amino acid changes due to speciation and enables the specific protein pair to govern the correlation strength. The output of the pair-wise correlation

method is a Pearson correlation coefficient, or phylogenetic correlation coefficient. We found that the phylogenetic correlation coefficient for each RAMP with GPCRs and receptor complex gene pairs, but not receptor-ligand pairs, was significantly higher than random pairs (Figure 3-7C). The phylogenetic analysis was repeated across mammalians, but without normalization by 18S rRNA distance. In this case, the pairs of each RAMP with GPCRs, but not those of receptor complexes and receptor-ligand pairs showed significantly higher correlation coefficient than that expected by chance (Figure 3-7D).

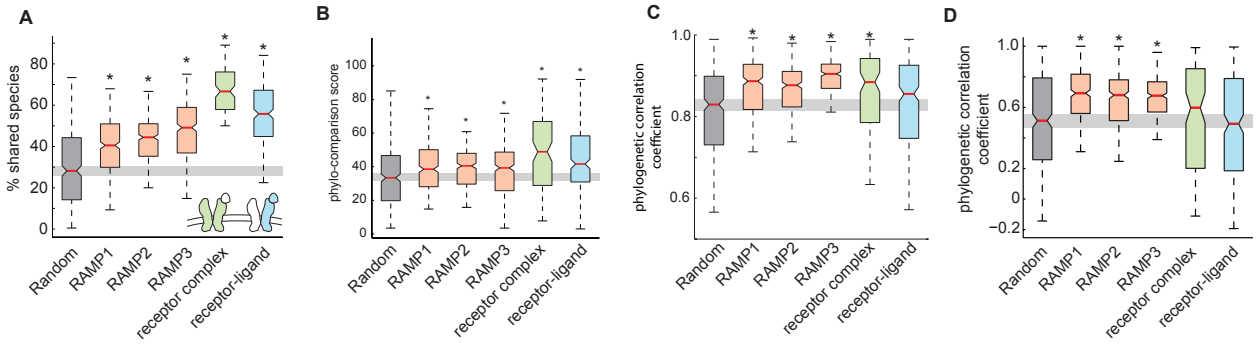

Figure 3-7. Shared species and phylogenetic tree comparison between GPCRs and RAMPs. (**A**) Boxplot for percent of shared species for gene pairs. (**B**) Boxplot for the global phylogenetic score as calculated by phylo-comparison for all GPCRs. (**C**) Boxplot for the phylogenetic correlation coefficient across all organisms, normalized by 18S rRNA sequence distance. (**D**) Boxplot for phylogenetic correlation coefficient across mammalians alone. Boxplots (as in Figure 3-3) are shown for 500 randomly chosen gene pairs (grey), RAMP1, RAMP2 or RAMP3 against non-olfactory GPCRs (orange), gene pairs that are members of the same receptor complex (green) or receptor-ligand gene pairs (blue). Asterisks denote that the median differs from that of randomly chosen proteins pairs, with $P<0.05$ (one-way ANOVA with Bonferroni correction).

3.4 Discussion

Previous studies have shown that eleven GPCRs, mostly focusing on the secretin-like receptors, interact with one or more RAMPs. Here, we address whether additional GPCRs also interact with RAMPs. We used computational methods to assess the coexpression and coevolution of all non-olfactory GPCRs with each RAMP on a global scale. Coevolution and coexpression of two genes suggest that the proteins they encode interact, whether directly or indirectly. Our findings show that GPCRs and RAMPs are significantly coevolved and coexpressed, suggesting that more GPCRs interact with RAMPs than is currently appreciated.

To ensure that the four methods we used – coexpression, percent shared species, tree comparison, and pair-wise tree correlation – could detect protein-protein interactions on a global level, we first compared the signal from known interacting gene pairs to random gene pairs. We found that each of the four methods implemented successfully identified protein-complex and protein-ligand coexpression and coevolution on a global level. The RAMP-GPCR gene pairs also demonstrated significant signal from each computational method implemented, but this signal was generally lower than that of known interacting protein pairs. The weaker signal is likely related to the previous findings that (i) not all GPCRs interact with a RAMPs and/or (ii) GPCRs that do interact with RAMPs often do not require complex formation to respond to known endogenous ligands.

To determine coexpression, I analyzed 8,555 human transcriptomes across 53 distinct tissues from data provided by the GTEx consortium. I found that RAMPs are ubiquitously expressed in the human body, as previously shown by northern blot analysis *(93)*. I also identified higher gene coexpression across human tissues for GPCRs and RAMPS than predicted

by chance. The high gene coexpression was driven by a subset of rhodopsin-like GPCR clusters, which included GPCRs that respond to a variety of different ligands. Thus, it is likely that additional rhodopsin-like GPCRs interact with RAMPs. To date, the only reported RAMP-interacting GPCR in the rhodopsin-like family is GPER1 *(9)*.

While the coexpression analyses provide a global overview of RAMP-GPCR interaction, we would also surmise that known interacting GPCRs demonstrate a positive correlation with cognate RAMPs. As expected, I found that the most well-studied RAMP-interacting GPCR, CALCRL, shows a positive correlation with each RAMP. In agreement with our coexpression analysis with RNA-Seq data, a coexpression analysis using microarray data shows that RAMP2 and CALCRL have high expression correlation in human tissues *(100)*.

Multiple RAMPs often interact with the same GPCR, which could have implications for the regulation of RAMP-GPCR complex formation *(97)*. In this study, I found that RAMP2 and RAMP3 have similar tissue distribution, high coexpression with the same clusters of GPCRs, and the strong correlation of Spearman rhos for each GPCR. These observations are in line with my later findings (see Chapter 4) showing that interacting GPCRs either form complexes with all three RAMPs or with just RAMP2 and RAMP3. Given that RAMP2 and RAMP3 are expressed in similar tissues and appear to interact with similar GPCRs, it is plausible that RAMP2 and RAMP3 may modulate the activity of each other by competing for specific GPCRs.

All three methods that we employed for estimation of gene coevolution – percent shared species, tree comparison, and pair-wise tree correlation – showed similar, identifiable coevolution among each of the RAMPs and non-olfactory GPCRs. The percent shared species analysis provides the most basic estimate of coevolution because it shows the tendency of a gene pair to exist in the same species. It is important to note that CALCRL is more evolutionarily

ancient than the RAMP family of proteins. RAMPs are found only in vertebrates, while the calcitonin subfamily of receptors can be found in invertebrate species such as *Drosophila melanogaster* and *Caenorhabditis elegans*. Therefore, CALCRL in invertebrate species likely functions without RAMPs *(100)*. This situation could cause the percentage of shared species to be more modest even in cases of interacting protein pairs. Thus, coexpression and coevolution measured by pair-wise tree correlations and tree comparison may be a better indicator of interaction because these methods consider only species that contain both a RAMP and GPCR.

In vitro, high-throughput protein-protein interactions can be probed by direct chemical assays, including yeast two-hybrid and tandem mass spectrometry *(101, 102)*. However, GPCRs are not amenable to these high-throughput methods. In large protein networks or families, such as GPCRs, it is impractical to study all possible biochemical interactions in a pair-wise manner. Thus, the use of bioinformatics methods, such as assessing coexpression and coevolution, are useful. Computational approaches also have the advantage that they are independent of the quality and validation of antibody affinity or other technical parameters that are required to carry direct experimentation. However, computational methods, as well as in vitro methods, are subject to limitations, including false detection ("false positives") and misdetection ("false negatives"). Thus, any potential interaction should be validated by multiple methods.

In summary, our results support the hypothesis that a global GPCR-RAMP interaction map exists. First, RNA-Seq data revealed that RAMPs are ubiquitously expressed across human tissue types, suggesting that RAMPs are essential to many physiological functions. Second, we determined that RAMPs are significantly coexpressed and coevolved with GPCRs. We also determined a high level of correlation between coexpression coefficients of RAMP2 and RAMP3

with each GPCR. These results imply that more GPCRs interact with RAMPs than what is currently reported.

CHAPTER 4. Multiplexed Analysis of the Secretin-like GPCR-RAMP Interactome

4.1 Introduction

We next wanted to use a direct biochemical assay to determine which GPCRs interact with RAMPs. Given that there are ~400 non-olfactory GPCRs that might, in principle, interact with each of the three RAMPs, the ideal experimental system should be high-throughput and provide a quantitative assessment of GPCR-RAMP complexes. Towards this end, I employed a suspension bead array (SBA) approach. The SBA strategy is based on the use of magnetic microspheres with different bar-codes. Each bar-coded bead population is coupled to a specific antibody (Ab), allowing the parallel capture and detection of multiple unique, identifiable protein epitopes from a complex mixture of proteins in solution. The SBA technology, in combination with the Human Protein Atlas (HPA) Ab collection, has been successfully implemented to identify soluble proteins in human serum samples *(85, 103)*. Here I demonstrate an experimental approach to define the secretin-like GPCR-RAMP interactome and develop an assay capable of testing the hypothesis that GPCRs and RAMPs interact on a global level.

4.2 Design and validation of GPCR and RAMP constructs

4.2.1 Design of GPCR and RAMP constructs

Immunoassays, such as a suspension bead array, require the use of validated Abs. However, GPCR Abs are notoriously difficult to produce because of the sequence similarity

amongst species and cross-reactivity between closely related GPCRs *(24)*. In addition, Abs to RAMPs have not been adequately validated *(97)*. To overcome the issue of using protein-specific Abs, I created dual, epitope-tagged RAMP, secretin-like GPCR, and ADGRF5 DNA constructs. Constructs of the chemokine receptors were developed for previous studies in our lab *(104–106)*. Each of the three RAMPs was tagged with a FLAG epitope and OLLAS epitope at its N- and C-terminal tail, respectively *(107)*. Each of the 23 GPCRs was epitope-tagged at its N-terminal tail with an HA epitope and/or at its C-terminal tail with a 1D4 epitope (Figure 4-1).

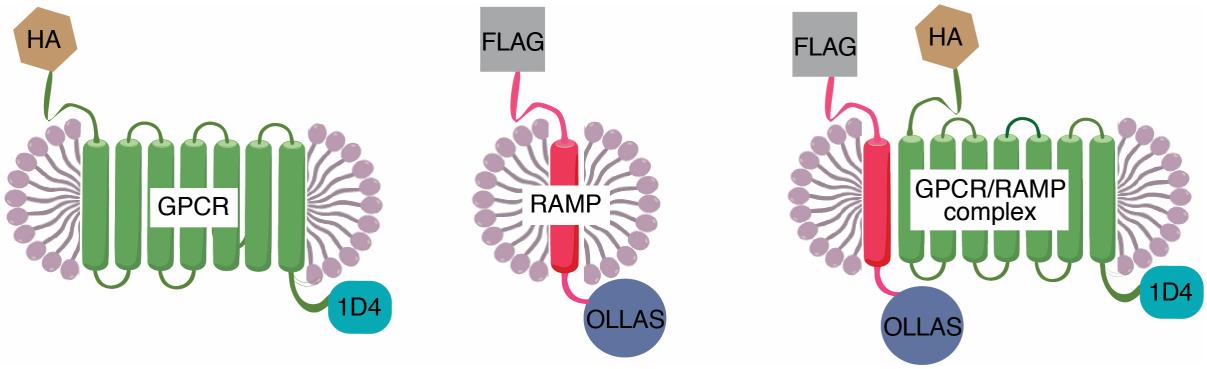

Figure 4-1. Epitope-tagged GPCR and RAMP DNA constructs. The GPCR constructs have an N-terminal HA tag, and a C-terminal 1D4 tag. The RAMP constructs have an N-terminal FLAG tag and a C-terminal OLLAS tag.

4.2.2 Validation of GPCR and RAMP constructs

To ensure that the epitope tags added onto the RAMP and GPCRs did not alter functionality, I ran a battery of tests. To begin with, I determined that the dual-epitope secretin-like GPCR and ADGRF5 were expressed in HEK293F cells, as detected by immunoblot using

anti-1D4 and anti-HA mAbs (Figure 4-2A). Dual-tagged RAMP constructs expressed in HEK293F cells were detected by immunoblot using anti-FLAG and anti-OLLAS Abs (Figure 4-2B). RAMPs traffic to the cell surface when co-expressed with CALCRL *(41)*. Thus, I determined the cell surface localization of each RAMP construct expressed alone or coexpressed with CALCRL by flow cytometry using an anti-FLAG Ab. As expected, each RAMP constructs demonstrated an increase in cell surface localization upon coexpression with CALCRL (Figure 4-2C). Finally, we compared the ability of adrenomedullin to induce cAMP accumulation in cells expressing dual-tagged CALCRL alone, CALCRL with coexpression of dual-tagged RAMP2 or CALCRL with coexpression of untagged RAMP2. No cAMP accumulation was observed in cells transfected with vector, dual-tagged CALCRL or dual-tagged RAMP2. A similar dose-response curve was observed in cells coexpressing dual-tagged CALCRL with either untagged RAMP2 or dual-tagged RAMP2 (Figure 4-2D). Therefore, the epitope tags on RAMP2 and CALCRL do not affect the ability of the CALCRL-RAMP2 heterocomplex to respond to the agonist adrenomedullin through stimulation of cAMP production. Taken together, these experiments indicate that the epitope tags do not affect functionality of RAMPs or CALCRL.

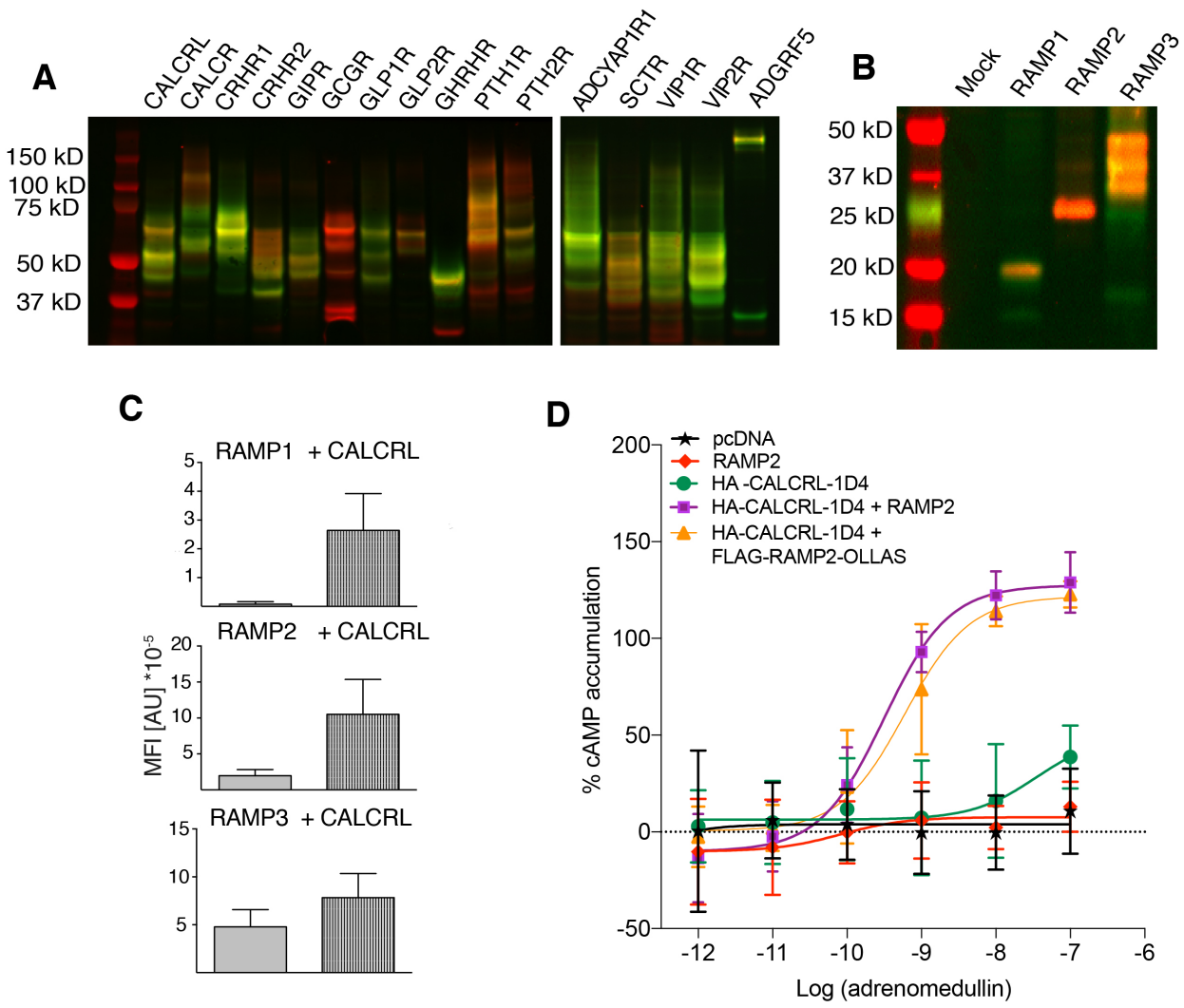

Figure 4-2. Expression and function of epitope-tagged GPCRs and RAMPs. **(A)** Dual-tagged GPCRs expressed in HEK293F cells were detected by immunoblot with an anti-HA Ab (green) and anti-1D4 Ab (red). **(B)** Dual-tagged RAMPs expressed in HEK293F cells were detected by immunoblot using an anti-FLAG Ab (green) or anti-OLLAS Ab (red). **(C)** Cell surface localization of each FLAG-RAMP-OLLAS expressed in HEK293F cells alone (solid bar) or coexpressed with HA-CALCRL-1D4 (striped bar) was measured by flow cytometry using an anti-FLAG Ab conjugated to PE. **(D)** Adrenomedullin-induced cAMP accumulation was measured in HEK293T cells expressing pcDNA3.1(+), RAMP2 alone, HA-CALCLRL-1D4 alone, HA-CALCRL-1D4 plus RAMP2, or HA-CALCRL-1D4 plus FLAG-RAMP2-OLLAS.

4.3 SBA analysis of GPCR-RAMP complexes

4.3.1 Selection of GPCRs to screen for RAMP interaction

To adapt the SBA method and develop an assay to measure GPCR-RAMP interactions, I focused on the family of 15 secretin-like GPCRs, and eight additional GPCRs, to screen for their ability to interact with each of the three RAMPs. All of the secretin-like receptors were included in the test set because this GPCR family encompasses the majority of GPCR-RAMP interactions described to date. Based on an earlier coevolution and coexpression analyses, we also included GPR4 and GPR182 from the rhodopsin-like GPCR family and ADGRF5 from the adhesion GPCR family *(108)*. In addition, the chemokine cluster of GPCRs demonstrated a significantly higher median coexpression with RAMP2 and RAMP3 in comparison with all GPCRs (Figure 3-5). Thus, we included members of the chemokine receptor family: C-C chemokine receptor 5 (CCR5), C-C chemokine receptor 7 (CCR7), C-X-C chemokine receptor 3 (CXCR3), C-X-C chemokine receptor 4 (CXCR4), and atypical chemokine receptor 3 (ACKR3), also known as C-X-C chemokine receptor 7 (CXCR7). A list of each of the 23 GPCRs chosen for SBA analysis and the epitope tag(s) present on each GPCR construct is presented in Table 4-1.

Table 4-1. A list of 23 GPCRs included in this study. Included are the common abbreviations of each GPCR, GPCR family designation, and engineered epitope tag on the N- and C-terminal tails. GPCRs are listed in alphabetical order. Secretin-family receptors are shown in bold. Y, yes; N, No.

GPCR	Abbreviation	GPCR family	N-terminal HA epitope tag	C-terminal 1D4 epitope tag
Atypical chemokine receptor 3/ C-X-C chemokine receptor 7	ACKR3/ CXCR7	Rhodopsin	Y	Y
Pituitary adenylate cyclase-activating polypeptide type 1	ADCYAP1R1	Secretin	Y	Y
Adhesion G protein-coupled receptor F5	ADGRF5	Adhesion	Y	Y
Calcitonin receptor-like receptor	CALCRL	Secretin	Y	Y
Calcitonin receptor	CALCR	Secretin	Y	Y
C-C chemokine receptor type 5	CCR5	Rhodopsin	N	Y
C-C chemokine receptor type 7	CCR7	Rhodopsin	N	Y
Corticotropin-releasing hormone receptor 1	CRHR1	Secretin	Y	Y
Cortocotropin-releasing hormone receptor 2	CRHR2	Secretin	Y	Y
C-X-C chemokine receptor type 3	CXCR3	Rhodopsin	Y	N
C-X-C chemokine receptor type 4	CXCR4	Rhodopsin	N	Y
Gastric inhibitory polypeptide receptor	GIPR	Secretin	Y	Y
Glucagon receptor	GCGR	Secretin	Y	Y
Growth hormone releasing hormone	GHRHR	Secretin	Y	Y
Glucagon-like receptor 1	GLP1R	Secretin	Y	Y
Glucagon-like receptor 2	GLP2R	Secretin	Y	Y
G protein-coupled receptor 4	GPR4	Rhodopsin	Y	N
G protein-coupled receptor 182	GPR182	Rhodopsin	Y	N
Parathyroid hormone receptor 1	PTH1R	Secretin	Y	Y
Parathyroid hormone receptor 2	PTH2R	Secretin	Y	Y
Secretin receptor	SCTR	Secretin	Y	Y
VIP and PACAP receptor 1	VIPR1	Secretin	Y	Y
VIP and PACAP receptor 2	VIPR2	Secretin	Y	Y

I aimed to create an SBA comprising a set of both GPCR-specific and RAMP-specific Abs, as well as monoclonal antibodies (mAbs) against epitope tags that were engineered onto expressed GPCR and RAMP constructs. The complete list of all anti-GPCR and anti-RAMP Abs coupled to the beads is presented in Table 4-2. A total of 55 Abs from the HPA were available to target 21 of the 23 GPCRs in the test set. The HPA Abs were produced by using 50 to 150 amino-acid-long peptides as immunogens to raise rabbit polyclonal Abs *(109)*. The nine anti-RAMP Abs employed were obtained from the HPA and various commercial sources. In addition, beads were coupled to four, validated anti-epitope tag mAbs (anti-HA, anti-1D4, anti-FLAG, and anti-OLLAS) *(107, 110)*. These four beads were included to capture GPCRs or RAMPs that were engineered to contain an epitope-fusion tag (Figure 4-1). For controls, we used rabbit IgG, mouse IgG, and uncoupled beads. The final SBA comprised 70 unique Abs coupled to unique bead IDs, and pooling created the basis for the multiplex assay (Figure 4-3A).

Table 4-2. The specific Abs coupled to a unique bead ID. Also included are the source of the Ab, and product code. The labels in bold correspond to secretin-like GPCRs. Underlined product codes indicate validated Abs.

Bead ID	Protein Name	Antibody Source	Product Code
61	**GLP2R**	HPA	HPA027929
72	**VIPR1**	HPA	HPA046516
73	**CRHR2**	HPA	HPA046683
74	**ADCYAP1R1**	HPA	HPA030739
75	ACKR3	HPA	HPA049718
77	ACKR3	HPA	HPA032003
78	**CRHR1**	HPA	HPA063352
79	**GCGR**	HPA	HPA066333
80	**GIPR**	HPA	HPA068054
81	CXCR4	HPA	HPA068321
82	**GCGR**	HPA	HPA071228
83	CCR5	HPA	HPA070587
84	CXCR4	HPA	HPA051623
85	**CRHR1**	HPA	HPA055287
86	**CRHR1**	HPA	HPA071484
87	**CRHR2**	HPA	HPA073345
88	**ADCYAP1R1**	HPA	HPA073908
89	ACKR3	HPA	HPA057492
90	**GHRHR**	**HPA**	HPA077545
91	**VIPR2**	**HPA**	HPA062707
92	**GPR182**	**HPA**	HPA027037
93	**GCGR**	**HPA**	HPA057075
94	**CRHR1**	**HPA**	HPA046066
95	**GHRHR**	**HPA**	HPA070884
96	**GCGR**	**HPA**	HPA074345
293	**SCTR**	**HPA**	HPA007312
299	**PTH1R**	**HPA**	HPA007978
300	**PTH2R**	**HPA**	HPA010534
304	**CRHR1**	**HPA**	HPA032018
306	**GHRHR**	**HPA**	HPA034645
307	**GHRHR**	**HPA**	HPA034644
309	CXCR3	HPA	HPA045942
313	**CRHR1**	**HPA**	HPA052441
319	**GLP2R**	**HPA**	HPA064671
320	**GLP1R**	**HPA**	HPA065175
321	ADGRF5	HPA	HPA065251
325	**GHRHR**	HPA	HPA068576
326	ADGRF5	HPA	HPA068796
334	**PTH1R**	HPA	HPA075879
336	**GLP1R**	HPA	HPA077988
337	GPR182	HPA	HPA027037
343	Empty	N/A	N/A
339	**VIPR1**	HPA	HPA026777
349	RAMP2	HPA	HPA064452
350	rabbit IgG	Bethyl	P120
355	RAMP1	Abcam	ab156575
356	RAMP1	HPA	HPA010654
357	RAMP2	HPA	HPA052020
358	RAMP1	HPA	HPA057814
359	OLLAS	In house	N/A
360	FLAG	Sigma	F3165
361	RAMP1	RnD	AF6428
362	RAMP2	RnD	AF6427
363	RAMP3	RnD	AF4875
364	RAMP1	Santa	sc-11379
365	mouse	Bio Rad	PMP01X
366	1D4	In house	N/A
367	HA	Biolegend	16B12
373	CXCR3	HPA	HPA003189
374	**SCTR**	HPA	HPA007269
375	**PTH1R**	HPA	HPA007491
376	**CALCRL**	HPA	HPA007586
377	**VIPR1**	HPA	HPA007588
378	**CALCRL**	HPA	HPA008070
379	**PTH1R**	HPA	HPA007978
380	**PTH2R**	HPA	HPA010534
381	**PTH2R**	HPA	HPA010655
382	**GIPR**	HPA	HPA017428
383	GPR4	HPA	HPA019207
384	CXCR4	HPA	HPA027832

Each of the three epitope-tagged RAMP constructs was expressed in HEK293F cells alone or coexpressed with each of the 23 epitope-tagged GPCR constructs. Following transfection, each cell preparation was solubilized in a dodecyl maltoside detergent solution to create a heterogeneous micelle mixture of RAMPs, GPCRs and GPCR-RAMP complexes, in addition to other cellular protein components (Figure 4-3A). This strategy created a set of 73 unique lysates cotransfected with each combination of the RAMPs and 23 GPCRs, plus three RAMP controls, and empty-vector, or mock, transfected controls.

Next, we distributed each lysate in duplicate into 96-well plates and added aliquots of the pooled SBA to each well. Four replicate plates were processed in parallel, one for each detection mAb. For detection of the proteins or protein complexes bound to the beads, each plate was then incubated with a different anti-epitope tag detection mAb (a PE-conjugated version of either anti-HA, anti-FLAG, anti-1D4 or anti-OLLAS) (Figure 4-1). The fluorescence from the PE-conjugated detection mAbs was measured by a flow cytometer (Luminex FlexMap 3D) and matched to the bar-code of each bead. The SBA strategy allowed us to evaluate protein expression, Ab specificity, and GPCR-RAMP complex formation in a single experiment (Figure 4-3B).

Figure 4-3. Schematic of SBA procedure. **(A)** Unique Abs were coupled to different bar-coded beads to create an SBA with 70 distinct populations of capture beads, and the beads were subsequently pooled. DNA constructs encoding each of three epitope-tagged RAMPs and 23 epitope-tagged GPCRs were cotransfected in HEK293F cells such that all possible combinations of GRCPs and RAMPs were represented. The cells were solubilized in a detergent solution, which resulted in heterogeneous mixtures of solubilized proteins, including the RAMPs, GPCRs, and putative GPCR-RAMP complexes. An aliquot of each cell lysate was incubated with an aliquot of SBA. Four identical assay plates were prepared in this manner. Following wash steps, a different PE-conjugated anti-epitope tag detection mAb was added to each of the four plates. **(B)** A Luminex 3D FlexMap instrument was used to measure the reporter fluorescence produced by the PE-conjugated detection mAb while simultaneously reading the bar-code of each individual bead. From a single well, the specificity of RAMP Abs and GPCR Abs could be determined. Simultaneously, GPCR-RAMP complexes could be captured using either anti-epitope tag Abs, anti-GPCR Abs, or anti-RAMP Abs

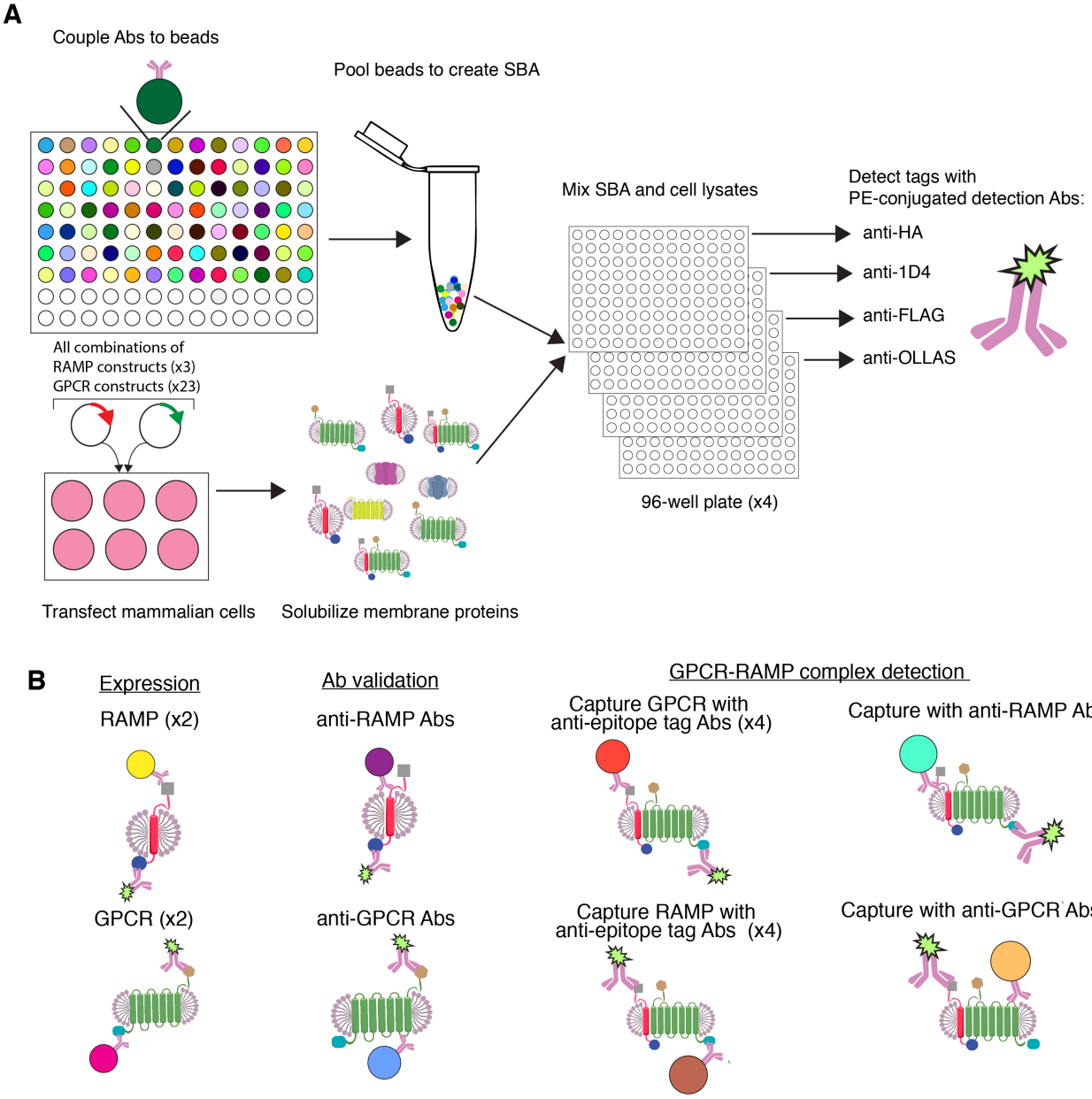
A
Couple Abs to beads
Pool beads to create SBA
Mix SBA and cell lysates
Detect tags with
PE-conjugated detection Abs:
anti-HA
anti-1D4
anti-FLAG
anti-OLLAS
All combinations of
RAMP constructs (x3)
GPCR constructs (x23)
96-well plate (x4)
Transfect mammalian cells
Solubilize membrane proteins
B
Expression
RAMP (x2)
GPCR (x2)
Ab validation
anti-RAMP Abs
anti-GPCR Abs
GPCR-RAMP complex detection
Capture GPCR with
anti-epitope tag Abs (x4)
Capture with anti-RAMP Abs
Capture RAMP with
anti-epitope tag Abs (x4)
Capture with anti-GPCR Abs

4.3.2 Capture and detection of RAMPs and GPCRs using anti-epitope tag mAbs.

We first determined that the epitope-tagged GPCRs and RAMPs could be captured and detected by mAbs targeting the epitope tags. Expression of each dual-epitope tagged RAMP was demonstrated by capture with one of the anti-epitope tag mAb beads (OLLAS or FLAG) and detection with the PE-conjugated version of the other anti-epitope tag mAb (OLLAS or FLAG) (Figure 4-4A and B). Similarly, expression of each dual-epitope tagged GPCR was demonstrated by capture and subsequent detection with the anti-1D4 and anti-HA mAbs (Figure 4-4C and D).

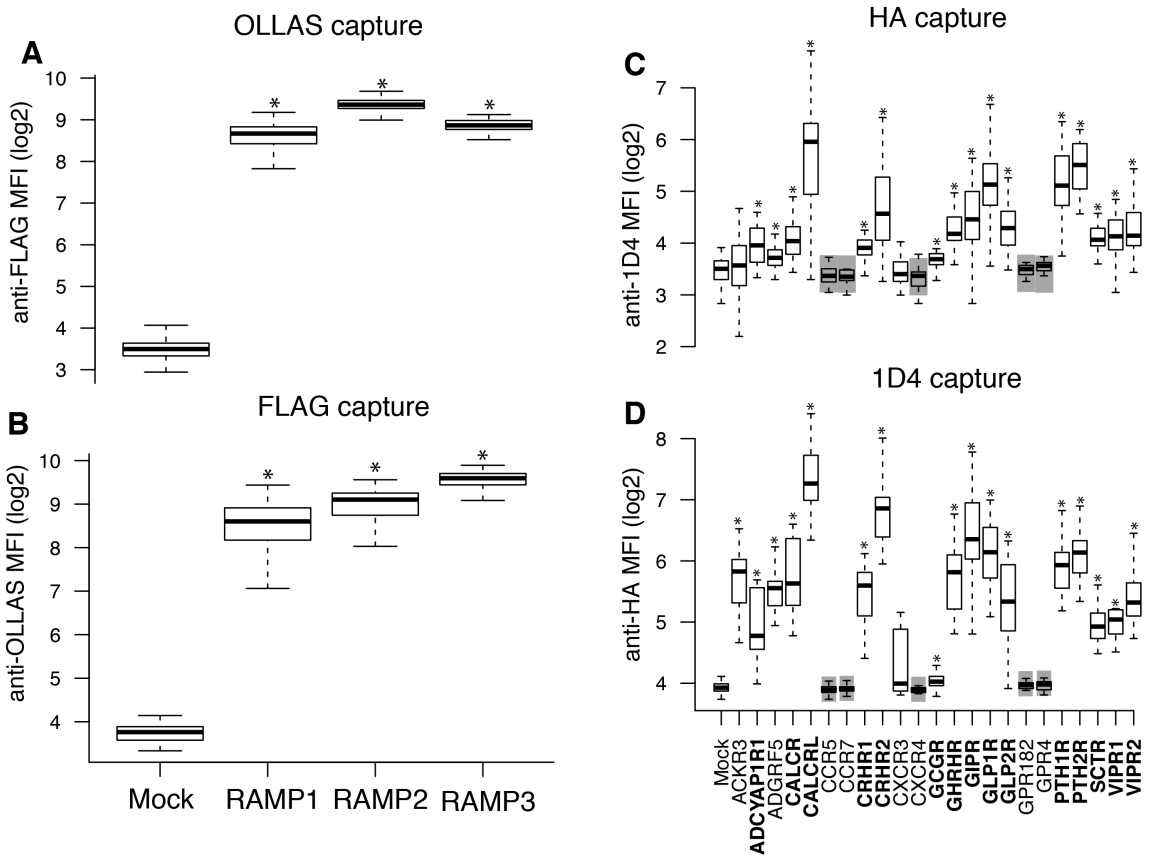

Figure 4-4. Validation of epitope tag mAbs to capture and detect RAMPs and GPCRs. Lysates from cells transfected with each epitope-tagged RAMP construct (FLAG and OLLAS) were incubated with the SBA, which included mAbs targeting FLAG or OLLAS. Each RAMP was **(A)** captured with anti-OLLAS mAb beads and detected with PE-conjugated anti-FLAG mAb or **(B)** captured with anti-FLAG mAb beads and detected with a PE-conjugated anti-OLLAS mAb. Lysates from cells transfected with each epitope-tagged GPCR construct (HA and/or 1D4) were incubated with the SBA, which included mAbs targeting HA or 1D4. Each GPCR was **(C)** captured with anti-HA mAb beads and detected with a PE-conjugated anti-1D4 mAb, or **(D)** captured with anti-1D4 mAb beads and detected with a PE-conjugated anti-HA mAb. Grey boxes around the occasional data set indicate that the GPCR does not have both engineered epitope tags, and thus would not be expected to show signal in this experiment. The labels in

bold correspond to secretin-like GPCRs. Data is median fluorescence intensity (MFI) and representative of at least nine experiments performed in duplicate.

4.3.3 Capture and detection of GPCR-RAMP complexes using anti-epitope tag mAbs

Having validated that both GPCRs and RAMPs can be captured with one of the anti-epitope tag beads and detected with one of four PE-conjugated, anti-epitope tag mAbs, it follows that we should also be able to detect GPCR-RAMP complexes that were captured by the Abs of the SBA. In the basic experimental setup using epitope tag mAbs, there are eight possible capture-detection mAb pairs that can be used to capture or detect either a RAMP or a GPCR in a given GPCR-RAMP complex: 1D4-FLAG, 1D4-OLLAS, HA-FLAG, HA-OLLAS, FLAG-1D4, FLAG-HA, OLLAS-1D4 and OLLAS-HA (Figure 4-5). For single epitope-tagged GPCRs, four capture-detection mAb pairs could be used to detect a GPCR-RAMP complex. Several GPCRs formed complexes with one or more of the RAMPs, including CALCRL. CALCRL has previously been shown to create a stable complex which each RAMP *(111)*. The significance of the detection signal for the complex depended on the capture-detection Ab pair used (Table 4-3).

Figure 4-5. Capture and detection of GPCR-RAMP complexes using anti-epitope tag mAbs. Lysates from cells transfected with each epitope-tagged RAMP construct and cotransfected with each epitope-tagged GPCR construct were incubated with the SBA, which included beads that were conjugated to mAbs targeting the four tags. Complexes were captured in multiplex fashion using one of the four mAbs. There are eight possible capture-detection schemes. The GPCR is captured using anti-1D4 mAb, and the GPCR-RAMP complex is detected using **(A)** PE-conjugated FLAG mAb or **(B)** PE-conjugated anti-OLLAS mAb. The GPCR is also captured using anti-HA mAb, and the GPCR-RAMP complex is detected using **(C)** PE-conjugated anti-FLAG mAb or **(D)** PE-conjugated anti-OLLAS mAb. The RAMP is captured using anti-FLAG mAb, and the GPCR-RAMP complex is detected using **(E)** PE-conjugated 1D4 mAb or **(F)** PE-conjugated anti-HA mAb. The RAMP is also captured using anti-OLLAS mAb, and the GPCR-RAMP complex is detected using **(G)** PE-conjugated 1D4 mAb or **(H)** PE-conjugated anti-HA mAb. Data are presented for each of the three RAMPs. GPCR names are listed at the bottom of each RAMP panel, and the boxes are color-coded. The occasional grey box indicates that the GPCR did not have the appropriate epitope tag to be captured or detected. The labels in bold correspond to secretin-like GPCRs.

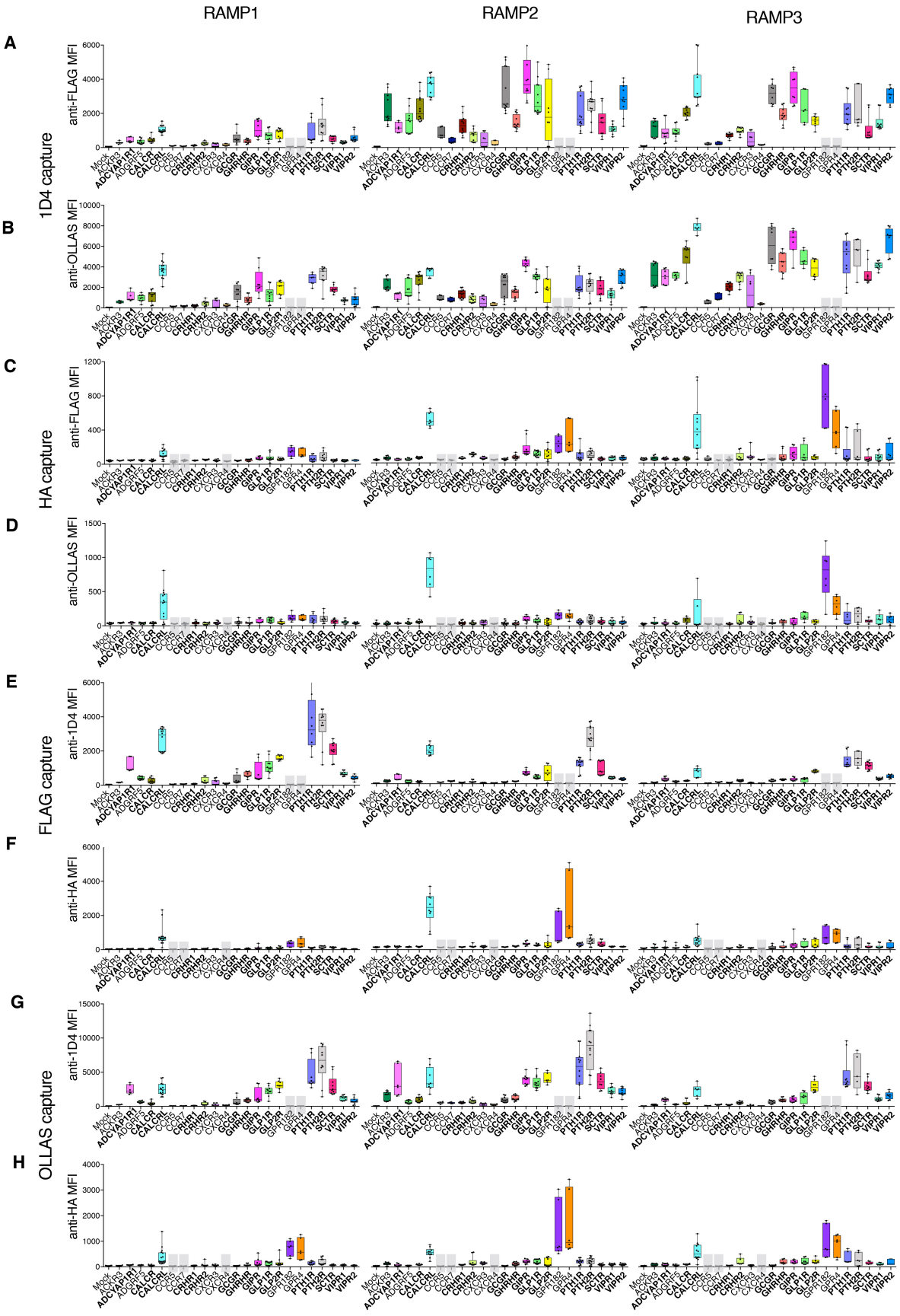
RAMP1
RAMP2
RAMP3
A
B
C
D
E
F
G
H
1D4 capture
HA capture
FLAG capture
OLLAS capture
anti-FLAG MFI
anti-OLLAS MFI
anti-1D4 MFI
anti-HA MFI

Table 4-3. Statistical significances of complex formation between each GPCR and RAMP complex pair reported as p-values. The data sets are from GPCR-RAMP complexes capture and detected by mAbs targeting epitope tags on the GPCR and RAMP constructs (Figure 4-5). Statistical significance of signal between mock transfected cell lysates and lysates from cells co-transfected with each dual-tagged RAMP construct plus each dual or single-tagged GPCR construct (Ordinary one-way ANOVA, Dunnett's multiple comparisons test). N/A indicates that the GPCR does not have the epitope tag to be captured or detected with the corresponding Ab. Secretin-like receptors are shown in bold.

	Interaction with RAMP1							
Capture Ab	1D4	1D4	HA	HA	OLLAS	OLLAS	FLAG	FLAG
Detection Ab	FLAG	OLLAS	FLAG	OLLAS	1D4	HA	1D4	HA
ACKR3	0.8796	0.8534	0.9999	0.9998	0.9994	0.9999	0.9993	0.9999
ADCYAP1R1	0.2328	0.0423	0.9998	0.9996	0.0002	0.9998	0.0001	0.9994
ADGRF5	0.4556	0.0370	0.9999	0.9999	0.6631	0.9998	0.5635	0.9995
CALCR	0.1073	0.0054	0.9999	0.9999	0.9835	0.9998	0.9363	0.9997
CALCRL	0.0001	0.0001	0.0001	0.0001	0.0001	0.0001	0.0001	0.0001
CCR5	0.9996	0.9996	N/A	N/A	0.9999	N/A	0.9999	N/A
CCR7	0.9998	0.9995	N/A	N/A	0.9999	N/A	0.9999	N/A
CRHR1	0.9994	0.9993	0.9999	0.9998	0.9998	0.9999	0.9998	0.9998
CRHR2	0.9457	0.8771	0.9992	0.9999	0.9883	0.9997	0.9936	0.9990
CXCR3	0.9993	0.9854	N/A	N/A	0.9993	N/A	0.9994	N/A
CXCR4	0.9991	0.9991	N/A	N/A	0.9997	N/A	0.9997	N/A
GCGR	0.0238	0.0001	0.9999	0.9993	0.8747	0.9999	0.4756	0.9999
GHRHR	0.3372	0.1207	0.9994	0.9996	0.1304	0.9996	0.1245	0.9993
GIPR	0.0001	0.0001	0.6682	0.9957	0.0382	0.9946	0.0006	0.5220
GLP1R	0.0018	0.0001	0.0613	0.4153	0.0001	0.9956	0.0001	0.6313
GLP2R	0.0001	0.0001	0.9884	0.9995	0.0001	0.9956	0.0001	0.4058
GPR182	N/A	N/A	0.0001	0.1198	N/A	0.0390	N/A	0.0001
GPR4	N/A	N/A	0.0001	0.2359	N/A	0.0056	N/A	0.0001
PTH1R	0.0001	0.0001	0.8781	0.5164	0.0001	0.9988	0.0001	0.8046
PTH2R	0.0001	0.0001	0.0054	0.0423	0.0001	0.8586	0.0001	0.0933
SCTR	0.0358	0.0001	0.9999	0.9994	0.0001	0.9869	0.0001	0.9994
VIPR1	0.6674	0.2842	0.9999	0.9991	0.0717	0.9997	0.0142	0.9994
VIPR2	0.0038	0.0508	0.9994	0.9999	0.5351	0.9999	0.1127	0.9997

	Interaction with RAMP2							
Capture Ab	1D4	1D4	HA	HA	OLLAS	OLLAS	FLAG	FLAG
Detection Ab	FLAG	OLLAS	FLAG	OLLAS	1D4	HA	1D4	HA
ACKR3	0.0001	0.0001	0.9940	0.9999	0.6094	0.9999	0.0186	0.9991
ADCYAP1R1	0.0288	0.0117	0.9999	0.9997	0.0044	0.9998	0.0001	0.9997
ADGRF5	0.0001	0.0001	0.9997	0.9993	0.9029	0.9999	0.9181	0.9999
CALCR	0.0001	0.0001	0.9732	0.9867	0.9442	0.9998	0.2488	0.9994
CALCRL	0.0001	0.0001	0.0001	0.0001	0.0001	0.0001	0.0001	0.0001
CCR5	0.2940	0.1073	N/A	N/A	0.9988	N/A	0.9944	N/A
CCR7	0.9939	0.3372	N/A	N/A	0.8242	N/A	0.9989	N/A
CRHR1	0.0002	0.0001	0.9947	0.5879	0.9990	0.9999	0.9654	0.9995
CRHR2	0.3328	0.0709	0.0342	0.9997	0.8729	0.9988	0.7280	0.9397
CXCR3	0.9939	0.8620	N/A	N/A	0.9997	N/A	0.9994	N/A
CXCR4	0.9993	0.9988	N/A	N/A	0.9997	N/A	0.9996	N/A
GCGR	0.0001	0.0001	0.9997	0.9995	0.9947	0.9999	0.2862	0.9999
GHRHR	0.0001	0.0001	0.6943	0.9999	0.7817	0.9997	0.0839	0.9988
GIPR	0.0001	0.0001	0.0001	0.0341	0.0001	0.7177	0.0001	0.1563
GLP1R	0.0001	0.0001	0.0064	0.6186	0.0001	0.9992	0.0001	0.9128
GLP2R	0.0001	0.0001	0.0165	0.9859	0.0001	0.9990	0.0001	0.9935
GPR182	N/A	N/A	0.0001	0.0001	N/A	0.0197	N/A	0.0001
GPR4	N/A	N/A	0.0001	0.0006	N/A	0.0001	N/A	0.0001
PTH1R	0.0001	0.0001	0.3975	0.9935	0.0001	0.9988	0.0001	0.6975
PTH2R	0.0001	0.0001	0.0165	0.0572	0.0001	0.5891	0.0001	0.6220
SCTR	0.0001	0.0001	0.9994	0.8982	0.0001	0.9949	0.0001	0.9994
VIPR1	0.0091	0.0001	0.9989	0.9886	0.0010	0.9998	0.0001	0.9993
VIPR2	0.0001	0.0001	0.9872	0.9741	0.0433	0.9998	0.0004	0.9993

	Interaction with RAMP3							
Capture Ab	1D4	1D4	HA	HA	OLLAS	OLLAS	FLAG	FLAG
Detection Ab	FLAG	OLLAS	FLAG	OLLAS	1D4	HA	1D4	HA
ACKR3	0.0080	0.0001	0.9998	0.9995	0.9993	0.9988	0.9996	0.9993
ADCYAP1R1	0.0355	0.0001	0.9999	0.9997	0.0017	0.9868	0.1854	0.9994
ADGRF5	0.0151	0.0001	0.9999	0.9998	0.7451	0.9988	0.9991	0.9997
CALCR	0.0001	0.0001	0.9998	0.9853	0.2823	0.9947	0.8329	0.9993
CALCRL	0.0001	0.0001	0.0001	0.0749	0.0001	0.0001	0.0001	0.0001
CCR5	0.9994	0.9938	N/A	N/A	0.9998	0.9999	N/A	N/A
CCR7	0.9993	0.4219	N/A	N/A	0.9878	0.9999	N/A	N/A
CRHR1	0.2018	0.0001	0.9999	0.9999	0.9991	0.9998	0.9994	0.9998
CRHR2	0.0221	0.0001	0.9993	0.9830	0.1470	0.9938	0.8527	0.7529
CXCR3	0.8261	0.0015	N/A	N/A	0.9997	N/A	0.9998	N/A
CXCR4	0.9996	0.9991	N/A	N/A	0.9999	N/A	0.9999	N/A
GCGR	0.0001	0.0001	0.9999	0.9999	0.6740	0.9948	0.8946	0.9998
GHRHR	0.0001	0.0001	0.9990	0.9992	0.0284	0.7504	0.2015	0.8697
GIPR	0.0001	0.0001	0.9821	0.9991	0.0053	0.0290	0.1588	0.0120
GLP1R	0.0001	0.0001	0.9853	0.8632	0.0722	0.2798	0.0539	0.5420
GLP2R	0.0001	0.0001	0.9996	0.9991	0.0001	0.0290	0.0001	0.7387
GPR182	N/A	N/A	0.0001	0.0001	N/A	0.0001	N/A	0.0001
GPR4	N/A	N/A	0.0001	0.0001	N/A	0.0001	N/A	0.0001
PTH1R	0.0001	0.0001	0.5993	0.6640	0.0001	0.1738	0.0001	0.0915
PTH2R	0.0001	0.0001	0.2537	0.0302	0.0001	0.0162	0.0001	0.0531
SCTR	0.0013	0.0001	0.9994	0.9952	0.0001	0.8881	0.0001	0.9936
VIPR1	0.0001	0.0001	0.9996	0.8788	0.0015	0.8429	0.0544	0.9991
VIPR2	0.0001	0.0001	0.9562	0.9378	0.0001	0.7792	0.0044	0.9685

We calculated an overall statistic for the significance of each GPCR-RAMP complex pair to combine the significances of interaction for each of the eight capture and detection pairs (Table 4-4). First, the statistical significances from the data presented in Figure 4-5 were calculated (Table 4-3). An ordinary one-way ANOVA, with Dunnett's multiple comparison's test was used to compare signal between mock transfected cell lysates and cell lysates cotransfected with each RAMP or GPCR construct. Resulting P-values of <0.0001 were assigned 4, <0.001 a 3, <0.01 a 2, and <0.05 a 1. The values were summed and divided by the number of capture and detection pairs that we expected to be capable of measuring the relevant complex. For dual-tagged GPCRs, we divided by eight and for single-tagged GPCRs we divided by four to obtain a normalized value.

Table 4-4. Overall statistic for GPCR-RAMP complex formation. P-values are presented in Table 4-3. P-values <0.0001 were assigned 4, <0.001 a 3, <0.01 a 2, and <0.05 a 1. The values were summed and divided by the number of capture and detection pairs that we expected to be capable of measuring the relevant complex. For dual-tagged GPCRs, we divided by eight and for single-tagged GPCRs we divided by four to obtain a normalized value. Secretin-like receptors are shown in bold. * indicates that the complex formation was confirmed by PLA and † that complex formation was not confirmed by PLA (Figure 4-14).

	RAMP1	RAMP2	RAMP3	Previously published RAMP interaction
ACKR3	0	1.125	0.75	Unknown
ADCYAP1R1	1	0.75	0.75	Unknown
ADGRF5	0.125	0.875	0.625	Unknown
CALCR	0.25	1	1	RAMP1, 2 and 3 *(41)*
CALCRL	4	4*	3.5	RAMP1, 2 and 3 *(44, 45)*
CCR5	0	0	0	Unknown
CCR7	0	0	0	Unknown
CRHR1	0	0.625	0.375	RAMP2 *(53, 55)*
CRHR2	0	0	0.75	None *(53)*
CXCR3	0	0†	0.25	Unknown
CXCR4	0	0	0	Unknown
GCGR	0.625	1	2	Unknown
GHRHR	0	2	1.125	RAMP2 *(50, 51, 54)*
GIPR	1.125	2.375	1.125	None *(54)*
GLP1R	1.75	1.875	1.25	None *(50, 54, 55)*
GLP2R	2	2	2	None *(54)*
GPR182	2.25	2.25*	4	Unknown
GPR4	2.5	3.25*	4	Unknown
PTH1R	2	2*	2.125	RAMP2 *(54)*
PTH2R	2.25	2	2.125	RAMP3 *(54)*
SCTR	1.625	2	1.75	RAMP3 *(56)*
VIPR1	0	1.125	1.25	RAMP1, 2 and 3 *(54)*
VIPR2	0.25	1.25	1.625	RAMP1, 2, and 3 *(55)*

4.3.4 Validation of Abs targeting RAMPs and GPCRs

My next aim was to validate the SBA approach as a method to identify GPCR-RAMP interactions without having to rely upon the use of epitope tags engineered onto both the GPCR and the RAMP. Thus, I needed to assess the available protein-specific Abs to each GPCR and each RAMP, which were obtained from either commercial sources or HPA. In order to validate the utility of each anti-RAMP Ab, the cell lysates containing epitope-tagged RAMPs were incubated with the SBA, which included nine anti-RAMP Abs. The captured RAMPs were detected using the PE-conjugated OLLAS and PE-conjugated FLAG mAbs. I found that five out of the nine HPA and commercial anti-RAMP Abs (56%) selectively captured their intended RAMP. In addition, each anti-RAMP Ab showed little cross-reactivity with the other two non-targeted RAMPs (Figure 4-6). Validated Abs are underlined in Table 4-2.

Figure 4-6. Validation of Abs used to capture RAMPs. In order to validate anti-RAMP Abs, lysates from cells transfected with each epitope-tagged RAMP construct (FLAG and OLLAS) were incubated with the SBA, which included beads conjugated with nine capture Abs targeting the three RAMPs. **(A)** PE-conjugated anti-FLAG and **(B)** PE-conjugated anti-OLLAS mAbs were used to detect any RAMPs captured by the beads. Data are median fluorescence intensity (MFI) and represent at least 200 experiments, each performed in duplicate. At a statistical significance of $p \leq 0.05$ (Kruskal-Wallis ANOVA), we validated at least one capture Ab for each of the three RAMPs (a total of 5 RAMP capture Abs). Validated Abs are underlined. Bead ID numbers are listed after each RAMP name and the corresponding Ab name is provided in Table 4-2.

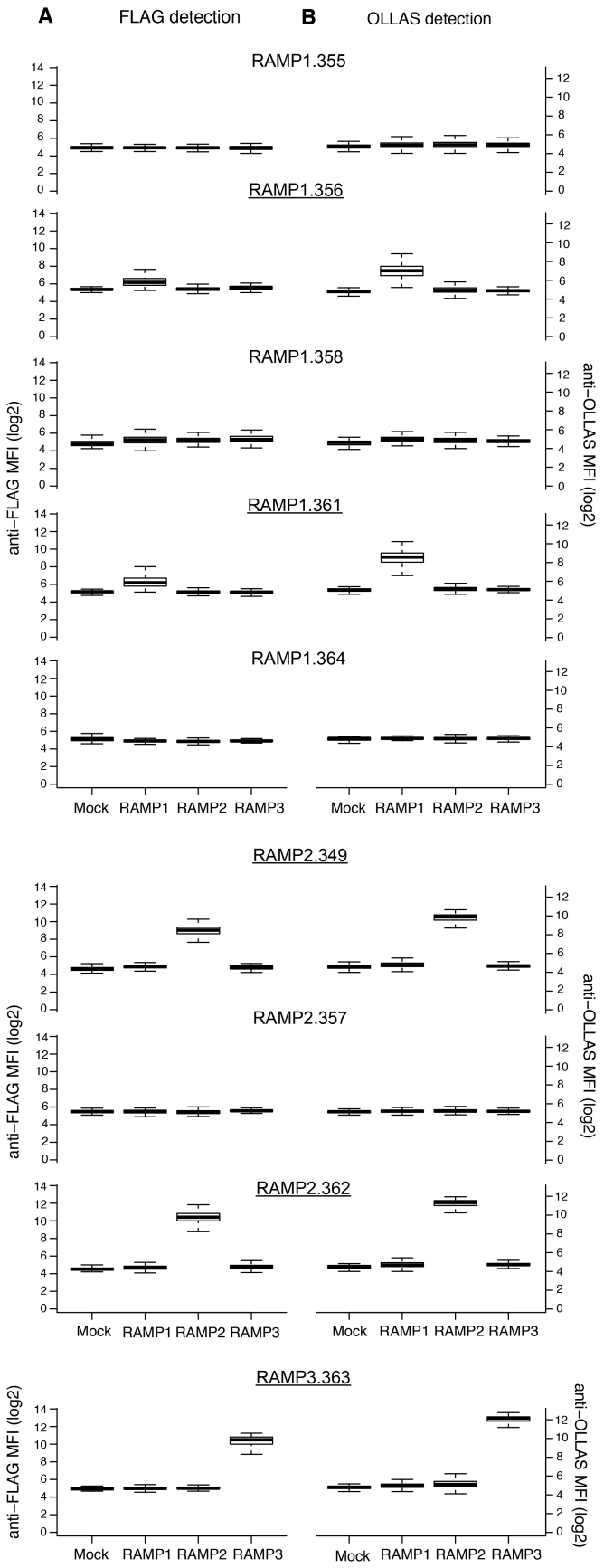
A
FLAG detection
B
OLLAS detection
RAMP1.355
RAMP1.356
RAMP1.358
RAMP1.361
RAMP1.364
RAMP2.349
RAMP2.357
RAMP2.362
RAMP3.363
anti–FLAG MFI (log2)
anti–OLLAS MFI (log2)
Mock
RAMP1
RAMP2
RAMP3

In parallel, the collection of anti-GPCR Abs was validated for GPCR capture using cell lysates containing the 23 epitope-tagged GPCRs. In this case, the detection mAbs used were anti-1D4 and anti-HA. When using either PE-conjugated anti-1D4 or PE-conjugated anti-HA as the detection mAb, 31 out of the 55 anti-GPCR Abs (~56%) tested captured their intended GPCR targets (Figure 4-7). Overall, I found that the anti-HA mAb was not as sensitive to detect GPCRs as the anti-1D4 detection mAb. To judge the ability of an Ab to capture its intended GPCR target, I used a Z-score cutoff of 1.645 (corresponding to the 95% confidence interval of a single-tailed Z-test). I found that at least one HPA Ab for 19 of the 21 GPCRs (90%) included in this study, and with HPA Abs available, fulfilled the criteria (Table 4-2).

Figure 4-7. Validation of Abs used to capture GPCRs. In order to validate anti-GPCR Abs, lysates from cells transfected with each epitope-tagged GPCR construct (HA and/or 1D4) were incubated with the SBA, which included beads conjugated with 55 Abs targeting 21 GPCRs. **(A)** PE-conjugated anti-HA or **(B)** PE-conjugated anti-1D4 were used to detect any GPCRs captured by the beads. GPCRs are shown in alphabetical order and the labels in bold correspond to secretin-like GPCRs. Each dot in each bee-swam plot represents a data point from one experiment. The blue dots indicate signal from lysates containing the intended GPCR target, while grey dots indicate signal from lysates containing an of the other epitope-tagged GPCR targets. Data are median fluorescence intensity (MFI) and representative of at least 200 experiments, each performed in duplicate. The occasional grey box indicates that the GPCR did not have the appropriate epitope tag to be captured or detected. At a statistical significance of $p \leq 0.05$ we validated a total of 31 capture Abs, with at least one capture Ab for 19 of the 21 GPCRs studied. Validated Abs are underlined. Bead ID numbers are listed after each GPCR name and the corresponding Ab name is provided in Table 4-2.

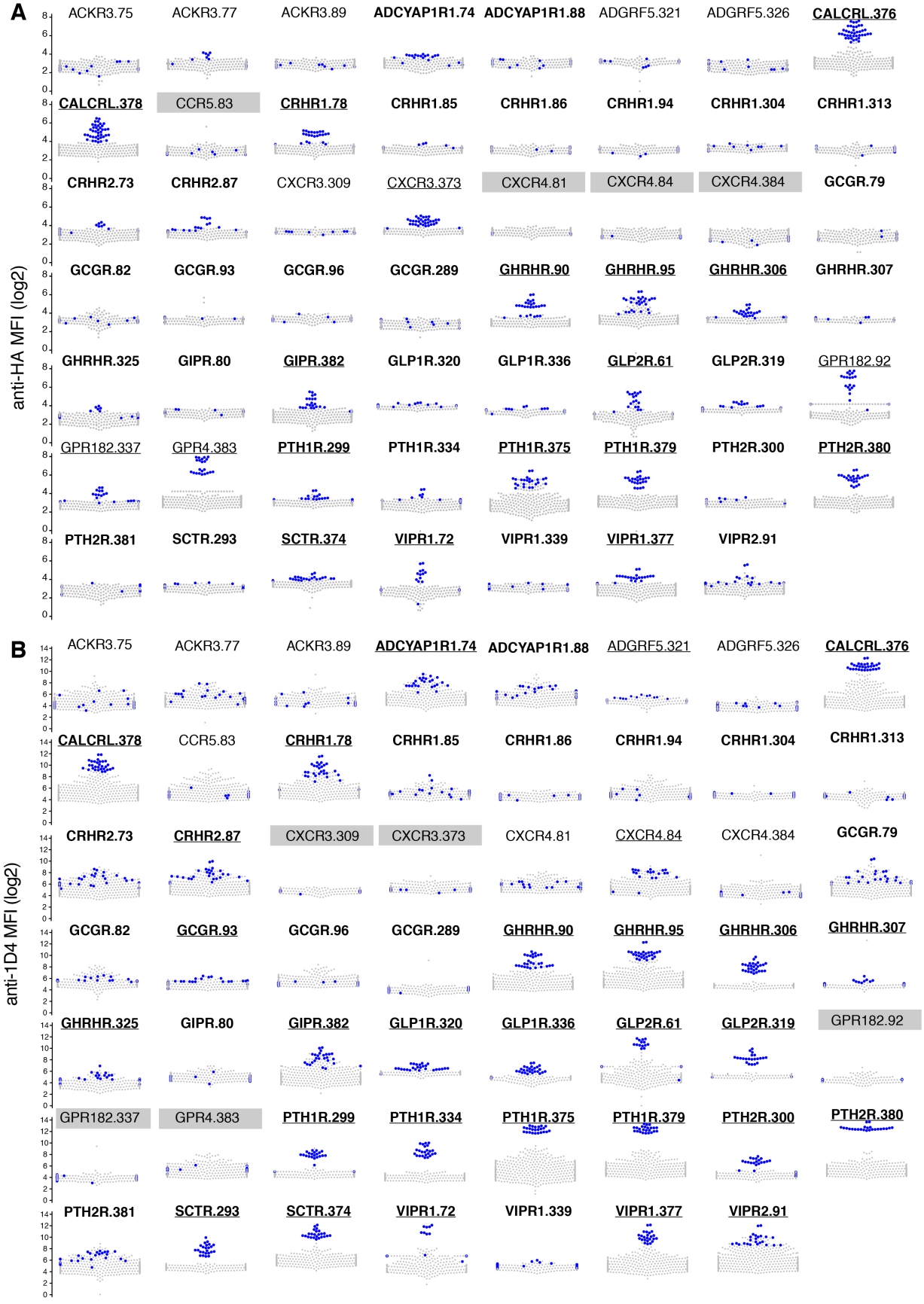
A
anti-HA MFI (log2)
ACKR3.75
ACKR3.77
ACKR3.89
ADCYAP1R1.74
ADCYAP1R1.88
ADGRF5.321
ADGRF5.326
CALCRL.376
CALCRL.378
CCR5.83
CRHR1.78
CRHR1.85
CRHR1.86
CRHR1.94
CRHR1.304
CRHR1.313
CRHR2.73
CRHR2.87
CXCR3.309
CXCR3.373
CXCR4.81
CXCR4.84
CXCR4.384
GCGR.79
GCGR.82
GCGR.93
GCGR.96
GCGR.289
GHRHR.90
GHRHR.95
GHRHR.306
GHRHR.307
GHRHR.325
GIPR.80
GIPR.382
GLP1R.320
GLP1R.336
GLP2R.61
GLP2R.319
GPR182.92
GPR182.337
GPR4.383
PTH1R.299
PTH1R.334
PTH1R.375
PTH1R.379
PTH2R.300
PTH2R.380
PTH2R.381
SCTR.293
SCTR.374
VIPR1.72
VIPR1.339
VIPR1.377
VIPR2.91
B
anti-1D4 MFI (log2)
ACKR3.75
ACKR3.77
ACKR3.89
ADCYAP1R1.74
ADCYAP1R1.88
ADGRF5.321
ADGRF5.326
CALCRL.376
CALCRL.378
CCR5.83
CRHR1.78
CRHR1.85
CRHR1.86
CRHR1.94
CRHR1.304
CRHR1.313
CRHR2.73
CRHR2.87
CXCR3.309
CXCR3.373
CXCR4.81
CXCR4.84
CXCR4.384
GCGR.79
GCGR.82
GCGR.93
GCGR.96
GCGR.289
GHRHR.90
GHRHR.95
GHRHR.306
GHRHR.307
GHRHR.325
GIPR.80
GIPR.382
GLP1R.320
GLP1R.336
GLP2R.61
GLP2R.319
GPR182.92
GPR182.337
GPR4.383
PTH1R.299
PTH1R.334
PTH1R.375
PTH1R.379
PTH2R.300
PTH2R.380
PTH2R.381
SCTR.293
SCTR.374
VIPR1.72
VIPR1.339
VIPR1.377
VIPR2.91

In addition to validating Abs with high affinity to their intended target, the SBA also gives information on the cross-reactivity of the Abs to the other GPCRs included in this study. I found that none of the validated Abs demonstrated cross-reactivity (Figure 4-8).

Figure 4-8. Analysis of anti-GPCR Ab cross-reactivity. Lysates from cells transfected with each epitope-tagged GPCR construct (HA and 1D4) were incubated with the SBA, which included 55 Abs to 21 GPCRs. **(A)** PE-conjugated anti-1D4 and **(B)** PE-conjugated anti-HA were used to detect any GPCRs captured by the beads. The occasional grey boxes indicate that the GPCR did not have the appropriate epitope tag to be detected. The labels in bold correspond to secretin-like GPCRs and validated Abs are underlined. Heatmaps represent the z-scores of median fluorescence intensity (MFI) and indicates the ability of the GPCR Abs to capture each of the 23 GPCRs used in the study. Data represents the median z-score of at least three experiments performed in duplicate. Bead ID numbers are listed after each GPCR name and the corresponding Ab name is provided in Table 4-2.

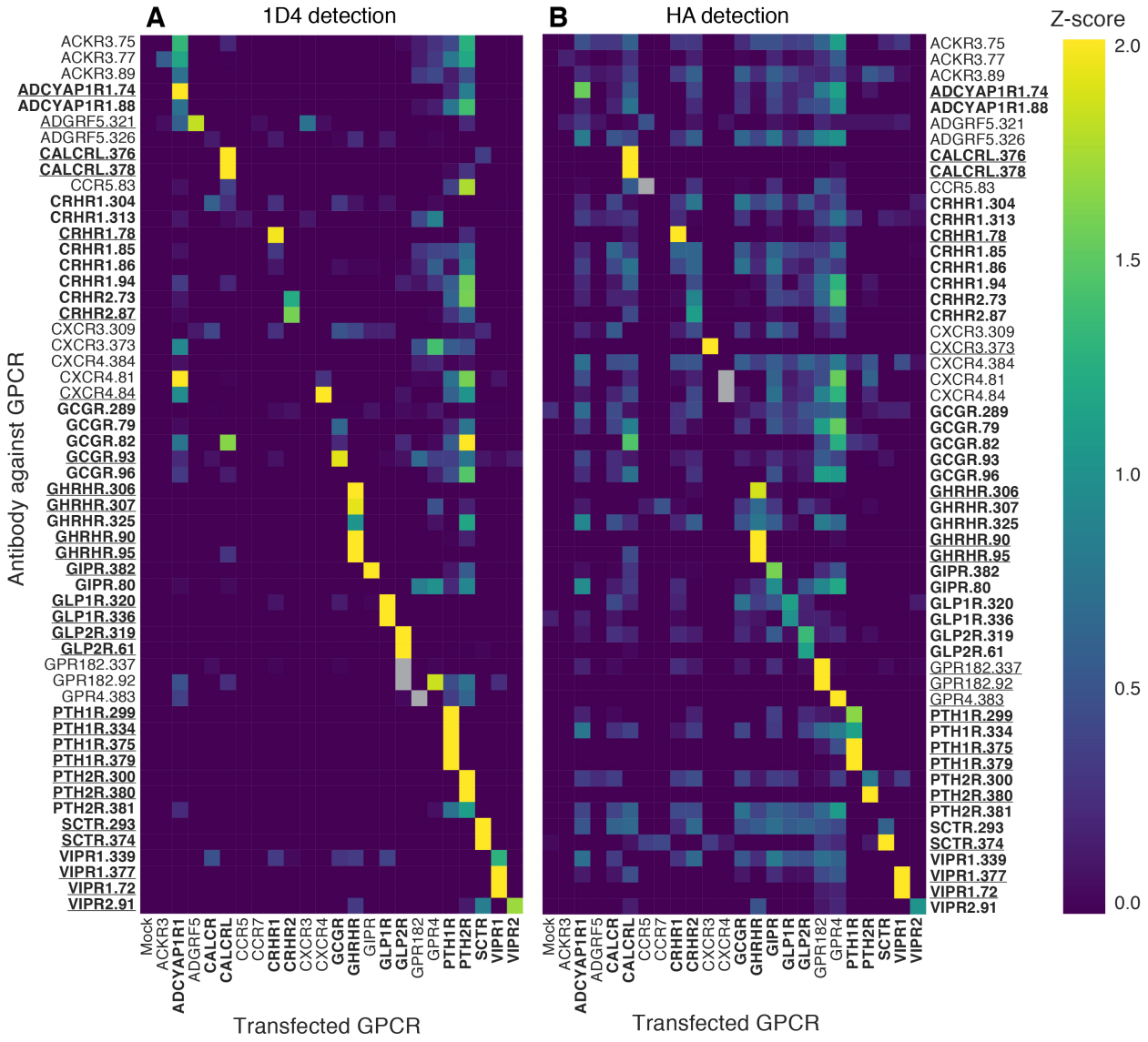
A
1D4 detection
B
HA detection
Z-score
2.0
1.5
1.0
0.5
0.0
Antibody against GPCR
ACKR3.75
ACKR3.77
ACKR3.89
ADCYAP1R1.74
ADCYAP1R1.88
ADGRF5.321
ADGRF5.326
CALCRL.376
CALCRL.378
CCR5.83
CRHR1.304
CRHR1.313
CRHR1.78
CRHR1.85
CRHR1.86
CRHR1.94
CRHR2.73
CRHR2.87
CXCR3.309
CXCR3.373
CXCR4.384
CXCR4.81
CXCR4.84
GCGR.289
GCGR.79
GCGR.82
GCGR.93
GCGR.96
GHRHR.306
GHRHR.307
GHRHR.325
GHRHR.90
GHRHR.95
GIPR.382
GIPR.80
GLP1R.320
GLP1R.336
GLP2R.319
GLP2R.61
GPR182.337
GPR182.92
GPR4.383
PTH1R.299
PTH1R.334
PTH1R.375
PTH1R.379
PTH2R.300
PTH2R.380
PTH2R.381
SCTR.293
SCTR.374
VIPR1.339
VIPR1.377
VIPR1.72
VIPR2.91
Mock
ACKR3
ADCYAP1R1
ADGRF5
CALCR
CALCRL
CCR5
CCR7
CRHR1
CRHR2
CXCR3
CXCR4
GCGR
GHRHR
GIPR
GLP1R
GLP2R
GPR182
GPR4
PTH1R
PTH2R
SCTR
VIPR1
VIPR2
Transfected GPCR
Transfected GPCR

4.3.5 GPCR-RAMP complexes captured by validated anti-GPCR Abs

Next, I explored the broader utility of using the anti-GPCR Abs to capture directly the GPCR-RAMP complexes. I examined the beads that were coupled to anti-GPCR Abs and measured signals arising from a bound RAMP using both PE-conjugated anti-FLAG and PE-conjugated anti-OLLAS mAbs (Figure 4-9). In this experimental design, GPCRs can be captured through their native sequence, ablating the need to create epitope-tagged constructs. With few exceptions (<0.05%) the majority of signals associated with complex capture using the anti-GPCR Abs that reached a Z-score ≥ 1.645 were obtained from lysates containing the target GPCR.

Figure 4-9. Detection of GPCR-RAMP complexes following capture by anti-GPCR Abs. Lysates from cells transfected with each epitope-tagged RAMP construct (FLAG and OLLAS) and cotransfected with each epitope-tagged GPCR construct (HA and 1D4) were incubated with the SBA, which included 55 Abs to 21 GPCRs included in this study. Complexes were captured in multiplex fashion using the anti-GPCR Ab beads. The presence of a GPCR-RAMP complex was detected using **(A)** PE-conjugated OLLAS mAb, or **(B)** PE-conjugated anti-FLAG mAb. The labels in bold correspond to secretin-like GPCRs and validated Abs are underlined. The heatmap displays the Z-score of median fluorescence intensity (MFI) and represents at least three experiments performed in duplicate. Bead ID numbers are listed after each GPCR name and the corresponding Ab name is provided in Table 4-2.

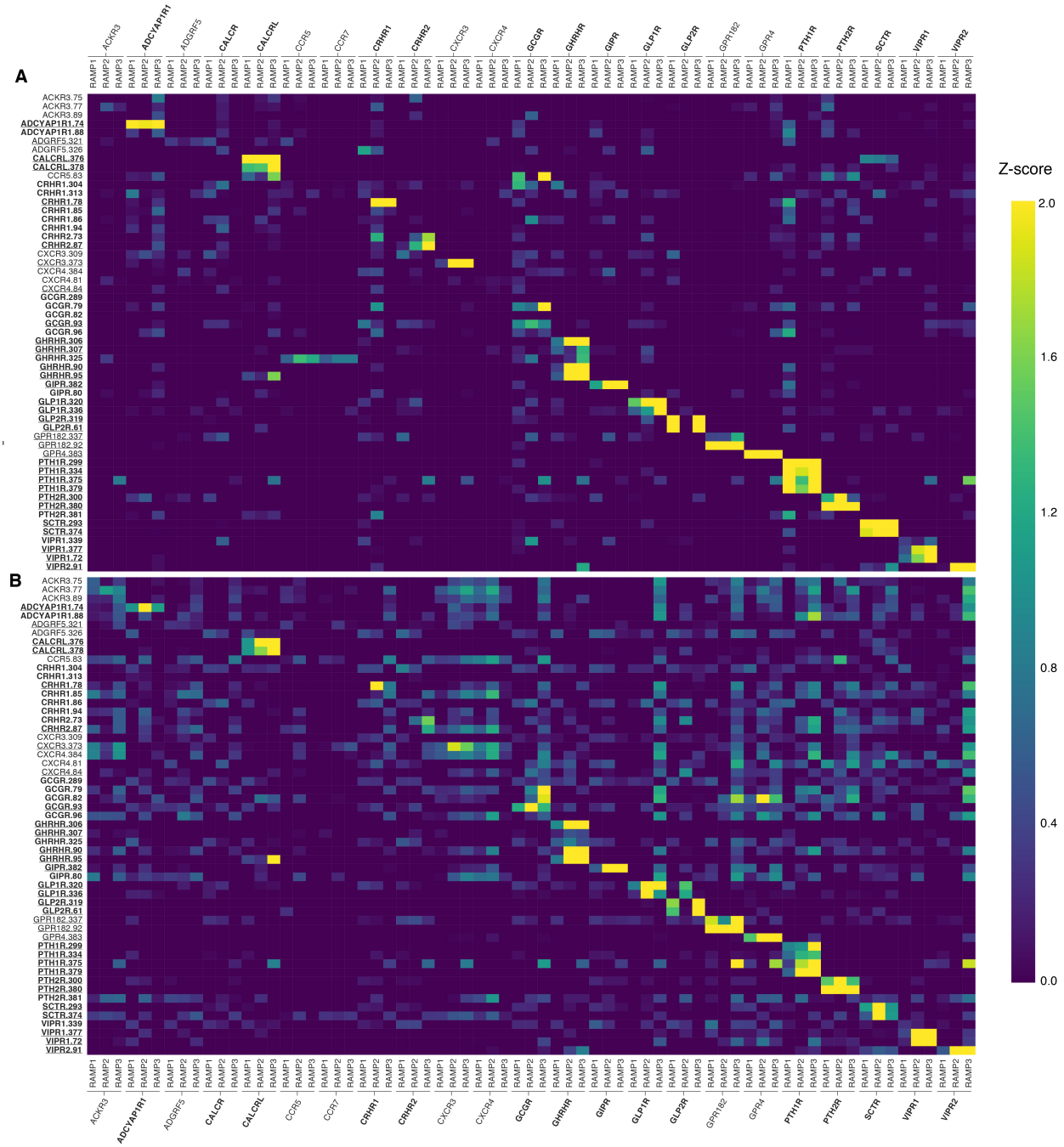
A
B
Z-score
2.0
1.6
1.2
0.8
0.4
0.0
ACKR3
ADCYAP1R1
ADGRF5
CALCR
CALCRL
CCR5
CCR7
CRHR1
CRHR2
CXCR3
CXCR4
GCGR
GHRHR
GIPR
GLP1R
GLP2R
GPR182
GPR4
PTH1R
PTH2R
SCTR
VIPR1
VIPR2
RAMP1
RAMP2
RAMP3

4.3.6 Statistical comparison of SBA data sets

I next determined whether the data obtained using anti-GPCR capture Abs recapitulated the results obtained with the epitope tag capture methods. I first converted the anti-GPCR data set (Figure 4-9) to a binary (0,1) matrix by using a Z-score threshold set to 1.645, which corresponds to a confidence interval of 95%, for a single-tailed test. I then created a hypothetical matrix of results based on the data set obtained from using epitope tags to capture GPCR-RAMP complexes and the overall statistic for GPCR-RAMP interaction from Table 4-4. For example, the two anti-CALCRL antibodies were assigned a 4 for interaction with RAMP1, RAMP2 and a 3.5 with RAMP3 but only with lysates coexpressing CALCRL and each RAMP (Figure 4-10).

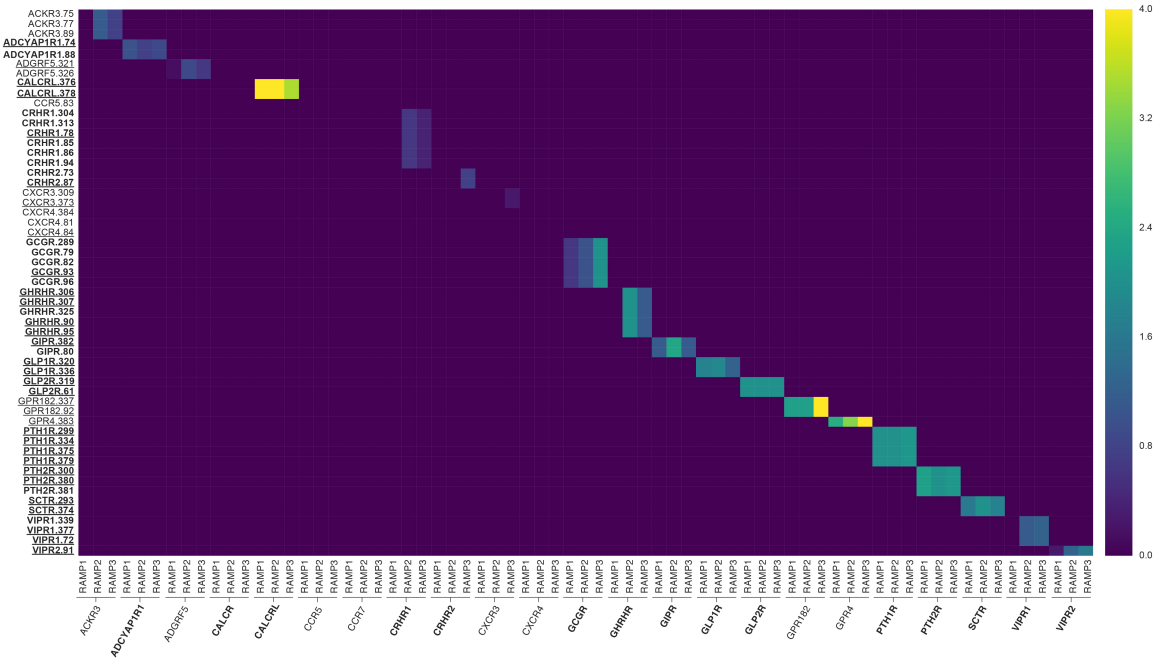

Figure 4-10. Hypothetical matrix of results for RAMP-GPCR heterocomplexes captured by GPCR Abs based on data from epitope tag capture and detection. Lysates from cells transfected with each epitope-tagged RAMP construct (FLAG and OLLAS) and cotransfected with each epitope-tagged GPCR construct (HA and 1D4) were incubated with the SBA, which included mAbs to the four engineered epitope tags. Complexes were captured in multiplex fashion using one of the four mAbs, with eight possible capture-detection schemes. An overall statistic for GPCR-RAMP complex formation was calculated by assigning P-values derived from Figure 4-5 of $p < 0.0001$ a 4, $p < 0.001$ a 3, $p < 0.01$ a 2, and $p < 0.05$ a 1 for each capture-detection mAb pair (Table 4-3 and Table 4-4). The values were summed and divided by the number of capture and detection pairs that we expected to be capable of measuring the relevant complex. The labels in bold correspond to secretin-like GPCRs. Heatmap represents the overall statistic and is the hypothetical expected data for Figure 4-9.

The threshold used to convert the epitope tag data to binary form was increased by an interval of 0.125 and then the following metrics were plotted: (a) overall percent agreement (P_0), (b) the percent of hits from the epitope tag data that are also found in the anti-GPCR Ab data (sensitivity), (c) the percent of non-hits from the epitope tag data that are also non-hits in the

anti-GPCR Ab data (specificity), (d) the probability of a positive result in the anti-GPCR Ab data also being a positive in the epitope tag data (positive predictive value), (e) the probability of a negative result in the anti-GPCR Ab data also being a negative in the epitope tag data (negative predictive value) and (6) the similarity of the two data sets (Jaccard Index) (Table 2-2).

Overall, using anti-GPCR Abs to capture GPCR-RAMP complexes results in data that corroborates with the results from using epitope tag mAbs (Figure 4-11). The overall agreement, specificity, and negative predictive value reach nearly 100% at the lowest threshold used to create a binary matrix from the anti-epitope tag capture data. The high correspondence for these metrics agrees with the observation that the majority of signals from GPCR Abs that reach a Z-score of 1.645 are seen only with lysates containing the intended GPCR target. The ability of anti-GPCR Abs to successfully capture the heterocomplexes is represented by the sensitivity, positive predictive value, and Jaccard index. All in three metrics, the OLLAS detection mAb performed better than the FLAG detection mAb. Unsurprisingly, the validated GPCR Abs demonstrated more congruency of positive results between the datasets. The Jaccard index represents the overall agreement of the positive results in both data sets and indicates at which threshold the agreement is maximized. The threshold that maximizes the agreement between the data sets was 1.125 in the case of both OLLAS and FLAG detection, and with all GPCR Abs and the validated GPCR Abs. However, the Jaccard index is only minimally smaller even at the lowest threshold (0.125), with a difference of 2-10%. In all, the population of false negatives arising from the anti-GPCR Ab data is very small. When using an OLLAS detection mAb and with pre-validated Abs, the anti-GPCR SBA was able to capture the majority of the GPCR-RAMP complexes.

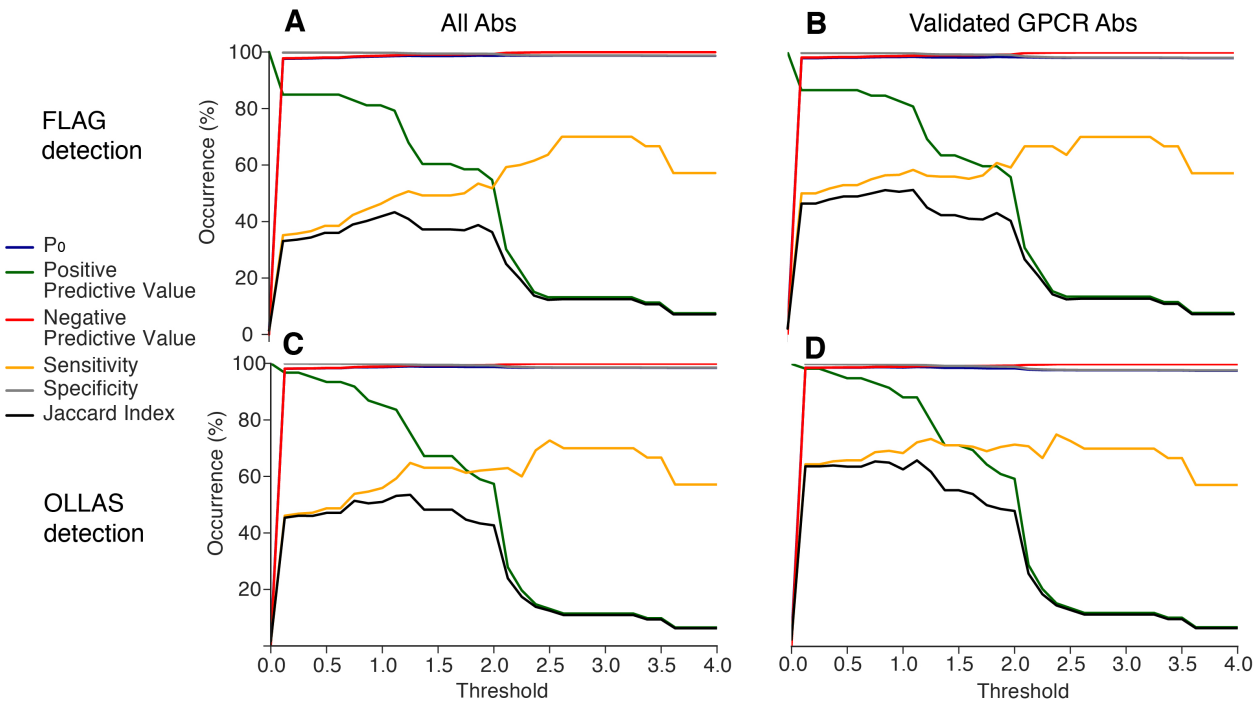

Figure 4-11. Statistical validation of GPCR-RAMP SBA data sets. Data obtained from the capture of the GPCR-RAMP complexes using anti-epitope mAbs (Figure 4-5) were compared with data obtained from the GPCR-RAMP complexes captured using anti-GPCR Abs (figure 4-9). PE-conjugated anti-FLAG was used to detect GPCR-RAMP complexes captured using **(A)** all anti-GPCR Abs or **(B)** validated anti-GPCR Abs. Alternatively, PE-conjugated anti-OLLAS mAb was used to detect GPCR-RAMP complexes captured using **(C)** all anti-GPCR Abs or **(D)** validated anti-GPCR Abs. The Z-score threshold for the anti-GPCR Ab data was set at 1.645. P_0 (blue), positive predictive value (green), negative predictive value (red), sensitivity (yellow), specificity (grey), and Jaccard Index (black) are plotted as a function of increasing threshold for the interaction results using epitope tags for capture and detection (Table 4-4). Table 2-2 shows the formulas and metrics used and provides a narrative description of each of the statistical terms. For example, the Jaccard Index represents the overall agreement of the positive results in both data sets and indicates at which threshold the agreement is maximized.

4.3.7 Summary of RAMP-GPCR complexes detected using an SBA assay

I used several detection and capture Ab pairs in a multiplexed fashion to identify GPCR-RAMP complexes. The complexes were captured through epitope tags engineered onto the GPCR or RAMP, and PE-conjugated anti-epitope tag mAbs were used to detect the putative interacting partner. In this experimental setup there were eight combinations of capture/detection pairs to identify complexes of dual-epitope tagged GPCRs with RAMPs, or four capture/detection pairs to identify complexes of single-epitope-tagged constructs. In addition, many of the Abs validated to capture the GPCRs or RAMPs also captured the GPCR-RAMP complexes. These data were collected in multiplexed fashion. A summary of the results obtained from all of the combinations of capture/detection Ab pairs employed are presented graphically in Figure 4-12. Generally, the GPCRs that exhibit complex formation with RAMPs either form complexes with all three RAMPs, or RAMP2 and RAMP3.

Figure 4-12. Graphical summary of GPCR-RAMP complexes detected using an SBA assay. Each circle depicts a unique GPCR along with each of the three RAMPs. Each GPCR is labeled and color coded. RAMP1 is colored grey, RAMP2 is colored lime, RAMP3 is colored tangerine. Curved lines within the circles show GPCR-RAMP interactions, and the thicknesses of the lines shows relative statistical significance (see below). The small labels around the circumference indicate the Abs used for the SBA experiments. In total four anti-epitope tag mAbs, 31 validated Abs to the 23 GPCRs included in the study, and five validated Abs to the three RAMPs are shown. Three GPCRs tested (CCR5, CCR7 and CXCR4) did not form complexes with RAMPs and are not shown here. The statistical significance derived for the particular interaction using the indicated capture/detection pair is represented by the thickness of the curved lines. P values of $p \leq 0.05$ are given an arbitrary thickness of 1, $p \leq 0.01$ a thickness of 2, $p \leq 0.001$ a thickness of 3, and $p \leq 0.0001$ a thickness of 4. Bead ID numbers are listed with each GPCR name and the corresponding validated Ab names are provided in Table 4-2.

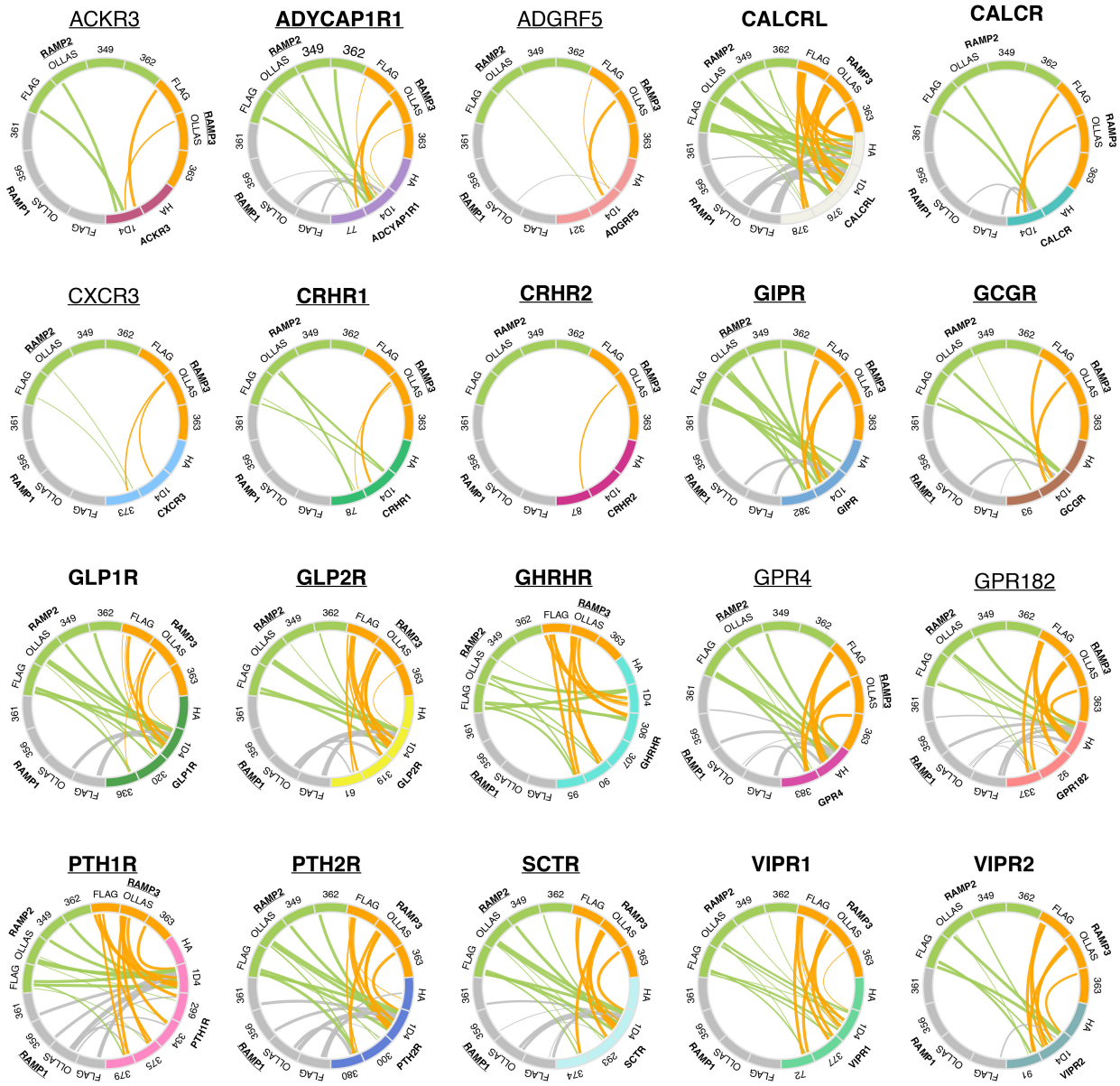
ACKR3
ADYCAP1R1
ADGRF5
CALCRL
CALCR
CXCR3
CRHR1
CRHR2
GIPR
GCGR
GLP1R
GLP2R
GHRHR
GPR4
GPR182
PTH1R
PTH2R
SCTR
VIPR1
VIPR2

4.4 Validation of GPCR-RAMP interactions by PLA

In order to show the presence of selected GPCR-RAMP complexes in membranes, we employed a proximity ligation assay (PLA). The PLA method enables detection of protein interactions, which are visualized as fluorescent puncta *(112)*. In principle, each PLA punctum corresponds to a single protein-protein complex that reacts with two primary Abs, one per protein. The distance constraints for PLA proximity detection are fairly stringent and the fluorescence signal is highly amplified using a rolling circle DNA polymerization that hybridizes with fluorescent complementary oligonucleotides. The PLA can be carried out *in situ* in a cell membrane environment, which provides evidence for the functional relevance of the SBA results.

4.4.1 Establishment of the PLA method to detect GPCR-RAMP complexes

To detect the extracellular epitopes, we employed anti-HA and anti-FLAG Abs for CALCRL and RAMP2, respectively. Following PLA processing, we used a DAPI stain to visualize the cell nucleus and to count cells. Images were taken in the blue channel to visualize the cell nucleus and red channel to identify PLA puncta (Figure 4-13A). Omitting either the anti-HA or anti-FLAG primary Abs during PLA processing of CALCRL and RAMP2 cotransfected cells measured primary Ab nonspecific binding, while omitting all primary Abs measures nonspecific binding of the PLA probes. Mock transfected cells treated with both Abs served as a negative control (Figure 4-13B). PLA puncta count from cells that were cotransfected with

CALCRL and RAMP2 and incubated with both primary Abs were significantly higher compared to control treatments and mock transfected cells (Figure 4-13C).

Next, we determined whether the puncta count from the CALCRL and RAMP2 cotransfected cells were localized to the cell membrane since misfolded protein can accumulate in the endoplasmic reticulum. The accumulation of misfolded protein in the endoplasmic reticulum could cause the PLA method to appear to detect false positive protein-protein interactions. Puncta count from RAMP2 and CALCRL cotransfected cells were compared when using a permeabilizing fixation reagent, methanol, and a non-permeabilizing fixation reagent, formaldehyde (FA). There was no significant difference between puncta count using the two different fixation reagents (Figure 4-13D).

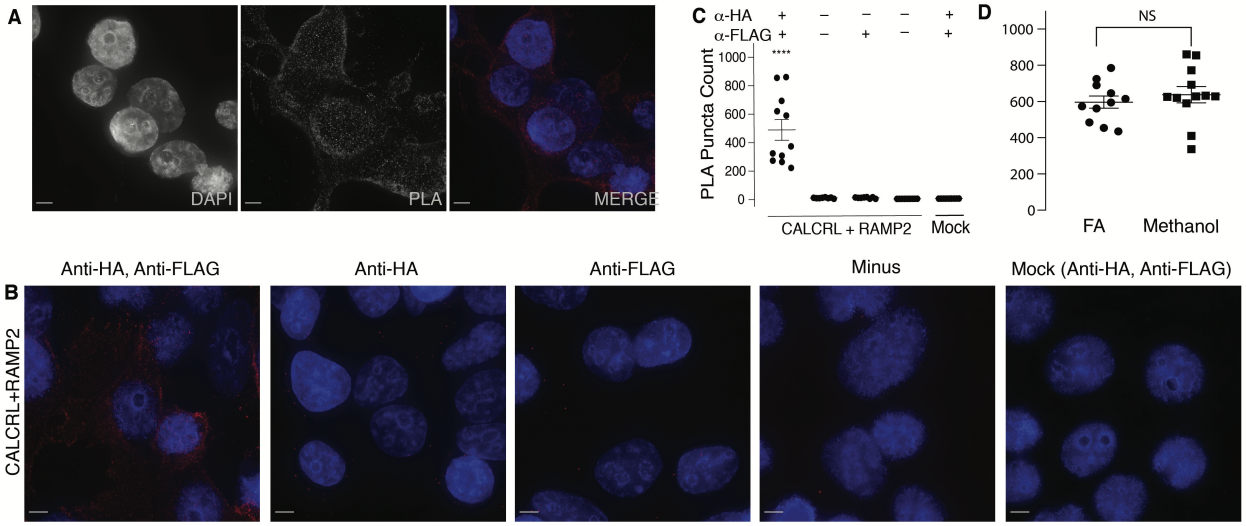

Figure 4-13. Detection of CALCRL-RAMP2 interactions in cell membranes using PLA. Cells were cotransfected with epitope-tagged GPCR and RAMP2 then incubated with α-HA and α-FLAG Abs. PLA was then carried out to quantitate GPCR-RAMP2 interactions. The number of PLA puncta per cell for each Z-stack captured was measured. Each Z-stack is of a different field of view. **(A)** Representative PLA images showing greyscale split-channel view of a Z-stack maximum projection for cells cotransfected with CALCRL and RAMP2 and treated with both primary Abs. The merge is presented in color. Scale bars, 5µm for both (A) and (C). Blue = DAPI, red = PLA puncta. **(B)** Representative images of PLA performed on CALCRL and RAMP2 cotransfected cells with Ab incubation detection as noted. Images show maximum projection of Z-stack, which is the maximum signal intensity for each channel at each point across all slices in the Z-stack. **(C)** Quantitation of control PLA experiments performed on CALCRL and RAMP2 cotransfected cells. PLA puncta counts were compared between samples that received both primary Abs and samples that received only anti-HA Ab, only anti-FLAG Ab, no primary Abs, or mock transfection with both primary Abs. Data are from two experiments performed with at least three replicates. **(D)** PLA puncta counts per cell for cells cotransfected with CALCRL and RAMP2, fixed with either FA or methanol and subjected to PLA. Data are from at least two experiments performed with at least five replicates. Significance determined by two-tailed P-test. Scale bars, 5µm. Blue = DAPI, red = PLA puncta.

4.4.2 Validation of RAMP-GPCR interactions using the PLA method.

We next used PLA to test GPCR-RAMP2 interactions in cell membranes for a variety of other GPCRs that were also studied using the SBA method. We focused on quantifying interactions between RAMP2 and CALCRL, PTH1R, GPR182, GPR4 and CXCR3 (Figure 4-14A). These GPCRs showed a range of capabilities to interact with RAMP2 in the SBA under conditions of detergent solubilization. Puncta were quantified over multiple Z-stacks, creating a 3D image of puncta (Figure 4-14B). The PLA results indicated that there were differences in puncta count among the receptor-RAMP2 pairs studied. Overall, the results of the PLA on a limited number of GPCR-RAMP pairs were consistent with the results of the SBA.

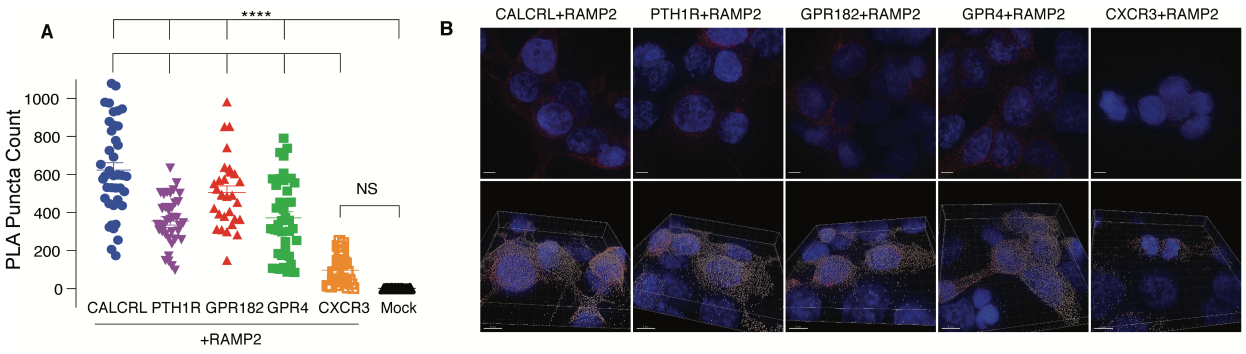

Figure 4-14. Validation of GPCR-RAMP complex formation in cell membranes using PLA. Cells were cotransfected with epitope-tagged GPCR and RAMP2 then incubated with α-HA and α-FLAG Abs. PLA was then carried out to quantitate GPCR-RAMP2 interactions. The number of PLA puncta per cell for each Z-stack captured was measured. Each Z-stack is of a different field of view. **(A)** PLA puncta counts for cells cotransfected with RAMP2 and selected GPCRs. Data are from at least three experiments performed with at least five replicates. **(B)** Representative images of cells cotransfected with RAMP2 and selected GPCRs and subjected to PLA. Top row shows maximum projection of Z-stack, which is the maximum signal intensity for each channel at each point across all slices in the Z-stack. The bottom row shows snapshots from puncta quantification performed in Imaris. Scale bars, 5μm top row, 8μm bottom row. Blue = DAPI, red = PLA puncta, grey = Imaris spots. The statistical test for significance used was a one-way ANOVA followed by Dunnett's multiple comparisons test (****P<0.0001, NS = not significant).

4.5 Discussion

We present a novel method to detect interactions between GPCRs and RAMPs that may have general utility to detect interacting partners of membrane proteins more broadly. The method relies on the preparation and validation of Abs for a suspension bead-based assay, which allows multiplexed immunocapture and detection of a large number of discrete proteins from a lysate mixture. The SBA we developed contains uniquely bar-coded beads conjugated to four

mAbs against epitope tags engineered at the N- and C-terminal tails of the expressed GPCRs and RAMPs, nine Abs against three different RAMPs, 55 Abs against 21 of the 23 GPCRs studied, and control beads. Captured GPCRs, RAMPs, or GPCR-RAMP complexes were detected by mAbs against the engineered epitope tags. In a single multiplexed experiment, we could use a variety of capture and detection strategies to identify complexes. The complexes were captured using the epitope tags on the GPCRs and detected using the epitope tags on the RAMPs, and *vice versa*. Finally, GPCR-RAMPcomplexes were captured by protein-specific Abs, demonstrating the possibility to detect these complexes without the need for protein engineering to introduce the epitope tags. We found that the results obtained using validated anti-GPCR or anti-RAMP Abs were concordant to those obtained using the anti-epitope tag mAbs for complex capture.

Using the SBA assay strategy, we identified previously reported secretin-like GPCR-RAMP complexes. For example, we show that CALCRL forms stable complexes with each of the three RAMPs, which have been well characterized in the literature *(111)*. In addition, we also detected and confirmed the formation of other complexes between secretin-like GPCRs and RAMPs that have been previously reported: CALCR with all three RAMPs, CRHR1 with RAMP2, GCGR with RAMP2, PTH1R with RAMP2, PTH2R with RAMP3, SCTR with RAMP3, VIPR1 with RAMP2 and RAMP3, and VIPR2 with all three RAMPs *(44, 45, 50, 51, 54–56)*. However, we failed to observe one previously reported complex, VIPR1 with RAMP1. The presence of a putative VIPR1-RAMP1 complex was inferred earlier because the cell surface expression of RAMP1 increased upon coexpression of VIPR1 *(54)*. The majority of the GPCR-RAMP interactions reported earlier were also based upon reciprocal effects of heterologous overexpression, and to our current knowledge, not on any type of direct binding assay. Many of the GPCR-RAMP interactions had remained unverified by other experimental methods. Our

findings using the SBA assay system to capture and detect actual GPCR-RAMP complexes appear to validate most of the earlier indirect findings. The results also validate the Abs and assay procedure as a robust method to detect and quantitate the presence of GPCR-RAMP complexes from cell lysates.

In addition, we discovered several new secretin-like GPCR-RAMP complexes that have not been described previously. We found that GIPR and ADCYAP1R1 formed complexes with all three RAMPs. To our knowledge, GIPR and ADCYAP1R1 have not been studied earlier with respect to their ability to interact with RAMPs. In addition, we found that several secretin-like GPCRs that were previously reported to not interact with RAMPs did indeed form complexes that were detected in the SBA assay. In particular, both GLP1R and GLP2R demonstrated complex formation with all three RAMPs, and GHRHR formed a complex with RAMP2 and RAMP3, but not with RAMP1. CRHR2 showed a very low probability of complex formation with RAMP3, but not with RAMP1 and RAMP2. These receptors had been judged not to form complexes with RAMPs because overexpression of the receptors in HEK293 or COS-7 cells did not cause coexpressed RAMPs to translocate to the cell surface *(53, 54)*. Our results show directly the existence of GPCR-RAMP complexes and suggests that RAMP translocation studies may not be sensitive to detect all GPCR-RAMP interactions *(113)*. The method we present detects interactions occurring anywhere in the cells, as opposed to just the cell membrane. Of note, preliminary data from another report did suggest that RAMPs were detected at the cell surface when coexpressed with GLP2R in HEK293T cells *(114)*.

Interactions between RAMPs and GPCRs beyond the secretin-like family have remained largely unexplored, with the exception of GPER30 and CaSR *(9, 57, 58)*. Here, among the few non-secretin-like receptors targeted by our SBA, we discovered interactions of RAMPs with

chemokine receptors and orphan receptors. The orphan receptors GPR4 and GPR182 interacted with all three RAMPs. Intriguingly, GPR4 demonstrates cell-type selectivity in response to lysolipids, potentially a result of differential RAMP expression in different cell types *(115)*. The chemokine receptors ACKR3/CXCR7 and CXCR3 also interacted weakly with RAMP2 and RAMP3.

Notably, two of the GPCRs that were demonstrated to interact with RAMP2 and RAMP3 have been linked to ligands targeting CALCRL in complex with one of the three RAMPs. These GPCRS, ACKR3/CXCR7 and GPR182, have not been previously reported to interact with RAMPs. GPR182 has been reported to be a receptor for adrenomedullin, a peptide ligand that signals through the CALCRL/RAMP2 complex *(116)*. GPR182 was reclassified as an orphan receptor when these results could not be reproduced *(117)*. ACKR3/CXCR7, a chemokine receptor, was originally described as a receptor for both adrenomedullin and calcitonin-gene related (CGRP), a peptide ligand that signals through the CALCRL/RAMP1 complex *(118)*. More recently, ACKR3/CXCR7 was demonstrated to act as decoy receptor for adrenomedullin *(79)*. This opens up the possibility that RAMPs can facilitate adrenomedullin or CGRP binding to these receptors.

Results obtained using mAbs to capture and detect RAMP-GPCR complexes through epitope tags showed variation among the different combinations of detection and capture Abs. For example, using OLLAS and 1D4 mAbs as the capture-detection pair was generally more sensitive than using HA and FLAG mAbs. Of note, the well-validated interaction between CALCR and each of the RAMPs was only detected by several, but not all mAb capture-detection pairs. Of course, the main reason for the variation in signal sensitivity among the different mAb pairs employed could be related to differences in Ab affinity and sensitivity. In line with this

hypothesis, the anti-OLLAS mAb has been demonstrated to have at least 100-fold higher affinity than anti-FLAG mAbs *(107)*.

Recent structural studies provide insight into the potential role of GPCR-RAMP complex formation. A cryogenic electron microscopy structure of the CALCRL-RAMP1 complex shows that RAMP1 forms extensive contacts with transmembrane helices 3, 4 and 5 as well as with extracellular loop 2 (ECL2) of CALCRL *(49)*. The agonist ligand of CALCRL-RAMP1 makes contacts with the with ECL2 of CALCRL. In contrast, there are very minimal direct contacts between the ligand and RAMP1, suggesting that the complex should exist in the absence of ligand *(48)*. The extensive contact surface between CALCRL and RAMP1 suggests that the complex should be stable under conditions used here in the SBA assay. Given that the CALCRL-RAMP1 structure is generalizable to other possible GPCR-RAMP complexes, Abs that would capture the GPCR through ECL2 might fail to recognize the same GPCR in complex with a RAMP. In line with this hypothesis, we found that a subset of validated anti-GPCR Abs were unable to capture a GPCR-RAMP complex that were identified through capture using other anti-GPCR Abs or anti-epitope tag mAbs.

We validated a set of Abs to detect GPCR-RAMP complexes in order to avoid artifacts inherent in having to rely upon insufficiently characterized Abs *(119, 120)*. Cross-reactivity of anti-GPCR Abs is a particular problem due to structural and amino acid sequence similarity among GPCRs *(24)*. The multiplexed nature of the SBA assay allowed us to both validate Abs to the RAMPs and GPCRs and check for potential cross-reactivity and off-target binding to all other GPCRs included in the study. We assessed Ab cross-reactivity even in the absence of the intended GPCR while unintended GPCR targets were overexpressed. Using the SBA, we found at least one Ab that targeted the intended GPCR with high selectivity for 19 of the 21 targets

with HPA Abs available. We also found at least one Ab to each RAMP that specifically captured the targeted RAMP. Future experiments will validate additional anti-GPCR Abs as they become available. In addition, the SBA strategy can be used to screen for therapeutic mAbs that show the lowest cross-reactivity with other GPCRs.

By being able to use protein-specific, anti-GPCR Abs in the multiplexed SBA assay, the requirement to use engineered epitope tags and a heterologous overexpression system would be eliminated. This would alleviate the potential of identifying non-physiological interactions, since the requirement for overexpressing both proteins would be removed. Thus, we determined whether anti-GPCR Abs can capture the GPCR-RAMP complexes directly. The pre-validated anti-GPCR Abs used in the SBA were able to capture the majority of the GPCR-RAMP complexes as demonstrated by using OLLAS mAb detection.

In order to show the presence of selected GPCR-RAMP complexes in membranes, we used PLA, which is an immunolocalization assay in which the proximity of two different Abs is detected using oligonucleotide-labeled secondary Abs. The PLA can be carried out *in situ* in a cell membrane environment, which provides evidence for the functional relevance of the SBA results. While PLA has been used to detect GPCR heteromers *(121)*, to our knowledge there have been no reports on its use to detect GPCR-RAMP complexes. Cells cotransfected with CALCRL and RAMP2 and treated with both primary Abs showed a significant PLA signal in comparison to all the negative controls, indicating that the assay is robust. We also compared results from the PLA using methanol-fixed cells to those using FA-fixed cells. The difference between the methanol and FA data sets was not significant, ensuring that most of the signal came from protein complexes on the membrane.

Although transient protein overexpression by cotransfection is subject to experimental variation, PLA puncta can be quantified, which together allows a semi-quantitative assessment of the extent of GPCR-RAMP interactions within the cellular context. We used the PLA to test a subset of GPCRs (PTH1R, GPR4, GPR182, and CXCR3) that were shown to interact with RAMP2 in the SBA assay. However, the CXCR3-RAMP2 interaction was detected only with one capture Ab at a low statistical significance. In concordance with the SBA results trend, we confirmed complex formation between RAMP2 and the PTH1R, GPR4 and GPR182, but the signal for CXCR3 did not meet statistical significance. Therefore, the PLA results highlight the importance of confirming the SBA results by a complementary method, especially when a RAMP-GPCR complex was observed with only one capture Ab.

In summary, the multiplexed SBA assay we developed enables the validation and use of Abs for the detection of GPCR-RAMP interactions. As a proof-of-concept, we defined the complete interactome between secretin-family GPCRs and RAMPs (Fig. 4). We also identified a number of novel GPCR-RAMP interactions, including some interacting partners among rhodopsin-family GPCRs that we selected for study based on earlier bioinformatics analysis. We used the *in situ* PLA to verify the extent of the interaction between several GPCR-RAMP2 pairs tested in the SBA. The SBA is scalable, allowing up to 500 beads to be conjugated with different Abs and decoded in the Luminex system. Therefore, we intend to expand the existing SBA, which consisted of 70 beads, based on the validation of additional Abs using epitope-tagged controls. We also look forward to using the SBA strategy to study other protein-protein interactions, including, but not limited to, GPCR heterodimerization. We consider the SBA technology to be potentially transformative with respect to studies of membrane protein systems.

CHAPTER 5. Future Perspectives

5.1 Additional computational methods for validating and predicting GPCR-protein interactions

We used two computational approaches to demonstrate that interactions between GPCRs and RAMPs are likely widespread – coexpression and coevolution. There are additional computational methods for predicting protein-protein interactions (PPIs) that were not used here. For example, machine learning algorithms to predict PPIs can find features shared among protein pairs with known interaction but not seen in non-interactors. Once the common features of a particular protein-protein complex are determined, the algorithm can classify new protein pairs as interactors or non-interactors *(122)*. Information obtained about GPCRs that interact with RAMPs from the SBA assay will allow the implementation of machine learning to find additional GPCRs likely to interact with RAMPs.

Another computational method to predict new PPIs is homology modeling, which requires a well-resolved three-dimensional structure as a reference structure. Recently, a new publication has described a CALCRL-RAMP1 structure at 3.3 Å resolution *(49)*. This structure will assist in the prediction of new GPCR-RAMP interactions, validation of experimentally determined interactions and elucidation of the molecular mechanisms of GPCR specificity for RAMPs. The power of homology modeling has been highlighted in a study regarding RAMP interactions with CRHR1 and CRHR2. CRHR2 does not interact with RAMP2, while the closely related CRHR1 does interact with RAMP2. Homology modeling of the ectodomains revealed that in CRHR1, two negatively charged residues are attracted to a histidine in RAMP2. But in

CRHR2, one of the corresponding residue is histidine, causing electrostatic repulsion away from RAMP2 *(53)*. Also, of note, I found that RAMP2 and RAMP3 show very similar coexpression patterns with GPCRs and form complexes with the same GPCRs. Thus, a specific component found in RAMP2 and RAMP3, but not RAMP1, may contribute to GPCR specificity. Interestingly, RAMP1 and RAMP3 show more general structural similarity at the extracellular region, with a shorter N-terminal tail than RAMP3. However, both RAMP2 and RAMP3 are glycosylated and contain glutamic acid at position 74. In RAMP1, the corresponding residue is tryptophan, which is an essential residue in conferring antagonist specificity *(123)*. In addition, the role of the transmembrane region of RAMP has yet to be investigated for its potential role in conferring GPCR-interaction specificity. These features may contribute to receptor specificity and warrant further analysis.

5.2 Scaling up the SBA method for high-throughput GPCR-protein interaction assay

To our knowledge, no robust proteomics approaches are available to address GPCR-protein interactions. GPCRs are underrepresented in mass spectrometry data, in part due to the lack of efficient proteolysis procedures *(86)*. Affinity assays to screen for GPCR-protein interactions, or membrane protein-protein interactions in general, have been lacking due to difficulties in (i) generating Abs that are functional in the intended assay system *(24, 124)* and (ii) extracting GPCRs from the native environment while maintaining both their binding capabilities and their accessibility for Ab-based detection. Using the SBA assay system, we validated at least one Ab from the HPA Ab library for 19 GPCRs. We were unable to validate Abs for only two of the GPCRs tested. It is feasible that a far more complete set of GPCRs can

be captured by an SBA-based assay once additional GPCR Abs are investigated. It is important to note that many additional anti-GPCR Abs, validated by other immunoassays, became available from HPA following the performance of the experiments described here. Also, we plan to investigate Abs from other commercial sources to identify and validate a complete set of useful anti-GPCR Abs.

Once a complete set of anti-GPCR Abs has been identified, the SBA method can be used to investigate additional GPCR-RAMP as well as other GPCR-protein interactions. One of the potential pitfalls in identifying GPCR-RAMP interactions is the need to overexpress both the GPCR and RAMP in a heterologous system, which can inadvertently drive non-physiological complex formation by mass action. Thus, we were interested in determining if the SBA method has the potential to detect GPCR-RAMP interactions of endogenously expressed GPCRs. To detect GPCR interactions from cells endogenously expressing GPCRs, anti-GPCR Abs must be able to capture the complex. Here, I showed that protein-specific anti-GPCR Abs were capable of capturing the majority of RAMP-GPCRs interactions identified (Figure 4-9). These experiments still required the use of engineered epitope tags on the RAMP proteins for detection of the GPCR-RAMP complex. To detect endogenous interactions, GPCR-RAMP complexes should be able to be captured using anti-GPCR Abs and detected using anti-RAMP Abs, thus alleviating the need for epitope tags on either protein. I found that CALCRL-RAMP2 and CALCRL-RAMP3 complexes could be detected without the need for epitope tags (Figure 5-1). However, these experiments were performed on lysates overexpressing both the GPCR and RAMP. Thus, we will use next determine if we can capture endogenous GPCR-RAMP interactions by investigating lysates from cell lines and tissues that are known to endogenously express a RAMP and CALCRL, such as the SK-N-MC cell line and human lung tissue. For an

endogenous GPCR-RAMP interaction experiment, lysates of interest will be incubated with an SBA containing Abs to GPCRs expressed in the lysate and GPCR-RAMP interactions will be detected with a PE-conjugated anti-RAMP Ab. It is possible that a GPCR-interacting protein of interest does not have a well-validated, protein-specific Ab. In this case, heterologous expression of an epitope-tagged putative GPCR-interacting protein can be used to identify interactions. Even in this case, the requirement for heterologous expression of the hundreds of GPCRs can be avoided by using cell lines or tissues that endogenously express GPCRs of interest.

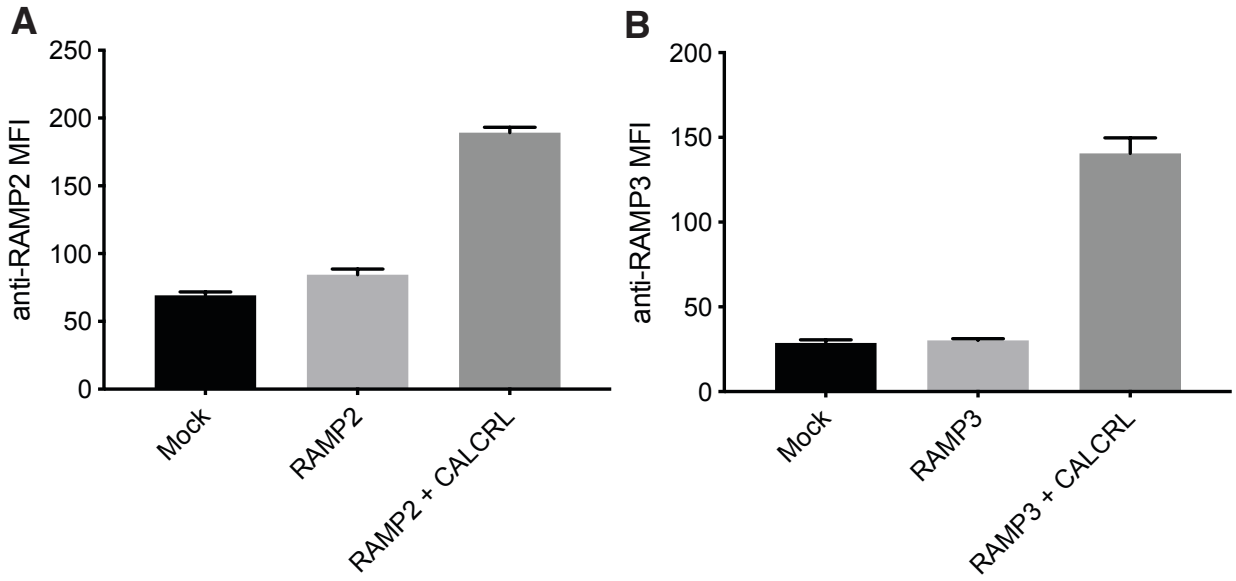

Figure 5-1. Capture and detection of CALCRL-RAMP complexes using protein-specific Abs.Lysates from cells transfected with mock (black), the indicated RAMP alone (light grey), or cotransfected with CALCRL and the indicated RAMP (dark grey) were incubated with the SBA, which included beads conjugated to a validated Ab targeting CALCRL. The GPCR was captured using anti-CALCRL Ab and the CALCRL-RAMP complex is detected using **(A)** PE-conjugated anti-RAMP2 Ab or **(B)** PE-conjugated anti-RAMP3 Ab. Data are median fluorescence intensity (MFI) and represent 3 experiments, each performed in duplicate.

I demonstrated the capability of the SBA method, especially in combination with bioinformatics, to identify global GPCR-RAMP interactions. However, the approaches I demonstrated are not limited to the study of GPCR-RAMP interactions. Both the SBA method, as well as the bioinformatics approach, may be extended to other single transmembrane proteins that interact with GPCRs, including receptor transporting proteins (RTPs), receptor expression enhancing proteins (REEPs), melanocortin receptor accessory proteins (MRAP), and the M10 major histocompatbility proteins (MHC). An SBA could also be utilized to identify stable transmembrane interactions of GPCR heterocomplexes. Such experiments using the SBA method can elucidate a map of GPCR-transmembrane interactions, which is vital for understanding the full regulation of GPCRs *(125, 126)*.

Finally, the SBA strategy can also be used to screen for therapeutic anti-GPCR mAbs with low cross-reactivity to other GPCRs. MAbs targeting GPCRs are of increasing interest as therapeutic agents *(24)*. However, GPCR Abs suffer from cross-reactivity due to high amino acid sequence homology among closely related GPCRs. To screen putative therapeutic mAbs, the anti-GPCR mAbs could be coupled to unique beads as capture mAbs to create an SBA. Then lysates containing an epitope-tagged GPCR of interest, as well as closely related GPCRs, could be incubated with the SBA and anti-epitope mAbs targeting the GPCR would be used for detection. Highly specific capture mAbs would show signal only with the lysate containing the tagged GPCR of interest and could thus be identified for further development.

5.3 Implications of RAMP interactions with additional GPCRs

Since GPCRs participate in numerous molecular processes and are targeted by ~40% of pharmaceuticals, mapping GPCR interactions with RAMPs has important implications for both basic biology as well as translational medicine *(127)*. For example, nearly 30% of non-olfactory GPCRs remain orphan receptors, whose endogenous ligands are unknown. Despite evidence that orphan receptors are important in many pathophysiological states, the rate of GPCR de-orphanization has decreased drastically in the last few decades *(128)*. We found that RAMPs interacted with orphan GPCRs GPR4 and GPR182 and observed that RAMPs are globally coevolved and coexpressed with GPCRs. Since the discovery of RAMPs led to the de-orphanization of CALCRL, it is feasible to expect that the identification of novel orphan GPCR-RAMP interactions would bolster the field of GPCR deorphanization.

A particularly compelling orphan GPCR we found to interact with RAMPs is GPR182. As mentioned previously, GPR182 was once thought to be the receptor for adrenomedullin. Adrenomedullin is now known to signal through the CALCRL-RAMP2 or CALCRL-RAMP3 complex. It is possible that a RAMP interaction is required for GPR182 to respond to adrenomedullin. We plan to investigate the modulation of GPR182 activity by RAMP2 and RAMP3. We will use an ERK phosphorylation assay since it is currently unclear which G protein subtype is activated by GPR182 and ERK phosphorylation involves signaling components downstream of each Gα protein subtypes and β-arrestin (11). Supporting the use of an ERK phosphorylation assay, GPR182 acts as a negative regulator of ERK phosphorylation *(129)*.

In addition, RAMPs may provide new opportunities for drug development. Currently, the only FDA-approved drug that targets a GPCR-RAMP complex is erenumab, a mAb which inhibits CGRP signaling through CALCRL-RAMP1 *(130, 131)*. The identification of new GPCR-RAMP interactions will help guide GPCR-focused drug development *(132)*. One possibility in RAMP-focused drug discovery is to develop bitopic ligands that target a RAMP and interacting GPCR. By targeting both proteins, bitopic ligands are likely to have increased specificity to the GPCR or GPCR-RAMP complex and can be used to target a GPCR in particular tissue(s) that coexpress a specific RAMP and GPCR *(133)*.

New GPCR-RAMP interactions have the potential to address a significant problem in translational biology - the failure of preclinical model systems to predict drug success *(127)*. Since RAMPs can dramatically modulate the ligand-binding affinity and activity of a GPCR, the presence or absence of a RAMP in the model system could alter the potency or activity of a drug. When investigating a drug targeting a RAMP-interacting GPCR, an appropriate model system would need to express the same RAMP(s) that are expressed in the intended target tissues. Several of the GPCRs determined to interact with RAMPs by the SBA experiments have investigational drug candidates in either preclinical development or clinical trials *(22)*.

Given that GPCR signaling is an essential process in nearly every physiological aspect of human cells, the need for a detailed GPCR-RAMP interactome map is necessary. Ideally, a full map would detail which GPCR interacts with which RAMP and would provide information about the corresponding molecular impact, including changes in GPCR ligand specificity, trafficking and signaling. Our work to develop a robust multiplexed assay used to determine the secretin-like GPCR-RAMP interactome provides a first step toward that goal.

APPENDIX A: G Protein Subtype-specific Signaling Bias in a Series of CCR5 Chemokine Analogs

A.1 Abstract

Chemokines and some chemical analogs of chemokines prevent cellular HIV-1 entry when bound to the HIV-1 coreceptors C-C chemokine receptor 5 (CCR5) or C-X-C chemokine receptor 4 (CXCR4), which are G protein-coupled receptors (GPCRs). The ideal HIV-1 entry blocker targeting the coreceptors would display ligand bias and avoid activating G protein-mediated pathways that lead to inflammation. We compared CCR5-dependent activation of second messenger pathways in a single cell line. We studied two endogenous chemokines [RANTES (also known as CCL5) and MIP-1α (also known as CCL3)] and four chemokine analogs of RANTES (5P12-, 5P14-, 6P4- and PSC-RANTES). We found that CCR5 signaled through both $G_{i/o}$ and $G_{q/11}$. IP1 accumulation and Ca^{2+} flux arose from $G_{q/11}$ activation, rather than from Gβγ subunit release after $G_{i/o}$ activation as had been previously proposed. The 6P4 and PSC RANTES analogs were superagonists for $G_{q/11}$ activation, whereas the 5P12 and 5P14 RANTES analogs displayed a signaling bias for $G_{i/o}$. These results demonstrate that RANTES analogs elicit G protein subtype-specific signaling bias and can cause CCR5 to couple preferentially to $G_{i/o}$ rather than $G_{q/11}$ signaling pathways. We propose that G protein subtype-specific signaling bias may be a general feature of GPCRs that can couple to more than one G protein subtype.

A.2 Introduction

Canonically, GPCR signaling involves sequential activation of a single type of Gα protein class followed by β-arrestin-dependent activation of non-canonical signal pathways. According to the concept of functional selectivity or ligand bias, signaling intensity can be skewed toward either the G protein pathway or the β-arrestin pathway *(12, 134)*. Biased ligands are potentially desirable therapeutic agents that modulate specific signaling pathways relevant to disease processes *(135)*. However, designing biased ligands requires a thorough understanding of receptor pharmacology and the appropriate cell-based assay systems to characterize the properties of drug candidates.

One disease target for biased ligands is HIV-1 infection, an ongoing epidemic with approximately 2.1 million new cases worldwide in 2015. A strategy to reduce transmission of HIV-1 is to prevent its cellular entry *(136)*. C-C chemokine receptor 5 (CCR5) is an obligate co-receptor required for cellular viral entry. Cells lacking CCR5 on their surface are not susceptible to most strains of HIV-1 infection *(137)*. Although endogenous chemokine agonists reduce the population of CCR5 on the cell surface by inducing receptor internalization, CCR5 agonists are not used as therapeutic agents for two reasons. First, they cause internalization of only a subset of CCR5, allowing HIV-1 to use receptors remaining on the cell surface for cellular entry *(138)*. Second, stimulation of G proteins by activated CCR5 also promotes targeted migration of immune cells, leading to undesirable inflammatory side effects and enhanced HIV-1 infection at the site of inflammation *(139, 140)*. In principle, a biased ligand that causes maximal receptor internalization, in the absence of G protein activation to avoid generating an inflammatory response, would be an ideal HIV-1 cellular entry blocker *(141)*.

The desire for a biased, therapeutically viable HIV-1 drug that targets CCR5 has motivated the development of several analogs of RANTES with N-terminal modifications (Figure A-1A): PSC-, 6P4-, 5P12-, and 5P14-RANTES (PSC, 6P4, 5P12, and 5P14 hereafter). These RANTES analogs appear to show pronounced signaling bias. Optimization of AOP-RANTES, the first potent, non-signaling chemokine analog that blocks HIV-1 entry *(142)*, has generated to PSC *(143)*. PSC behaves as a pharmacological superagonist because it appears to be more efficacious than RANTES at eliciting the release of intracellular Ca^{2+} stores and is more effective at causing internalization of CCR5 *(141, 144)*. Recombinant RANTES analogs including 6P4, 5P12, and 5P14 have high anti-HIV-1 potency and induce CCR5 internalization. Like PSC, 6P4 behaves as a strong agonist that induces both Ca^{2+} flux and receptor internalization. In contrast, 5P14 does not cause Ca^{2+} flux signaling, but induces receptor internalization, suggestive of an internalization or β-arrestin-biased ligand. Finally, 5P12 binds to CCR5 but does not demonstrate apparent Ca^{2+} flux or receptor internalization *(141)*.

These RANTES analogs show promise in being capable of tuning the CCR5 signaling pathways to avoid the undesired side effect of inflammation. However, the signaling pathways that link CCR5 activation to its numerous physiological functions, including inflammation, remain poorly characterized. In addition to inducing Ca^{2+} flux, activation of G proteins through CCR5 also leads to inhibition of cAMP generation, an effect of $G_{i/o}$ protein activation. However, it is less clear if Ca^{2+} flux is a result of G_q protein activation or release of Gβγ subunits following $G_{i/o}$ protein activation in the context of CCR5 *(145)*. 5P14, which does not trigger CCR5-mediated Ca^{2+} flux, does inhibit cAMP production *(146)*. These results suggest that CCR5-mediated Ca^{2+} flux and inhibition of cAMP generation are not linked and may be mediated by different G proteins. Some GPCRs can signal through more than one Gα protein class depending

on the cellular environment and the activating ligand *(147)*. CCR5 has been suggested to switch from $G_{i/o}$ to G_q signaling, but the relationship between the well-established $G_{i/o}$ signaling pathway and other G protein signaling pathways remains to be determined *(148)*.

Here, we tested the ability of endogenous chemokines and RANTES analogs to activate different Gα protein classes in the same human cell line in culture. It was important to use the same cell line because compositional differences of effectors between cell types can make it possible for a ligand to appear to be biased when different pathways are evaluated in different cells, a bias that is not detected if the same cell types are used for all of the assays *(149)*. We measured G protein activation through several downstream pathways, including inhibition of cAMP generation, Ca^{2+} flux, and IP1 accumulation. In addition, we identified the activated Gα protein subtype that was responsible for these downstream events by performing assays in the presence of transfected individual G proteins, or in cells treated with pertussis toxin (PTX) to inactivate $G_{i/o}$ or an inhibitor (YM-254890) to block activation of G_q *(150, 151)*. We found that each of the chemokines induced $G_{i/o}$ protein activation, but the chemokines varied in their ability to activate G_q proteins. In comparison with the endogenous chemokines RANTES (also known as CCL5) and MIP-1α (also known as CCL3), 6P4 and PSC acted as superagonists at G_q, whereas 5P12 showed no G_q activation and was $G_{i/o}$ biased.

A.3 Methods and Materials

A.3.1 Materials

Coelenterazine 400A for $BRET^2$ experiments was from Biotium. The IP-One homogenous time resolved fluorescence (HTRF) assay kit was from Cisbio. Forskolin, PTX and poly-D-lysine were from Sigma. YM-254890 was from Wako Pure Chemical Industries. Dulbecco's modified Eagle's medium Glutamax (DMEM-Q), Hank's balanced salt-solution (HBSS) and Lipofectamine 2000 were from Life Technologies. Fetal bovine serum (FBS) was from Atlanta Biologicals. Bovine serum albumin (BSA) fraction V, fatty acid-free was from Roche and 96-well white, clear bottom microplate, and 384-well black, clear bottom microplates were from Corning. RANTES and MIP-1α were from Peprotech. The RANTES analogs 5P12, 5P14, 6P4 and PSC were a gift from Prof. Oliver Hartley (Université de Genève).

A.3.2 Transfection constructs

The human CCR5 cDNA in pcDNA3.1(+) encoded a C-terminal 1D4 epitope tag (TETSQVAPA). The EPAC2 reporter was a gift from Prof. Michel Bouvier (Université de Montréal). G_q and G_{i2} α-subunit plasmids are wild-type human cDNA cloned in pcDNA3.1(+) (cDNA Resource Center). G_{qi5} refers to a construct in which the α-subunit of G_q is modified so that its C-terminal tail amino acids residues are derived from the α-subunit of G_{i2} (such that EYNLV-COOH in G_q becomes to DCGLF-COOH in G_{qi5}). G_{qi5} was cloned into pcDNA1 (Addgene) *(152)*.

A.3.3 Cell culture and transfection

HEK293T cells were maintained in DMEM-Q with 10% FBS. Transient transfections were performed using Lipofectamine 2000 according to the manufacturer's instructions with some modifications as previously described *(104)*. Cells were transfected in different plate formats with the following amounts of total DNA: 2 μg per well in 6-well plates; 100 ng per well in 96-well plates and 20 ng per well in 384-well plates. Total transfected plasmid DNA was kept constant by adding empty vector pcDNA3.1(+) when necessary.

A.3.4 Adenylyl cyclase activity assay

Inhibition of forskolin-stimulated cAMP production in response to each chemokine was monitored in HEK293T cells cotransfected with CCR5 and an EPAC reporter protein that shows a decrease in BRET upon cAMP binding *(84)*. For each well of a 96-well plate, HEK293T cells (100,000 in 0.1 mL DMEM) were transfected with 12 ng RLuc3-EPAC-GFP, a $BRET^2$ cAMP sensor, with or without cotransfection of 24 ng CCR5 wt. Cells were then plated at 100 μL/well into 96-well white, clear bottom microplates previously coated with 0.01% (w/v) poly-D-Lysine. Twenty-four hours post-transfection, medium was replaced with BRET buffer [phosphate buffer saline (PBS) containing 0.5mM $MgCl_2$ and 0.1% BSA]. Coelenterazine 400A was added to a final concentration of 5 μM followed by a 5 min incubation at room temperature. Cells were then stimulated with chemokine in the presence or absence of 5 μM of forskolin at RT for 5 min prior to $BRET^2$ reading to yield dose-response curves. Luminescence and fluorescence readings were collected using the Synergy NEO2 plate reader (BioTek) and Gen5 software. $BRET^2$ readings

between RLuc3 and GFP10 were collected by sequential integration of the signals detected in the 365- to 435- nm (RLuc3) and 505- to 525- nm (GFP10) windows. $BRET^2$ ratios were calculated as previously described previously *(84)* and are shown as a percentage of the forskolin-stimulated response. For experiments involving PTX, cells were treated with 100 ng/mL PTX for 16 hours at 37°C and 5% CO_2 before stimulation with forskolin and chemokines. All experimental manipulations were performed while cells remained attached to the 96-well plates.

A.3.5 Ca^{2+} flux assay

Ca^{2+} mobilization was monitored by loading CCR5-transfected HEK293T cells with a Ca^{2+}-sensitive fluorescent dye and measuring changes in cytosolic Ca^{2+} concentrations immediately following chemokine addition. For each well of a 384-well plate, HEK293T cells (20,000 in 0.02 mL DMEM) were transfected with 10 ng CCR5 or 20 ng of empty vector. Where applicable, 5 ng of G_q, G_{i2}, or G_{qi5} vector constructs were cotransfected. Cells were then plated at 20 µL/well into 384-well black clear bottom microplates previously coated with 0.01% (w/v) poly-D-lysine hydrobromide. Twenty-four hours post-transfection 20 µL/well FLIPR Ca^{2+} 6 dye (Molecular Devices) was added to the cells and incubated for 1.5 hours at 37°C with 5% CO_2. The dye was dissolved in HBSS-H (HBSS with 20 mM HEPES, pH 7.4) with 0.4% BSA. Prior to measurement, the plate was incubated at 37°C for an additional 30 mins in a pre-warmed FlexStation II 384 Plate Reader (Molecular Devices). Chemokine at a 5x final concentration was diluted in HBSS-H with 0.2% BSA. Fluorescence readings were collected using the FlexStation plate reader with excitation at 485 nm, emission at 535 nm and the dichroic mirror at 525 nm. The FlexStation took measurements over a 100 second time course, with 10 µL of ligand added

to the cells 20 seconds after the start of measurement. Relative fluorescence units (RFU) are reported as the peak magnitude signal minus the basal signal in each well. For experiments involving PTX, cells were treated with 100 ng/mL PTX for 16 hours at 37°C and 5% CO_2 before chemokine stimulation. For experiments involving YM-254890, 10 μM of YM-254890 (dissolved as a 10 mM stock in DMSO) or equivalent DMSO vehicle was added to the cells and incubated for 30 min at 37°C.

A.3.6 IP1 accumulation assay

IP1 concentrations in CCR5-transfected cells was measured using a competitive HTRF assay following incubation with each chemokine for three hours. For each well of a low-volume, 384-well plate, HEK293T cells (5,000 in 7 μL DMEM) were transfected with 11 ng CCR5 vector or 11 ng of empty vector. Where applicable, 5.5 ng of G_q, G_{i2}, or G_{qi5} vector constructs were cotransfected. Twenty-four hours post-transfection, cells were stimulated by chemokine diluted in 7 μL 1X Stimulation Buffer (HEPES 10 mM, $CaCl_2$ 1 mM, $MgCl_2$ 0.5 mM, KCl 4.2 mM, NaCl 146 mM, glucose 5.5 mM, LiCl 50 mM, pH 7.4) with 0.2% BSA and 50 mM of LiCl (to prevent IP1 degradation). The chemokine was incubated at 37°C for 3 hours. Following incubation, cells were lysed by addition of 3 μL/well of d2-fluorophore-labeled, IP1 analog as the fluorescence acceptor and the Terbium cryptate-labeled, anti-IP1 mAb, as the fluorescence donor. Both fluorescent donor and acceptor were diluted in the kit-supplied lysis buffer. The plates were incubated overnight at 4°C, and time-resolved fluorescence signals were read using the BioTek Synergy NEO plate reader (BioTek) at 620 nm and 655 nm. Results were calculated as a 665 nm/620 nm signal ratio, and IP1 concentrations were interpolated from a standard curve

prepared using the supplied IP1 calibrator. Results are shown as pmoles of IP1 formed/well. For experiments involving PTX, cells were treated with 100 ng/mL PTX for 16 hours at 37°C and 5% CO_2 before stimulation. For experiments involving YM-254890, 10 μM of YM-254890 or equivalent DMSO vehicle was added to the cells and incubated for at 37°C for 30 min.

A.3.7 Data analysis

Data were graphed and analyzed using GraphPad Prism 6.0 software. Dose-response curves were fit by a three-parameter logistic equation.

A.4 Results

A.4.1 RANTES analogs induce CCR5-mediated inhibition of cAMP production which depends on $G_{i/o}$ protein activation

We first measured the ability of the RANTES analogs to induce $G_{i/o}$ activation, which is the canonical signaling pathway of CCR5. $G_{i/o}$ activation leads to the inhibition of adenylyl cyclase and a decrease in the amount of cellular cAMP. We tested the ligand-dependent inhibition of forskolin-stimulated cAMP production in cells transfected with CCR5 vector. Each ligand displayed a robust dose-dependent increase in inhibition of cAMP production (Figure A-1B). The EC_{50} values for inhibition of forskolin-stimulated cAMP accumulation determined for the ligands were all within 20-fold of each other, whereas the E_{max} values were within approximately a two-fold range (Table A-1). At the highest concentration of ligand used (100 nM), we found that the range of E_{max} values was 14 to 31% inhibition of the forskolin response.

The rank order of maximum signal was 5P14 > RANTES > MIP-1α = 6P4 = 5P12 > PSC. The EC_{50} values of ligands ranged from 0.1 to 2.1 nM with the following rank order: 6P4 > 5P14 >RANTES = PSC > MIP-1α = 5P12.

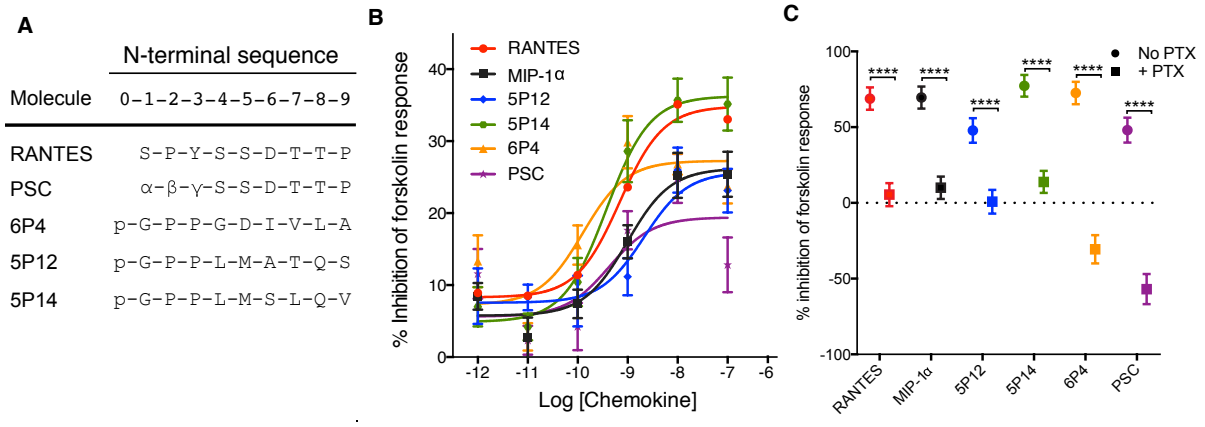

Figure A-1. CCR5-mediated $G_{i/o}$ protein activation by endogenous chemokines and RANTES analogs. (**A**) The RANTES analogs used in this study have modifications to the N-terminal tail region as shown, where p represents pyroglutamate, α represents N-nonanoyl, β represents L-thioproline and γ represents L-2-cyclohexylglycine. (**B**) HEK293T cells cotransfected with CCR5 and the EPAC reporter plasmid were stimulated with forskolin and incubated with the chemokines RANTES (red, circle), MIP-1α (black, square), 5P12 (blue, diamond), 5P14 (green, hexagon), 6P4 (yellow, triangle) and PSC (purple, star). (**C**) Transfected cells were pretreated with 100 ng/mL of PTX (squares) or control buffer (circles) for 16 hours, stimulated with forskolin, and incubated with 100 nM of chemokines. Data are expressed as a percentage of forskolin-stimulated response and are presented as the mean ± SEM for N ≥ 3 three independent experiments performed in at least technical triplicate. Shown are the statistical significance of the differences between PTX-treated and control condition for each chemokine: ****P <0.0001 (multiple t-tests). Each chemokine tested significantly inhibited cAMP generation ($p < 0.001$). PSC and 6P4 showed enhanced inhibition of forskolin-induced cAMP generation $p < 0.05$ (one-way ANOVA, Dunnett's multiple comparisons test).

Table A-1. Summary of fitted curve parameters for inhibition of cAMP accumulation. EC_{50}, pEC_{50}, and E_{max} values with SEM are given for Figure A-1B.

	RANTES	MIP-1α	5P12	5P14	6P4	PSC
CCR5						
EC_{50} (nM)	0.7	1	2.1	0.4	0.1	0.4
pEC_{50} ± SEM	-9.2 ± 0.19	-9.0 ± 0.26	-8.7 ± 0.38	-9.4 ± 0.22	-9.9 ± 0.31	-9.4 ± 0.56
E_{max} ± SEM	26 ± 2.3	20 ± 2.5	18 ± 3.2	31 ± 3.1	20 ± 3.0	14± 3.4

To confirm that inhibition of cAMP accumulation was due to $G_{i/o}$ protein activation, we measured cAMP accumulation in cells pretreated with PTX to prevent $G_{i/o}$ proteins from interacting with receptors. Similar to the results from the dose-response experiment, each chemokine demonstrated significant CCR5-mediated inhibition of cAMP accumulation in forskolin-treated cells. As expected, PTX pretreatment abrogated the ability of all ligands to inhibit forskolin-stimulated cAMP accumulation (Figure A-1C).

A.4.2 RANTES analogs have different effects on CCR5-dependent Ca^{2+} flux

In addition to inhibiting cAMP accumulation, CCR5 activation also leads to Ca^{2+} flux. Thus, we tested the ability of each chemokine and chemokine analog to induce CCR5-mediated Ca^{2+} flux. In contrast to inhibiting cAMP accumulation, not all of the ligands stimulated Ca^{2+} flux through CCR5 (Figure A-2A). The RANTES analogs induced varying amounts of Ca^{2+} flux with the rank order being 6P4 = PSC > RANTES > MIP-1α > 5P14 > 5P12. Thus, for Ca^{2+} flux, 6P4 and PSC are superagonists that are more efficacious than the endogenous CCR5 chemokines

RANTES and MIP-1α, whereas 5P14 acts as a partial agonist and 5P12 does not have agonist activity.

A.4.3 Ca^{2+} flux mediated by CCR5 is inhibited by G_{i2} cotransfection and increased by G_q or G_{qi5} cotransfection

Because of the differences in signaling profiles of the RANTES analogs between Ca^{2+} flux and inhibition of cAMP accumulation, we next investigated the G protein family that was responsible for eliciting Ca^{2+} flux through CCR5 activation. Classically, Ca^{2+} flux is a result of G_q protein activation, but chemokine receptors can also induce Ca^{2+} flux through the release of Gβγ subunits following $G_{i/o}$ protein activation *(153, 154)*. To investigate the individual contributions of each Gα protein subtype to the Ca^{2+} flux signal, we repeated the Ca^{2+} flux experiments in cells in which CCR5 was cotransfected with G_q, G_{i2} or G_{qi5} protein. G_{qi5} is an engineered G_q protein containing the last five amino acid residues of G_{i2}, which allows $G_{i/o}$-coupled GPCRs to signal through G_q downstream signaling pathways *(152)*.

Cotransfection of G_{i2} with CCR5 markedly inhibited the ability of RANTES and MIP-1α to induce Ca^{2+} flux through CCR5 (Fig A-2B). G_{i2} cotransfection also dampened the maximum Ca^{2+} flux signal elicited in response to PSC. In contrast, cotransfection of CCR5 and G_q enhanced the maximal Ca^{2+} flux signal for all ligands, except 5P12 (Figure A-2C). In cells cotransfected with CCR5 and a promiscuous G protein construct, G_{qi5}, each RANTES analog induced robust Ca^{2+} flux (Figure A-2D), confirming the ability of all the RANTES analogs to activate $G_{i/o}$ through CCR5.

Due to differences in the binding kinetics of ligands, measurements of ligand bias are sensitive to the experimental time scale *(155, 156)* . For example, Ca^{2+} flux assays measure a transient signal that is complete in two minutes, whereas cAMP accumulation is measured over durations of 15 minutes or more. To accurately compare the ability of each chemokine to activate CCR5-mediated Ca^{2+} flux and inhibition of cAMP accumulation, it was necessary to measure Ca^{2+} flux with an accumulation assay. Inositol triphosphate (IP3) is a product upstream of Ca^{2+} flux, and a degradation product of IP3 can be measured by an accumulation assay. Although IP3 is rapidly degraded, its degradation product, inositol monophosphate (IP1), is stabilized by the addition of lithium chloride, allowing it to accumulate in the cell after receptor stimulation. In CCR5-expressing cells, we observed IP1 accumulation in response to only PSC (Figure A-2E), demonstrating that PSC functions as a superagonist as measured by IP1 accumulation and Ca^{2+} flux.

Cotransfection of G_{i2} with CCR5 reduced IP1 accumulation in response to PSC (Figure A-2F). In contrast, G_q cotransfection with CCR5 enhanced IP1 accumulation in response to each of the chemokines, except 5P12 (Figure A-2G). Moreover, G_q cotransfection with CCR5 revealed agonist activity as measured by IP1 accumulation in response to 6P4, RANTES, MIP-1α, and 5P14, an effect not seen in cells transfected with only CCR5. In addition, the rank order of maximal IP1 accumulation signal amongst the RANTES analogs was similar to that shown for Ca^{2+} flux, with 6P4 = PSC > RANTES > 5P14 > 5P12. Moreover, each of the RANTES analogs showed robust IP1 accumulation in cells cotransfected with G_{qi5}, confirming that each ligand activates $G_{i/o}$ (Figure A-2H).

Together, our IP1 accumulation and Ca^{2+} flux data show that PSC and 6P4 are superagonists, whereas 5P12 lacks agonist activity in these assays. Furthermore, G_{i2}

cotransfection disrupts the ability of both endogenous CCR5 chemokines and RANTES analogs to induce Ca^{2+} flux and IP1 accumulation, whereas G_q cotransfection has the opposite effect.

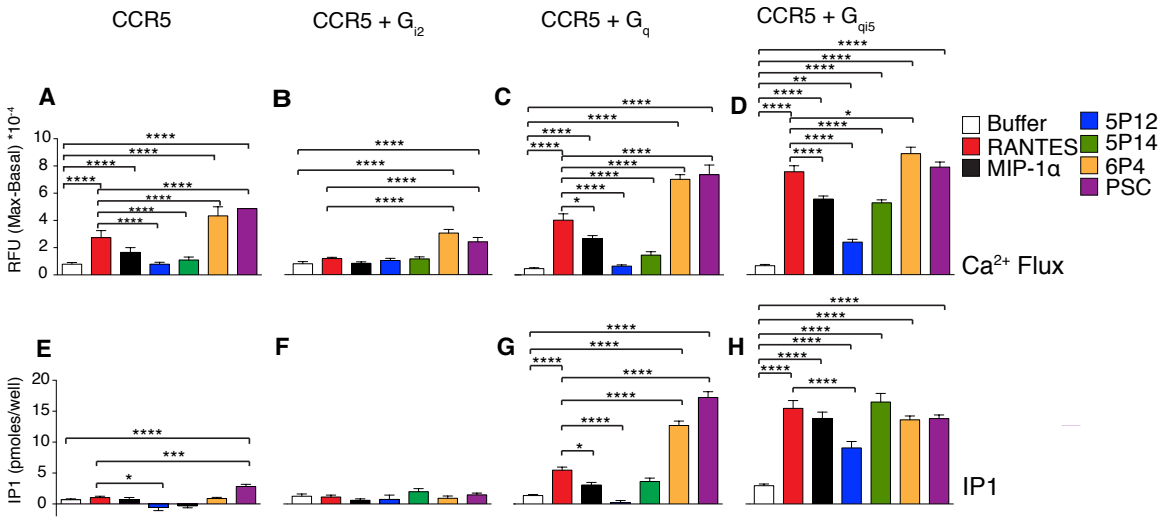

Figure A-2. The effects of G protein-subtype cotransfection on CCR5-mediated Ca^{2+} flux and IP1 accumulation in response to endogenous chemokines and RANTES analogs. Ca^{2+} flux in HEK293T cells transfected with (**A**) CCR5 alone or with G protein α subunits (**B**) G_{i2}, (**C**) G_q or (**D**) G_{qi5} was measured in response to 100 nM chemokine. Fluorescence data (maximal minus basal) are presented as mean relative fluorescence units (RFU) ± SEM for N=4 independent experiments performed in technical duplicate. IP1 accumulation in HEK293T cells transfected with (**E**) CCR5 alone or with G protein α subunits (**F**) G_{i2}, (**G**) G_q or (**H**) G_{qi5} was measured in response to 100 nM chemokine. Data are expressed as pmoles IP1 formed per well and are presented as mean ± SEM for N = 4 independent experiments performed in technical duplicate. Shown are the statistical significance of the differences between chemokine treatment and buffer control, and between chemokine treatment and RANTES treatment: *P<0.05, **P<0.01, ***P <0.001, ****P <0.0001 (two-way ANOVA, Tukey's multiple comparison's test).

A.4.4 CCR5-mediated Ca^{2+} flux is reduced by inhibiting $G_{i/o}$ protein activation and abolished by inhibiting G_q protein activation

To further differentiate between the contribution of $G_{i/o}$ and G_q proteins to CCR5-mediated signaling, we treated cells with Gα subtype-specific inhibitors. PTX prevents $G_{i/o}$ protein coupling to GPCRs by catalyzing the ADP-ribosylation of a Cys-residue in the C-terminal tail of $G_{i/o}$ alpha subunits *(157)*. YM-254890 prevents G_q activation by acting as a guanine-nucleotide dissociation inhibitor of G_q *(158)*. Both PTX and YM-254890 decreased CCR5-mediated Ca^{2+} flux (Figure A-3, A to D). However, YM-254890 abolished CCR5-mediated Ca^{2+} flux stimulated by all chemokines, while the effects of PTX was less pronounced. In CCR5-expressing cells, PTX reduced Ca^{2+} flux induced by the superagonists 6P4 and PSC and completely inhibited that induced by RANTES and MIP-1α (Figure A-3A). In cells cotransfected with CCR5 and G_{i2}, both PTX and YM-254890 decreased the remaining signal from PSC and 6P4 (Figure A-3B). However, in cells cotransfected with CCR5 and G_q, RANTES, MIP-1α, and 5P14 triggered a partially PTX-insensitive Ca^{2+} flux response (Figure A-3C). 6P4 and PSC also showed more PTX-insensitivity in cells cotransfected with G_q and CCR5 than in cells expressing CCR5 alone. Finally, the signal elicited by chemokines in cells cotransfected with CCR5 and the G_{qi5} chimera was reduced as a result of PTX treatment, except for that triggered by 5P12 (Figure A-3D). Overall, in contrast to PTX, disruption of G_q activation by YM-254890 abolished Ca^{2+} signaling by each ligand even when G_q or G_{qi5} were cotransfected.

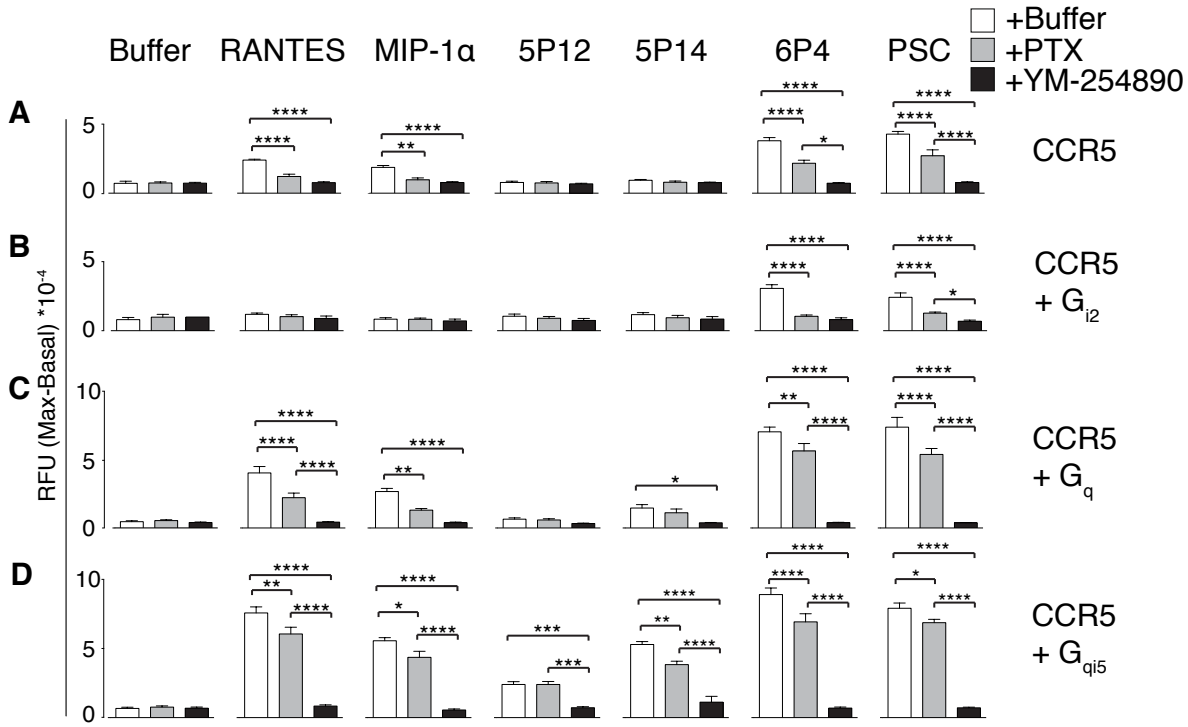

Figure A-3. The effects of PTX and YM-254890 treatment on CCR5-mediated Ca^{2+} flux in response to endogenous chemokines and RANTES analogs. Ca^{2+} flux in HEK293T cells transfected with (**A**) CCR5 alone or with G protein α subunits (**B**) G_{i2}, (**C**) G_q, or (**D**) G_{qi5} was measured in response to 100 nM of chemokine. Cells were pretreated with buffer (white bars), 100 ng/mL PTX (gray bars), or 1 μM YM-254890 (black bars). Fluorescence data (maximal minus basal) are presented as mean relative fluorescence units (RFU) ± SEM for N = 4 independent experiments performed in technical duplicate. Shown are the statistical significance of the differences between buffer control, PTX and YM-254890: *P<0.05, **P<0.01, ***P <0.001, ****P <0.0001 (two-way ANOVA, Tukey's multiple comparison's test).

A.4.5 CCR5-mediated IP1 accumulation is reduced by inhibiting $G_{i/o}$ protein activation and abolished by inhibiting G_q

Consistent with the Ca^{2+} flux experiments, YM-254890 prevented all of the chemokines from causing IP1 accumulation, regardless of the Gα protein subunit cotransfected (Figure A-4, A to D). In cells transfected with CCR5 alone, the PSC-induced IP1 signal was attenuated by PTX (Figure A-4A). PTX treatment of cells cotransfected with CCR5 and G_q only minimally reduced the IP1 signal induced by RANTES, MIP-1α, 6P4 and PSC, but had a greater effect on that induced by 5P14 (Figure A-4C). As with Ca^{2+} flux, PTX did not strongly reduce the signal elicited by the RANTES analogs when CCR5 was cotransfected with G_{qi5} (Figure A-4D). In summary, although PTX caused a modest decrease in chemokine responses, YM-254890 abolished the ability of each of the ligands tested to elicit IP1 accumulation and Ca^{2+} flux. Thus, both cotransfection and inhibition experiments suggest that G_q is the dominant G protein in stimulating Ca^{2+} flux following CCR5 activation, with $G_{i/o}$ playing a much smaller role.

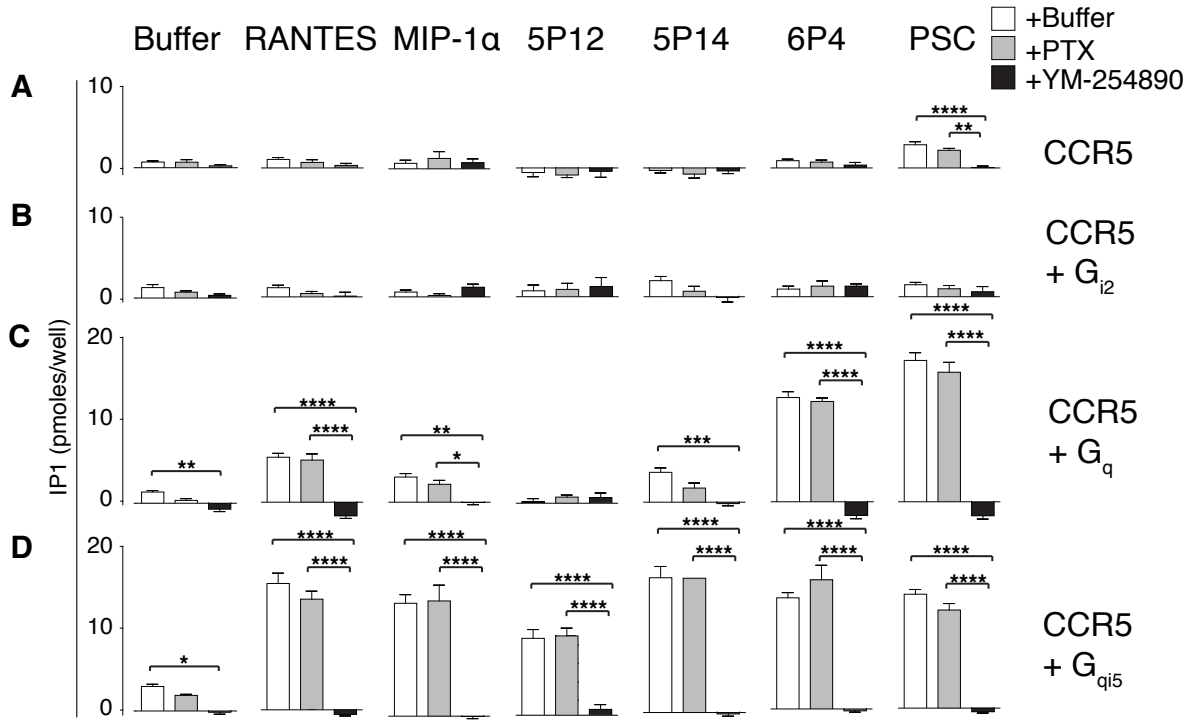

Figure A-4. The effects of PTX and YM-254890 treatment on CCR5-mediated IP1 accumulation in response to endogenous chemokines and RANTES analogs. IP1 accumulation in HEK293T cells transfected with (**A**) CCR5 alone or with G protein α subunits (**B**) G_{i2}, (**C**) G_q, or (**D**) G_{qi5} was measured in response to 100 nM of chemokine. Cells were pretreated with buffer (white bars), 100 ng/mL PTX (gray bars), or 1 μM YM-254890 (black bars). Data are expressed as pmoles IP1 formed per well and are presented as mean ± SEM for N = 4 independent experiments performed in technical duplicate. Shown are the statistical significances of the differences between buffer control, PTX and YM-254890: *P<0.05, **P<0.01, ***P <0.001, ****P <0.0001 (two-way ANOVA, Tukey's multiple comparison's test).

A.4.6 Cotransfection of CCR5 with $G_{i/o}$, G_q or G_{qi5} causes different effects on E_{max} values and EC_{50} values

The effects of G protein cotransfection with CCR5 could be a result of a change in ligand E_{max} (maximum signal) or EC_{50} (the concentration of ligand required for half-maximal signal). Performing and fitting dose-response curves for Ca^{2+} flux (Table A-2) showed that in cells transfected with CCR5, EC_{50} values ranged from 21.0 nM to 240 nM with the rank order of PSC = 6P4 = RANTES = 5P14 > MIP-1α (Figure A-5A). E_{max} values ranged from 2700 to 45000 RFU and the rank order was 6P4 > PSC > RANTES = MIP-1α > 5P14. Cotransfection of CCR5 and G_{i2} decreased Ca^{2+} flux such that only PSC and 6P4 could elicit any measurable Ca^{2+} flux response (Figure A-5B), which was due to reduced E_{max} values because EC_{50} values in cells transfected with CCR5 were similar to those in cells cotransfected with both CCR5 and G_{i2}. Similarly, the increase in response from each chemokine in cells cotransfected with CCR5 and G_q was not a result of altered EC_{50} values, but rather due to an increase in E_{max} values (Figure A-5C). In contrast to G_{i2} and G_q, cotransfection of G_{qi5} and CCR5 altered both EC_{50} and E_{max} values in dose-response Ca^{2+} flux experiments (Figure A-5D). The range of EC_{50} values amongst the ligands tested decreased, but the rank order was similar, with 6P4 = RANTES > PSC > 5P14 = MIP-1α > 5P12. In addition, the E_{max} value of each ligand increased, but the rank order also remained the same.

In cells transfected with CCR5 alone, only PSC showed any dose-dependent IP1 accumulation, with an EC_{50} of 190 nM (Figure A-5E) (Table A-3). No agonist-stimulated IP1 accumulation was observed in cells cotransfected with CCR5 and G_{i2} (Figure A-5F). Cells cotransfected with CCR5 and G_q displayed a range of EC_{50} values for IP1 accumulation of 4.3 nM to 72 nM with a rank order of 5P14 > 6P4 > RANTES = PSC. Theses EC_{50} values were similar to those for Ca^{2+} flux (Figure A-5C and G). The E_{max} values ranged from 1.0 to 8.4 pmoles/well with rank order of PSC > 6P4 > 5P14 > RANTES, although the curve fits for 5P12 and MIP-1α were ambiguous. This rank order of E_{max} values was similar to that observed with Ca^{2+} flux in CCR5-transfected cells both with and without cotransfection of G_q. As seen previously, cotransfection of G_{qi5} and CCR5 allowed each RANTES analog to cause IP1 accumulation (Figure A-5H). This increase in signal caused by G_{qi5} cotransfection with CCR5 could be attributed to a decrease in EC_{50} values for all ligands tested. In addition, an increase in E_{max} contributed to the higher signals for RANTES, MIP-1α, 5P12, and 5P14 in cells cotransfected with G_{qi5} and CCR5.

Figure A-5. Dose-response curves for CCR5-mediated Ca^{2+} flux and IP1 accumulation. Ca^{2+} flux in HEK293T cells transfected with (**A**) CCR5 alone or with G protein α subunits (**B**) G_{i2}, (**C**) G_q, or (**D**) G_{qi5} was measured in response to RANTES (red, circle), MIP-1α (black, square), 5P12 (blue, diamond), 5P14 (green, hexagon), 6P4 (yellow, triangle) and PSC (purple, star). Fluorescence data (maximal minus basal) are presented as mean relative fluorescence units (RFU) ± SEM for N = 4 independent experiments performed in technical triplicate. IP1 accumulation in HEK293T cells transfected with (**E**) CCR5 alone or with G protein α subunits (**F**) G_{i2}, (**G**) G_q, or (**H**) G_{qi5} was measured in response to RANTES (red, circle), MIP-1α (black, square), 5P12 (blue, diamond), 5P14 (green, hexagon), 6P4 (yellow, triangle) and PSC (purple, star). Data are expressed as pmoles IP1 formed per well and are presented as mean ± SEM for N=3 independent experiments performed in technical triplicate.

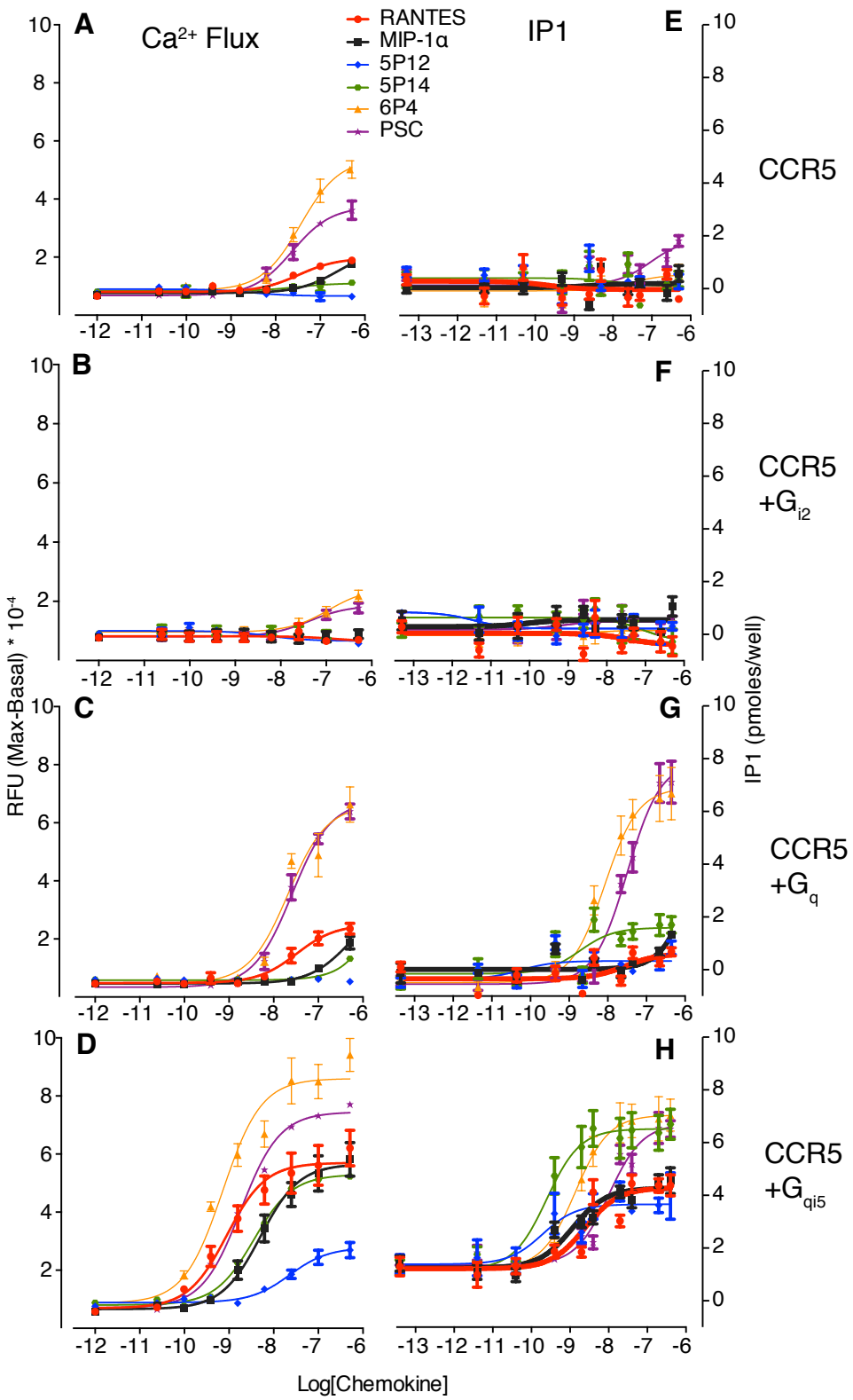
A
Ca2+ Flux
RANTES
MIP-1α
5P12
5P14
6P4
PSC
IP1
E
CCR5
B
F
CCR5
+Gi2
C
G
CCR5
+Gq
D
H
CCR5
+Gqi5
RFU (Max-Basal) * 10-4
IP1 (pmoles/well)
Log[Chemokine]

Table A-2. Summary of fitted curve parameters for Ca^{2+} flux. EC_{50}, pEC_{50}, and E_{max} values with SEM are given for Figure A-5, left column. ND, not detectable

	RANTES	MIP-1α	5P12	5P14	6P4	PSC
CCR5						
EC_{50} (nM)	32	240	ND	21	36	25
pEC_{50} ± SEM	-7.6 ± 0.2	-6.5 ± 0.2	ND	-7.7 ± 0.7	-7.4 ± 0.1	-7.6 ± 0.1
E_{max} ± SEM	12000 ± 1000	15000 ± 2000	ND	3000 ± 1000	45000 ± 2000	31000 ± 2000
CCR5 + G_{i2}						
EC_{50} (nM)	ND	ND	ND	ND	110	42
pEC_{50} ± SEM	ND	ND	ND	ND	-6.9 ± 0.3	-7.4 ± 0.3
E_{max} ± SEM	ND	ND	ND	ND	15000 ± 3000	10000 ± 2000
CCR5 + G_q						
EC_{50} (nM)	32	460	ND	ND	21	26
pEC_{50} ± SEM	-7.5 ± 0.1	-6.3 ± 0.3	ND	ND	-7.7 ± 0.1	-7.6 ± 0.1
E_{max} ± SEM	20000 ± 2000	27000 ± 8000	ND	ND	61000 ± 4000	64000 ± 2000
CCR5 + G_{qi5}						
EC_{50} (nM)	0.9	5.1	23	3.6	0.7	1.8
pEC_{50} ± SEM	-9.0 ± 0.1	-8.3 ± 0.1	-7.6 ± 0.1	-8.4 ± 0.1	-9.1 ± 0.1	-8.7 ± 0.1
E_{max} ± SEM	50000 ± 4000	50000 ± 3000	19000 ± 1000	45000 ± 2000	77000 ± 4000	67000 ± 3000

Table A-3. Summary of fitted curve parameters for IP1 accumulation. EC_{50}, pEC_{50}, and E_{max} values are given for Figure A-5, right column. ND, not detectable

	RANTES	MIP-1α	5P12	5P14	6P4	PSC
CCR5						
EC_{50} (nM)	ND	ND	ND	ND	ND	190
pEC_{50} ± SEM	ND	ND	ND	ND	ND	-6.7 ± 0.4
E_{max} ± SEM	ND	ND	ND	ND	ND	1.7 ± 0.3
CCR5 + G_{i2}						
EC_{50} (nM)	ND	ND	ND	ND	ND	ND
pEC_{50} ± SEM	ND	ND	ND	ND	ND	ND
E_{max} ± SEM	ND	ND	ND	ND	ND	ND
CCR5 + G_q						
EC_{50} (nM)	65	ND	ND	4.3	18	72
pEC_{50} ± SEM	-7.2 ± 0.4	ND	ND	-8.3 ± 0.3	-7.7 ± 0.1	-7.1 ± 0.1
E_{max} ± SEM	1.0 ± 0.2	ND	ND	1.6 ± 0.3	7.4 ± 0.1	8.4 ± 0.1
CCR5 + G_{qi5}						
EC_{50} (nM)	6	2.9	0.5	0.6	3.5	25
pEC_{50} ± SEM	-8.2 ± 0.1	-8.5 ± 0.1	-9.3 ± 0.4	-9.2 ± 0.2	-8.5 ± 0.1	-7.6 ± 0.1
E_{max} ± SEM	3.1 ± 0.3	3.0 ± 0.2	2.3 ± 0.4	5.3 ± 0.4	5.8 ± 0.5	5.4 ± 0.3

In summary, E_{max} values were altered when $G_{i/o}$ or G_q were cotransfected with CCR5, while both E_{max} and EC_{50} values were altered when G_{qi5} was cotransfected with CCR5. These results show that when CCR5 is cotransfected with either G_{i2} or G_q, the E_{max} values, but not the EC_{50} values, for agonist-dependent IP1 accumulation and Ca^{2+} flux were altered. In contrast, cotransfection of CCR5 and G_{qi5} caused a decrease in EC_{50} values for IP1 accumulation and Ca^{2+} flux for all ligands tested. In addition, coexpression of CCR5 and G_{qi5} led to an increase in E_{max} values for Ca^{2+} flux for all ligands, and an increase in E_{max} values for IP1 accumulation for most ligands tested.

A.5 Discussion

Several GPCR-targeted ligands have been described to cause signaling bias toward β-arrestin or G protein signaling pathways. However, reports of ligands that bias GPCR signaling towards a specific Gα protein class are rare, in part because of the difficulty in interpreting signaling assays in which crosstalk between different G protein signaling pathways occurs. In this study, we determined the specific Gα protein class that was responsible for CCR5-mediated inhibition of cAMP accumulation, Ca^{2+} flux, and IP3 production. Analogs of the endogenous chemokine RANTES with N-terminal modifications showed similar abilities to activate CCR5-mediated $G_{i/o}$ signaling, but either enhanced or decreased abilities to activate CCR5-mediated G_q signaling.

For inhibition of cAMP accumulation, each of the endogenous chemokines and the RANTES analogs tested acted as agonists with similar E_{max} values and EC_{50} values of 2.1 nM or

lower. EC_{50} values at least one order of magnitude higher were obtained earlier from CCR5-transfected CHO cells, which also showed a lack of detectable signal for 5P12 *(146)*. In addition to the use of different cells, the source of variation between these results could be due to the use of different ligand incubation times or different assays to detect cAMP (real-time changes of cAMP in live cells compared with measurement of cAMP after a single incubation time point) *(146)*.

The RANTES analogs showed different abilities to induce Ca^{2+} flux and IP1 accumulation through CCR5. In comparison to the endogenous chemokines RANTES and MIP-1α, the RANTES analogs 6P4 and PSC acted as superagonists, while 5P12 did not have agonist activity in the Ca^{2+} flux assays. Our measurements of EC_{50} and E_{max} values recapitulated the results from Ca^{2+} flux assays performed in CCR5-transfected Hela-P5L and PHA/IL-2-activated T blasts *(141)*. Cells expressing only CCR5 demonstrated IP1 accumulation in response only to PSC whereas CCR5-mediated Ca^{2+} flux was measured in response to RANTES, MIP-1α, 6P4, and PSC. The differences between results when assessing Ca^{2+} flux and IP1 accumulation is likely due to assay sensitivity *(159)*. Of note, the ability of the RANTES analogs to induce CCR5-mediated G_q signaling appears to correlate with their ability to induce β-arrestin recruitment and internalization. Analogous to the Ca^{2+} flux results, only 5P12 was unable to induce CCR5-internalization and β-arrestin recruitment to CCR5 *(160)*. In addition, cells treated with PSC demonstrated the strongest recruitment of β-arrestin to CCR5, followed by RANTES, and then 5P14 *(146, 161, 162)*.

The differences in the signaling profiles of the RANTES analogs suggests that different effectors are responsible for CCR5-mediated inhibition of cAMP accumulation or induction of Ca^{2+} flux. $G_{i/o}$ protein activation inhibits cAMP accumulation, a pathway further confirmed by

our results. 6P4 and PSC can stimulate cAMP production above levels induced by forskolin in the presence of PTX, suggesting that these ligands might also stimulate CCR5-mediated G_s protein activation. The differential regulation of adenylated cyclase subtypes in HEK293 cells could also be the source of this PTX-dependent cAMP production by 6P4 and PSC. Ca^{2+} can activate certain subtypes of adenylate cyclase, causing crosstalk between Ca^{2+} signaling and cAMP production *(163)*. Alternatively, 6P4 and PSC in presence of PTX could inhibit the degradation of forskolin-dependent cAMP, and these ligands would not induce cAMP production in the presence of PTX, but the absence of forskolin.

The Gα protein subunit that is responsible for Ca^{2+} flux and IP3 formation is less clear but could be G_q or $G_{i/o}$. Cotransfection of G_q augments CCR5-mediated Ca^{2+} flux and IP1 accumulation, responses that are inhibited by cotransfection of G_{i2}, which supports the hypothesis that G_q is responsible for Ca^{2+} flux. G_{i2} transfection could inhibit Ca^{2+} flux and IP1 accumulation through CCR5 by either preventing G_q recruitment by competitively binding to CCR5, or by acting as a Gβγ subunit scavenger, which would prevent the formation of heterotrimeric G_q proteins required for G protein activity.

We further differentiated the contributions of $G_{i/o}$ and G_q proteins to CCR5-mediated Ca^{2+} flux and IP3 signaling using inhibitors. The G_q inhibitor YM-254890 prevented all of the RANTES analogs from inducing CCR5-mediated Ca^{2+} flux and IP1 accumulation. However, the ability of PTX to at least partially inhibit Ca^{2+} flux and IP1 accumulation does not support the hypothesis that G_q mediates these signaling pathways through CCR5. This seemingly paradoxical result can be explained by the indirect effect of PTX decreasing binding of chemokines to CCR5 *(138)*. Reduction of agonist affinity is likely due to a reduction of $G_{i/o}$ protein pre-coupling to CCR5. Structural studies of β_2AR interacting with G protein has

confirmed the paradigm that a receptor must be bound to a transducer to stabilize the agonist-receptor interaction *(164)*. Likewise, the conformation of CCR5 molecules on the cellular surface is altered upon PTX-induced abrogation of $G_{i/o}$ pre-coupling *(165)*. Similar to our results, other reports have also described incomplete inhibition of CCR5-mediated Ca^{2+} flux by PTX, suggesting that $G_{i/o}$ plays a role in agonist binding but not in mediating Ca^{2+} flux *(166–168)*. Finally, it is unlikely that Gβγ subunits could induce Ca^{2+} flux in HEK293T cells because the closely related HEK293 cell line does not produce the phospholipase C subunit that links Gβγ release to Ca^{2+} flux *(169)*. Although we cannot rule out a contribution from Gβγ, our data suggest that Ca^{2+} flux signaling through CCR5 in this cellular system is mainly, if not completely, mediated by G_q protein activation.

Chemokine receptors are historically believed to couple to and signal through $G_{i/o}$ proteins exclusively. The Ca^{2+} flux response elicited by many chemokine receptors has been thought to be a result of Gβγ subunit release after activation of $G_{i/o}$ *(153)*. However, we provide evidence that CCR5 signals through both $G_{i/o}$ and $G_{q/11}$ proteins. We also demonstrate that IP1 accumulation and Ca^{2+} flux are products of G_q protein signaling in HEK293T cells. CCR5 mediates PTX-insensitive signaling responses, suggesting the CCR5 couples to and signals through other G proteins *(148, 166, 167)*. Indeed, CCR5 couples to and co-immunoprecipitates with G_q *(170, 171)*. Both G_q and $G_{i/o}$ protein signaling may contribute to the activities of other chemokine receptors. CXCR4 is proposed to switch from $G_{i/o}$ signaling to G_q signaling, leading to reduced migration and activation of the T cells *(148, 172)*. In addition, CXCR4 and CCR7-dependent chemotaxis of dendritic cells requires activation of both $G_{i/o}$ and G_q pathways *(173)*. Theoretically, the capacity of a receptor to couple to certain Gα protein subunits should be apparent from its primary structure. However, although residues in similar positions in different

GPCRs recognize G proteins, other distinct residues also make structural binding contacts. Therefore, without the availability of comparable structures of $G_{i/o}$ and G_q bound to activated GPCRs, it is difficult to surmise whether G_q coupling to other chemokine receptors can be predicted or validated by structural information *(174)*.

The capacity of each chemokine to bind to different conformations of CCR5 likely accounts for apparent differences to induce CCR5-mediated signaling through either $G_{i/o}$- or G_q-dependent pathways. The "spare receptor" concept posits that there are at least two pools of inactive CCR5: receptors pre-coupled to $G_{i/o}$ proteins, and "naked" receptors not pre-coupled to $G_{i/o}$ protein *(138, 175)*. CCR5 can assume multiple conformations, as shown by monoclonal antibody detection of different populations of CCR5 *(176)*. The endogenous chemokines RANTES and MIP-1α bind with high affinity to only $G_{i/o}$ protein-coupled CCR5, whereas PSC has a high affinity for both $G_{i/o}$ protein-coupled CCR5 and naked CCR5 *(138)*. Single molecule binding experiments have also shown that 5P12, 5P14, PSC and 6P4 bind to CCR5 with affinities of 374 pM, 493 pM, 10 nM, and 6.5 nM, respectively, in the absence of G protein. However, MIP-1α and RANTES do not show detectable binding to naked receptor up to concentrations of 10 μM *(177)*. Thus, PSC can activate a subset of CCR5 molecules that remains inactive after stimulation with RANTES *(175)*. The increased Ca^{2+} flux in response to PSC or 6P4 is likely due to the activation of naked CCR5, in addition to $G_{i/o}$-protein pre-coupled CCR5. In line with this hypothesis, PSC and 6P4 do not have substantially lower EC_{50} values than RANTES, but do have higher E_{max} values, suggesting that these chemokines are superagonists because they bind to more receptors, rather than because they bind with higher affinity.

We present a model to contextualize the results of our experiments and hypothesize about how RANTES analogs are capable of showing G protein-subtype specific signaling bias (Figure

A-6A). For RANTES and MIP-1α, $G_{i/o}$ subunit pre-coupling promotes binding of the ligand to the receptor, upon which $G_{i/o}$ is activated and dissociates from the receptor. A ligand that remains bound to the receptor can recruit and activate G_q or additional $G_{i/o}$ proteins. In contrast to RANTES and MIP-1α, PSC and 6P4 can bind to and activate CCR5-dependent signaling pathways, independently of whether the receptor is pre-coupled to $G_{i/o}$ or naked. By signaling through two pools of the receptor, PSC and 6P4 can produce more signal and thus act as superagonists. Although not apparent from our data, 5P12 binds to CCR5 in a G-protein independent fashion *(138)* and thus, binding of 5P12 to naked CCR5 preferentially activates $G_{i/o}$ (Figure A-6B) .

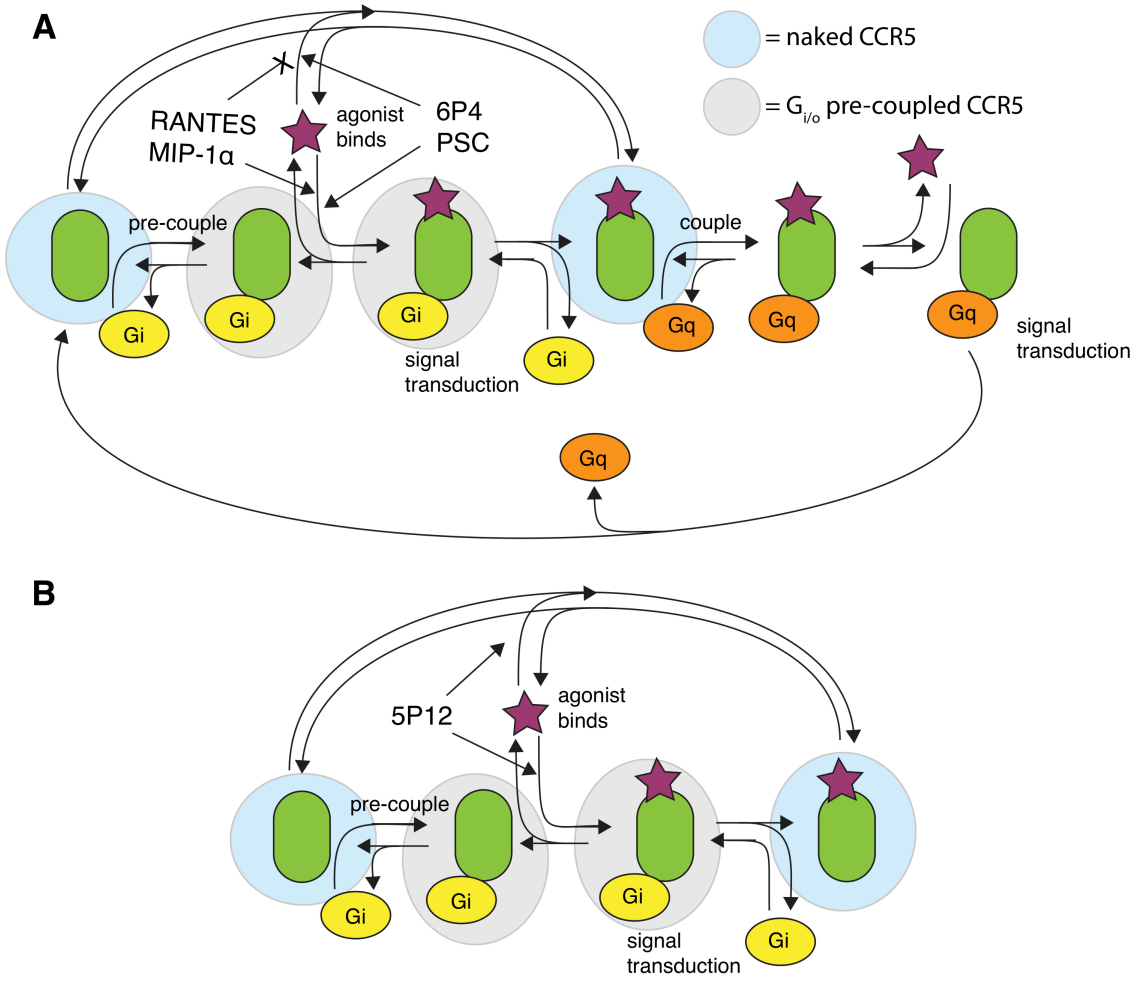

Figure A-6. Conceptual model depicting CCR5-mediated signaling through $G_{i/o}$ and G_q by endogenous chemokines and RANTES analogs. The CCR5 receptor exists in at least two populations, with a group of CCR5 molecules pre-coupled to $G_{i/o}$ (grey background) and another group in an uncoupled, or "naked" state (blue background). (**A**) RANTES and MIP-1α bind only to $G_{i/o}$-precoupled CCR5, which then leads to activation of $G_{i/o}$. Following activation of $G_{i/o}$, CCR5 then can recruit and activate G_q. 6P4 and PSC bind to both $G_{i/o}$-precoupled CCR5 and naked CCR5. Thus, activation of G_q protein occurs independently of $G_{i/o}$ proteins. (**B**) 5P12 binds to both $G_{i/o}$-precoupled CCR5 and naked CCR5, but binding leads to activation of $G_{i/o}$ only.

This study demonstrates a type of ligand bias that is G protein family specific. Another peptide receptor, pituitary adenylate cyclase-activating polypeptide (PACAP) receptor, responds to the two ligands PACAP-38 and PACAP-27 with similar EC_{50} values for the G_s signaling pathway. However, the two PACAP receptor ligands have EC_{50} values that are 100-fold different for a G_q signaling pathway *(178)*. The free fatty acid receptors (FFAR) also signal through multiple G protein families, but depending on the activating ligand, the FFARs can selectively signal through a single G protein family. For example, synthetic agonists targeting FFAR1 can signal through both G_q and G_s, whereas the endogenous agonists signal only through G_q *(179)*. In addition, an allosteric modulator targeting FFAR2 selectively activates $G_{i/o}$ signaling but not G_q signaling *(180)*. In our study, we described chemokines with similar capacity to evoke CCR5-mediated $G_{i/o}$ signaling, but with both diminished and enhanced G_q signaling.

How the modification of the N-terminal region of RANTES leads to such pronounced changes in CCR5-mediated G_q signaling, but not $G_{i/o}$ signaling, is unclear. Nonetheless, some insight can be garnered from crystal structures of CCR5, including CCR5 in complex with 5P7, another RANTES analog *(181, 182)*. 5P7 differs from 5P12 by one amino acid, Thr instead of Leu at position 7, and lacks agonist activity for Ca^{2+} flux *(141)*. When comparing the crystal structure of 5P7 to a model of CCR5 with RANTES, several different interactions are apparent that could be key for G_q protein activation. Whereas RANTES has polar residues in positions 4 to 7 that can engage a minor pocket polar network, 5P7 has bulky hydrophobic residues at these positions. Similarly, the G_q-inactive RANTES analogs 5P12 and 5P14 have bulky hydrophobic residues at positions 4 to 7, whereas the superagonist PSC has polar residues. However, the superagonist 6P4 has mostly less-bulky hydrophobic amino acids at these positions. A crystal

structure of CCR5 engaged with a superagonist will be necessary to understand precisely how G_q signaling is modulated by changes in the N-terminal sequences of RANTES.

The RANTES analogs 5P12 and 5P14, which fail to activate G_q, may be safer drugs because they discriminate between $G_{i/o}$ and G_q protein activation. In bypassing G_q signaling, several physiological effects of CCR5 activation that are PTX-resistant or downstream of Ca^{2+} flux would be avoided, including CCR5 recruitment to the immunological synapse during T cell stimulation *(148)*. In addition, an in vitro predictor of an inflammatory response, chemotaxis, requires additional GPCR signaling because $G_{i/o}$ signaling is necessary, but not sufficient, to induce chemotaxis *(154)*. Because Ca^{2+} flux is necessary for actin rearrangement, an important step in chemotaxis, it is plausible that this additional signaling component is G_q activation *(183)*. Although the RANTES chemokines have not been compared in their ability to induce chemotaxis, PSC does cause chemotaxis of CD4 T-cells *(138)*. The contribution of these two signaling arms to the physiological effects of CCR5 activation remain unknown. Thus, these RANTES analogs could serve as tools to determine the effects of $G_{i/o}$ signaling alone compared with G_q and $G_{i/o}$ protein signaling in combination. Future studies should utilize these chemokine analogs to determine how CCR5-mediated $G_{i/o}$ and G_q signaling affect events such as chemotaxis and T cell activation using physiologically-relevant cell types.

In conclusion, we investigated G protein subtype-specific biased signaling of the chemokine receptor CCR5 using a series of chemokine analogs developed as HIV-1 microbicides. Using a specific inhibitor, we found that $G_{q/11}$ is responsible for Ca^{2+} flux downstream of CCR5 in HEK293T cells, which earlier had been attributed to Gβγ subunit released from $G_{i/o}$. RANTES analogs had a wide range of efficacy for CCR5-mediated G_q signaling, but similar $G_{i/o}$ signaling efficacy, opening the possibility for selectively tuning

chemokine signaling. Non-canonical $G_{q/11}$ signaling bias in the chemokine receptor network to our knowledge has not been previously reported. Our findings also provide an experimental strategy in which a G_q-specific inhibitor is used to study G_q signaling bias relevant to Ca^{2+} flux signals from GPCRs thought to couple to $G_{i/o}$.

APPENDIX B: List of Publications

Listed below are all publications I contributed to during my PhD and QR codes to link. Not all the publications were discussed in this thesis. (184–186)

E. Lorenzen, T. Dodig-Crnković, I. B. Kotliar, E. Pin, E. Ceraudo, R. D. Vaughan, M. Uhlèn, T. Huber, J. M. Schwenk, T. P. Sakmar, Multiplexed analysis of the secretin-like GPCR-RAMP interactome, Sci. Adv. 5, eaaw2778 (2019).

Contributions: Designed and performed experiments, analyzed the data, wrote the manuscript.

E. Lorenzen, E. Ceraudo, Y. A. Berchiche, C. A. Rico, A. Fürstenberg, T. P. Sakmar, T. Huber, G protein subtype-specific signaling bias in a series of CCR5 chemokine analogs., Sci. Signal. 11 (2018).

Contributions: Designed and performed experiments, analyzed the data, wrote the manuscript.

E. Lorenzen, T. P. Sakmar, Receptor structures for a cauldron of cannabinoids., Cell 176, 409–411 (2019).

Contributions: Created the figure and edited the manuscript.

S. Barbash, **E. Lorenzen,** T. Persson, T. Huber, T. P. Sakmar, GPCRs globally coevolved with receptor activity-modifying proteins, RAMPs., Proc. Natl. Acad. Sci. USA 114, 12015–12020 (2017).

Contributions: Designed and performed experiments, analyzed the data, wrote the manuscript.

S. Barbash, T. Persson, **E. Lorenzen,** M. A. Kazmi, T. Huber, T. P. Sakmar, Detection of Concordance between Transcriptional Levels of GPCRs and Receptor-Activity-Modifying Proteins., iScience 11, 366–374 (2019).

Contributions: Designed experiments.

C. A. Rico, Y. A. Berchiche, M. Horioka, J. C. Peeler, **E. Lorenzen,** H. Tian, M. A. Kazmi, A. Fürstenberg, H. Gaertner, O. Hartley, T. P. Sakmar, T. Huber, High-Affinity Binding of Chemokine Analogs that Display Ligand Bias at the HIV-1 Coreceptor CCR5., Biophys. J. (2019).

Contributions: Designed and performed experiments, analyzed the data.

REFERENCES

1. R. A. Dixon, B. K. Kobilka, D. J. Strader, J. L. Benovic, H. G. Dohlman, T. Frielle, M. A. Bolanowski, C. D. Bennett, E. Rands, R. E. Diehl, R. A. Mumford, E. E. Slater, I. S. Sigal, M. G. Caron, R. J. Lefkowitz, C. D. Strader, Cloning of the gene and cDNA for mammalian beta-adrenergic receptor and homology with rhodopsin., *Nature* **321**, 75–79 (1986).

2. P. A. Hargrave, J. H. McDowell, D. R. Curtis, J. K. Wang, E. Juszczak, S. L. Fong, J. K. Rao, P. Argos, The structure of bovine rhodopsin., *Biophys Struct Mech* **9**, 235–244 (1983).

3. J. Gocayne, D. A. Robinson, M. G. FitzGerald, F. Z. Chung, A. R. Kerlavage, K. U. Lentes, J. Lai, C. D. Wang, C. M. Fraser, J. C. Venter, Primary structure of rat cardiac beta-adrenergic and muscarinic cholinergic receptors obtained by automated DNA sequence analysis: further evidence for a multigene family., *Proc. Natl. Acad. Sci. USA* **84**, 8296–8300 (1987).

4. F. Z. Chung, K. U. Lentes, J. Gocayne, M. Fitzgerald, D. Robinson, A. R. Kerlavage, C. M. Fraser, J. C. Venter, Cloning and sequence analysis of the human brain beta-adrenergic receptor. Evolutionary relationship to rodent and avian beta-receptors and porcine muscarinic receptors., *FEBS Lett.* **211**, 200–206 (1987).

5. K. Fukuda, T. Kubo, I. Akiba, A. Maeda, M. Mishina, S. Numa, Molecular distinction between muscarinic acetylcholine receptor subtypes., *Nature* **327**, 623–625 (1987).

6. Y. Masu, K. Nakayama, H. Tamaki, Y. Harada, M. Kuno, S. Nakanishi, cDNA cloning of bovine substance-K receptor through oocyte expression system., *Nature* **329**, 836–838 (1987).

7. R. J. Lefkowitz, Historical review: a brief history and personal retrospective of seven-transmembrane receptors., *Trends Pharmacol. Sci.* **25**, 413–422 (2004).

8. S. Takeda, S. Kadowaki, T. Haga, H. Takaesu, S. Mitaku, Identification of G protein-coupled receptor genes from the human genome sequence., *FEBS Lett.* **520**, 97–101 (2002).

9. P. M. Lenhart, S. Broselid, C. J. Barrick, L. M. F. Leeb-Lundberg, K. M. Caron, G-protein-coupled receptor 30 interacts with receptor activity-modifying protein 3 and confers sex-dependent cardioprotection., *J. Mol. Endocrinol.* **51**, 191–202 (2013).

10. V. V. Gurevich, E. V. Gurevich, GPCR signaling regulation: the role of grks and arrestins., *Front. Pharmacol.* **10**, 125 (2019).

11. N. R. Latorraca, A. J. Venkatakrishnan, R. O. Dror, GPCR dynamics: structures in motion., *Chem. Rev.* **117**, 139–155 (2017).

12. J. D. Violin, A. L. Crombie, D. G. Soergel, M. W. Lark, Biased ligands at G-protein-coupled

receptors: promise and progress., *Trends Pharmacol. Sci.* **35**, 308–316 (2014).

13. E. Lorenzen, E. Ceraudo, Y. A. Berchiche, C. A. Rico, A. Fürstenberg, T. P. Sakmar, T. Huber, G protein subtype-specific signaling bias in a series of CCR5 chemokine analogs., *Sci. Signal.* **11** (2018), doi:10.1126/scisignal.aao6152.

14. R. Fredriksson, H. B. Schiöth, The repertoire of G-protein-coupled receptors in fully sequenced genomes., *Mol. Pharmacol.* **67**, 1414–1425 (2005).

15. S. Montaner, I. Kufareva, R. Abagyan, J. S. Gutkind, Molecular mechanisms deployed by virally encoded G protein-coupled receptors in human diseases., *Annu. Rev. Pharmacol. Toxicol.* **53**, 331–354 (2013).

16. M. Versele, K. Lemaire, J. M. Thevelein, Sex and sugar in yeast: two distinct GPCR systems., *EMBO Rep.* **2**, 574–579 (2001).

17. R. Strotmann, K. Schröck, I. Böselt, C. Stäubert, A. Russ, T. Schöneberg, Evolution of GPCR: change and continuity., *Mol. Cell. Endocrinol.* **331**, 170–178 (2011).

18. A. de Mendoza, A. Sebé-Pedrós, I. Ruiz-Trillo, The evolution of the GPCR signaling system in eukaryotes: modularity, conservation, and the transition to metazoan multicellularity., *Genome Biol. Evol.* **6**, 606–619 (2014).

19. R. Fredriksson, M. C. Lagerström, L.-G. Lundin, H. B. Schiöth, The G-protein-coupled receptors in the human genome form five main families. Phylogenetic analysis, paralogon groups, and fingerprints., *Mol. Pharmacol.* **63**, 1256–1272 (2003).

20. R. Nusse, H. Clevers, Wnt/β-Catenin Signaling, Disease, and Emerging Therapeutic Modalities., *Cell* **169**, 985–999 (2017).

21. R. C. Stevens, V. Cherezov, V. Katritch, R. Abagyan, P. Kuhn, H. Rosen, K. Wüthrich, The GPCR Network: a large-scale collaboration to determine human GPCR structure and function., *Nat. Rev. Drug Discov.* **12**, 25–34 (2013).

22. A. S. Hauser, M. M. Attwood, M. Rask-Andersen, H. B. Schiöth, D. E. Gloriam, Trends in GPCR drug discovery: new agents, targets and indications., *Nat. Rev. Drug Discov.* **16**, 829–842 (2017).

23. A. Fang, S. Zhou, X. Su, C. Liu, X. Chen, Y. Wan, X. Lei, L. Xie, Y. Jia, W. Wang, L. Yang, X. Song, Y. Yao, RAMP3 is a prognostic indicator of liver cancer and might reduce the adverse effect of TP53 mutation on survival., *Future Oncol* **14**, 2615–2625 (2018).

24. C. J. Hutchings, M. Koglin, W. C. Olson, F. H. Marshall, Opportunities for therapeutic

antibodies directed at G-protein-coupled receptors., *Nat. Rev. Drug Discov.* **16**, 787–810 (2017).

25. S. C. Erlandson, C. McMahon, A. C. Kruse, Structural Basis for G Protein-Coupled Receptor Signaling., *Annu. Rev. Biophys.* (2018), doi:10.1146/annurev-biophys-070317-032931.

26. D. K. Grammatopoulos, Regulation of G-protein coupled receptor signalling underpinning neurobiology of mood disorders and depression., *Mol. Cell. Endocrinol.* **449**, 82–89 (2017).

27. D. M. Riddy, P. Delerive, R. J. Summers, P. M. Sexton, C. J. Langmead, G Protein-Coupled Receptors Targeting Insulin Resistance, Obesity, and Type 2 Diabetes Mellitus., *Pharmacol. Rev.* **70**, 39–67 (2018).

28. A. Nieto Gutierrez, P. H. McDonald, GPCRs: Emerging anti-cancer drug targets., *Cell Signal.* **41**, 65–74 (2018).

29. Y. Liu, S. An, R. Ward, Y. Yang, X.-X. Guo, W. Li, T.-R. Xu, G protein-coupled receptors as promising cancer targets., *Cancer Lett.* **376**, 226–239 (2016).

30. A. R. Moore, E. Ceraudo, J. J. Sher, Y. Guan, A. N. Shoushtari, M. T. Chang, J. Q. Zhang, E. G. Walczak, M. A. Kazmi, B. S. Taylor, T. Huber, P. Chi, T. P. Sakmar, Y. Chen, Recurrent activating mutations of G-protein-coupled receptor CYSLTR2 in uveal melanoma., *Nat. Genet.* **48**, 675–680 (2016).

31. D. O. Borroto-Escuela, I. Brito, W. Romero-Fernandez, M. Di Palma, J. Oflijan, K. Skieterska, J. Duchou, K. Van Craenenbroeck, D. Suárez-Boomgaard, A. Rivera, D. Guidolin, L. F. Agnati, K. Fuxe, The G protein-coupled receptor heterodimer network (GPCR-HetNet) and its hub components., *Int. J. Mol. Sci.* **15**, 8570–8590 (2014).

32. M. R. Whorton, M. P. Bokoch, S. G. F. Rasmussen, B. Huang, R. N. Zare, B. Kobilka, R. K. Sunahara, A monomeric G protein-coupled receptor isolated in a high-density lipoprotein particle efficiently activates its G protein., *Proc. Natl. Acad. Sci. USA* **104**, 7682–7687 (2007).

33. O. P. Ernst, V. Gramse, M. Kolbe, K. P. Hofmann, M. Heck, Monomeric G protein-coupled receptor rhodopsin in solution activates its G protein transducin at the diffusion limit., *Proc. Natl. Acad. Sci. USA* **104**, 10859–10864 (2007).

34. T. H. Bayburt, A. J. Leitz, G. Xie, D. D. Oprian, S. G. Sligar, Transducin activation by nanoscale lipid bilayers containing one and two rhodopsins., *J. Biol. Chem.* **282**, 14875–14881 (2007).

35. H. Tsukamoto, A. Sinha, M. DeWitt, D. L. Farrens, Monomeric rhodopsin is the minimal functional unit required for arrestin binding., *J. Mol. Biol.* **399**, 501–511 (2010).

36. S. Ferré, V. Casadó, L. A. Devi, M. Filizola, R. Jockers, M. J. Lohse, G. Milligan, J.-P. Pin, X. Guitart, G protein-coupled receptor oligomerization revisited: functional and pharmacological perspectives., *Pharmacol. Rev.* **66**, 413–434 (2014).

37. I. Gomes, W. Fujita, M. V. Chandrakala, L. A. Devi, Disease-specific heteromerization of G-protein-coupled receptors that target drugs of abuse., *Prog Mol Biol Transl Sci* **117**, 207–265 (2013).

38. S. Ferré, C. Lluis, J. L. Lanciego, R. Franco, Prime time for G-protein-coupled receptor heteromers as therapeutic targets for CNS disorders: the dopamine D_1-D_3 receptor heteromer., *CNS Neurol Disord Drug Targets* **9**, 596–600 (2010).

39. L. Achour, C. Labbé-Jullié, M. G. H. Scott, S. Marullo, An escort for GPCRs: implications for regulation of receptor density at the cell surface., *Trends Pharmacol. Sci.* **29**, 528–535 (2008).

40. L. Edvinsson, K. A. Haanes, K. Warfvinge, D. N. Krause, CGRP as the target of new migraine therapies - successful translation from bench to clinic., *Nat. Rev. Neurol.* **14**, 338–350 (2018).

41. L. M. McLatchie, N. J. Fraser, M. J. Main, A. Wise, J. Brown, N. Thompson, R. Solari, M. G. Lee, S. M. Foord, RAMPs regulate the transport and ligand specificity of the calcitonin-receptor-like receptor., *Nature* **393**, 333–339 (1998).

42. K. Husmann, W. Born, J. A. Fischer, R. Muff, Three receptor-activity-modifying proteins define calcitonin gene-related peptide or adrenomedullin selectivity of the mouse calcitonin-like receptor in COS-7 cells., *Biochem. Pharmacol.* **66**, 2107–2115 (2003).

43. S. Hilairet, S. M. Foord, F. H. Marshall, M. Bouvier, Protein-protein interaction and not glycosylation determines the binding selectivity of heterodimers between the calcitonin receptor-like receptor and the receptor activity-modifying proteins., *J. Biol. Chem.* **276**, 29575–29581 (2001).

44. G. Christopoulos, K. J. Perry, M. Morfis, N. Tilakaratne, Y. Gao, N. J. Fraser, M. J. Main, S. M. Foord, P. M. Sexton, Multiple amylin receptors arise from receptor activity-modifying protein interaction with the calcitonin receptor gene product., *Mol. Pharmacol.* **56**, 235–242 (1999).

45. S. L. Armour, S. Foord, T. Kenakin, W.-J. Chen, Pharmacological characterization of receptor-activity-modifying proteins (RAMPs) and the human calcitonin receptor, *J. Pharmacol. Toxicol. Methods* **42**, 217–224 (1999).

46. S. Kusano, M. Kukimoto-Niino, N. Hino, N. Ohsawa, K. Okuda, K. Sakamoto, M. Shirouzu,

T. Shindo, S. Yokoyama, Structural basis for extracellular interactions between calcitonin receptor-like receptor and receptor activity-modifying protein 2 for adrenomedullin-specific binding., *Protein Sci.* **21**, 199–210 (2012).

47. E. ter Haar, C. M. Koth, N. Abdul-Manan, L. Swenson, J. T. Coll, J. A. Lippke, C. A. Lepre, M. Garcia-Guzman, J. M. Moore, Crystal structure of the ectodomain complex of the CGRP receptor, a class-B GPCR, reveals the site of drug antagonism., *Structure* **18**, 1083–1093 (2010).

48. J. M. Booe, C. S. Walker, J. Barwell, G. Kuteyi, J. Simms, M. A. Jamaluddin, M. L. Warner, R. M. Bill, P. W. Harris, M. A. Brimble, D. R. Poyner, D. L. Hay, A. A. Pioszak, Structural Basis for Receptor Activity-Modifying Protein-Dependent Selective Peptide Recognition by a G Protein-Coupled Receptor., *Mol. Cell* **58**, 1040–1052 (2015).

49. Y.-L. Liang, M. Khoshouei, G. Deganutti, A. Glukhova, C. Koole, T. S. Peat, M. Radjainia, J. M. Plitzko, W. Baumeister, L. J. Miller, D. L. Hay, A. Christopoulos, C. A. Reynolds, D. Wootten, P. M. Sexton, Cryo-EM structure of the active, Gs-protein complexed, human CGRP receptor., *Nature* **561**, 492–497 (2018).

50. C. Weston, J. Lu, N. Li, K. Barkan, G. O. Richards, D. J. Roberts, T. M. Skerry, D. Poyner, M. Pardamwar, C. A. Reynolds, S. J. Dowell, G. B. Willars, G. Ladds, Modulation of Glucagon Receptor Pharmacology by Receptor Activity-modifying Protein-2 (RAMP2)., *J. Biol. Chem.* **290**, 23009–23022 (2015).

51. J. Cegla, B. J. Jones, J. V. Gardiner, D. J. Hodson, T. Marjot, E. R. McGlone, T. M. Tan, S. R. Bloom, RAMP2 influences glucagon receptor pharmacology via trafficking and signaling., *Endocrinology* **158**, 2680–2693 (2017).

52. D. L. Wootten, J. Simms, D. L. Hay, A. Christopoulos, P. M. Sexton, in *Membrane Proteins as Drug Targets*, Progress in Molecular Biology and Translational Science. (Elsevier, 2010), vol. 91, pp. 53–79.

53. S. Bailey, M. Harris, K. Barkan, I. Winfield, M. T. Harper, J. Simms, G. Ladds, M. Wheatley, D. Poyner, Interactions between RAMP2 and CRF receptors: The effect of receptor subtypes, splice variants and cell context., *Biochim. Biophys. Acta Biomembr.* **1861**, 997–1003 (2019).

54. A. Christopoulos, G. Christopoulos, M. Morfis, M. Udawela, M. Laburthe, A. Couvineau, K. Kuwasako, N. Tilakaratne, P. M. Sexton, Novel receptor partners and function of receptor activity-modifying proteins., *J. Biol. Chem.* **278**, 3293–3297 (2003).

55. D. Wootten, H. Lindmark, M. Kadmiel, H. Willcockson, K. M. Caron, J. Barwell, T. Drmota, D. R. Poyner, Receptor activity modifying proteins (RAMPs) interact with the VPAC2 receptor and CRF1 receptors and modulate their function., *Br. J. Pharmacol.* **168**, 822–834 (2013).

56. K. G. Harikumar, J. Simms, G. Christopoulos, P. M. Sexton, L. J. Miller, Molecular basis of association of receptor activity-modifying protein 3 with the family B G protein-coupled secretin receptor., *Biochemistry* **48**, 11773–11785 (2009).

57. T. Bouschet, S. Martin, J. M. Henley, Receptor-activity-modifying proteins are required for forward trafficking of the calcium-sensing receptor to the plasma membrane., *J. Cell Sci.* **118**, 4709–4720 (2005).

58. A. J. Desai, D. J. Roberts, G. O. Richards, T. M. Skerry, Role of receptor activity modifying protein 1 in function of the calcium sensing receptor in the human TT thyroid carcinoma cell line., *PLoS One* **9**, e85237 (2014).

59. T. Bouschet, S. Martin, J. M. Henley, Regulation of calcium-sensing-receptor trafficking and cell-surface expression by GPCRs and RAMPs., *Trends Pharmacol. Sci.* **29**, 633–639 (2008).

60. J. M. Bomberger, N. Parameswaran, C. S. Hall, N. Aiyar, W. S. Spielman, Novel function for receptor activity-modifying proteins (RAMPs) in post-endocytic receptor trafficking., *J. Biol. Chem.* **280**, 9297–9307 (2005).

61. J. M. Bomberger, W. S. Spielman, C. S. Hall, E. J. Weinman, N. Parameswaran, Receptor activity-modifying protein (RAMP) isoform-specific regulation of adrenomedullin receptor trafficking by NHERF-1., *J. Biol. Chem.* **280**, 23926–23935 (2005).

62. M. Morfis, N. Tilakaratne, S. G. B. Furness, G. Christopoulos, T. D. Werry, A. Christopoulos, P. M. Sexton, Receptor activity-modifying proteins differentially modulate the G protein-coupling efficiency of amylin receptors., *Endocrinology* **149**, 5423–5431 (2008).

63. M. Li, S. E. Wetzel-Strong, X. Hua, S. L. Tilley, E. Oswald, M. F. Krummel, K. M. Caron, Deficiency of RAMP1 attenuates antigen-induced airway hyperresponsiveness in mice., *PLoS One* **9**, e102356 (2014).

64. K. Tsujikawa, K. Yayama, T. Hayashi, H. Matsushita, T. Yamaguchi, T. Shigeno, Y. Ogitani, M. Hirayama, T. Kato, S. Fukada, S. Takatori, H. Kawasaki, H. Okamoto, M. Ikawa, M. Okabe, H. Yamamoto, Hypertension and dysregulated proinflammatory cytokine production in receptor activity-modifying protein 1-deficient mice., *Proc. Natl. Acad. Sci. USA* **104**, 16702–16707 (2007).

65. J. B. Pawlak, S. E. Wetzel-Strong, M. K. Dunn, K. M. Caron, Cardiovascular effects of exogenous adrenomedullin and CGRP in Ramp and Calcrl deficient mice., *Peptides* **88**, 1–7 (2017).

66. Z. Zhang, C. S. Winborn, B. Marquez de Prado, A. F. Russo, Sensitization of calcitonin gene-related peptide receptors by receptor activity-modifying protein-1 in the trigeminal

ganglion., *J. Neurosci.* **27**, 2693–2703 (2007).

67. S. J. Tepper, History and Review of anti-Calcitonin Gene-Related Peptide (CGRP) Therapies: From Translational Research to Treatment., *Headache* **58 Suppl 3**, 238–275 (2018).

68. U. Reuter, P. J. Goadsby, M. Lanteri-Minet, S. Wen, P. Hours-Zesiger, M. D. Ferrari, J. Klatt, Efficacy and tolerability of erenumab in patients with episodic migraine in whom two-to-four previous preventive treatments were unsuccessful: a randomised, double-blind, placebo-controlled, phase 3b study., *Lancet* **392**, 2280–2287 (2018).

69. T. Yoshizawa, T. Sakurai, A. Kamiyoshi, Y. Ichikawa-Shindo, H. Kawate, Y. Iesato, T. Koyama, R. Uetake, L. Yang, A. Yamauchi, M. Tanaka, Y. Toriyama, K. Igarashi, T. Nakada, T. Kashihara, M. Yamada, H. Kawakami, H. Nakanishi, R. Taguchi, T. Nakanishi, H. Akazawa, T. Shindo, Novel regulation of cardiac metabolism and homeostasis by the adrenomedullin-receptor activity-modifying protein 2 system., *Hypertension* **61**, 341–351 (2013).

70. D. O. Kechele, W. P. Dunworth, C. E. Trincot, S. E. Wetzel-Strong, M. Li, H. Ma, J. Liu, K. M. Caron, Endothelial Restoration of Receptor Activity-Modifying Protein 2 Is Sufficient to Rescue Lethality, but Survivors Develop Dilated Cardiomyopathy., *Hypertension* **68**, 667–677 (2016).

71. T. Koyama, L. Ochoa-Callejero, T. Sakurai, A. Kamiyoshi, Y. Ichikawa-Shindo, N. Iinuma, T. Arai, T. Yoshizawa, Y. Iesato, Y. Lei, R. Uetake, A. Okimura, A. Yamauchi, M. Tanaka, K. Igarashi, Y. Toriyama, H. Kawate, R. H. Adams, H. Kawakami, N. Mochizuki, A. Martínez, T. Shindo, Vascular endothelial adrenomedullin-RAMP2 system is essential for vascular integrity and organ homeostasis., *Circulation* **127**, 842–853 (2013).

72. R. Dackor, K. Fritz-Six, O. Smithies, K. Caron, Receptor activity-modifying proteins 2 and 3 have distinct physiological functions from embryogenesis to old age., *J. Biol. Chem.* **282**, 18094–18099 (2007).

73. Y. Ichikawa-Shindo, T. Sakurai, A. Kamiyoshi, H. Kawate, N. Iinuma, T. Yoshizawa, T. Koyama, J. Fukuchi, S. Iimuro, N. Moriyama, H. Kawakami, T. Murata, K. Kangawa, R. Nagai, T. Shindo, The GPCR modulator protein RAMP2 is essential for angiogenesis and vascular integrity., *J. Clin. Invest.* **118**, 29–39 (2008).

74. A. Yamauchi, T. Sakurai, A. Kamiyoshi, Y. Ichikawa-Shindo, H. Kawate, K. Igarashi, Y. Toriyama, M. Tanaka, T. Liu, X. Xian, A. Imai, L. Zhai, S. Owa, T. Arai, T. Shindo, Functional differentiation of RAMP2 and RAMP3 in their regulation of the vascular system., *J. Mol. Cell Cardiol.* **77**, 73–85 (2014).

75. C. J. Barrick, P. M. Lenhart, R. T. Dackor, E. Nagle, K. M. Caron, Loss of receptor activity-modifying protein 3 exacerbates cardiac hypertrophy and transition to heart failure in a sex-dependent manner., *J. Mol. Cell Cardiol.* **52**, 165–174 (2012).

76. K. M. Caron, O. Smithies, Extreme hydrops fetalis and cardiovascular abnormalities in mice lacking a functional Adrenomedullin gene., *Proc. Natl. Acad. Sci. USA* **98**, 615–619 (2001).

77. M. Kadmiel, B. C. Matson, S. T. Espenschied, P. M. Lenhart, K. M. Caron, Loss of receptor activity-modifying protein 2 in mice causes placental dysfunction and alters PTH1R regulation., *PLoS One* **12**, e0181597 (2017).

78. M. Kadmiel, K. Fritz-Six, S. Pacharne, G. O. Richards, M. Li, T. M. Skerry, K. M. Caron, Research resource: Haploinsufficiency of receptor activity-modifying protein-2 (RAMP2) causes reduced fertility, hyperprolactinemia, skeletal abnormalities, and endocrine dysfunction in mice., *Mol. Endocrinol.* **25**, 1244–1253 (2011).

79. K. R. Klein, N. O. Karpinich, S. T. Espenschied, H. H. Willcockson, W. P. Dunworth, S. L. Hoopes, E. J. Kushner, V. L. Bautch, K. M. Caron, Decoy receptor CXCR7 modulates adrenomedullin-mediated cardiac and lymphatic vascular development., *Dev. Cell* **30**, 528–540 (2014).

80. A. M. Altenhoff, N. Škunca, N. Glover, C.-M. Train, A. Sueki, I. Piližota, K. Gori, B. Tomiczek, S. Müller, H. Redestig, G. H. Gonnet, C. Dessimoz, The OMA orthology database in 2015: function predictions, better plant support, synteny view and other improvements., *Nucleic Acids Res.* **43**, D240-9 (2015).

81. T. M. W. Nye, P. Liò, W. R. Gilks, A novel algorithm and web-based tool for comparing two alternative phylogenetic trees., *Bioinformatics* **22**, 117–119 (2006).

82. F. Pazos, J. A. G. Ranea, D. Juan, M. J. E. Sternberg, Assessing protein co-evolution in the context of the tree of life assists in the prediction of the interactome., *J. Mol. Biol.* **352**, 1002–1015 (2005).

83. T. N. Petersen, S. Brunak, G. von Heijne, H. Nielsen, SignalP 4.0: discriminating signal peptides from transmembrane regions., *Nat. Methods* **8**, 785–786 (2011).

84. M. Leduc, B. Breton, C. Galés, C. Le Gouill, M. Bouvier, S. Chemtob, N. Heveker, Functional selectivity of natural and synthetic prostaglandin EP4 receptor ligands., *J. Pharmacol. Exp. Ther.* **331**, 297–307 (2009).

85. K. Drobin, P. Nilsson, J. M. Schwenk, Highly multiplexed antibody suspension bead arrays for plasma protein profiling., *Methods Mol. Biol.* **1023**, 137–145 (2013).

86. M. Wilhelm, J. Schlegl, H. Hahne, A. M. Gholami, M. Lieberenz, M. M. Savitski, E. Ziegler, L. Butzmann, S. Gessulat, H. Marx, T. Mathieson, S. Lemeer, K. Schnatbaum, U. Reimer, H. Wenschuh, M. Mollenhauer, J. Slotta-Huspenina, J.-H. Boese, M. Bantscheff, A. Gerstmair, F. Faerber, B. Kuster, Mass-spectrometry-based draft of the human proteome., *Nature* **509**, 582–

587 (2014).

87. N. Bhardwaj, H. Lu, Correlation between gene expression profiles and protein-protein interactions within and across genomes., *Bioinformatics* **21**, 2730–2738 (2005).

88. I. Tirosh, N. Barkai, Computational verification of protein-protein interactions by orthologous co-expression., *BMC Bioinformatics* **6**, 40 (2005).

89. M. Pellegrini, E. M. Marcotte, M. J. Thompson, D. Eisenberg, T. O. Yeates, Assigning protein functions by comparative genome analysis: protein phylogenetic profiles., *Proc. Natl. Acad. Sci. USA* **96**, 4285–4288 (1999).

90. G. W. Clark, V.-U.-N. Dar, A. Bezginov, J. M. Yang, R. L. Charlebois, E. R. M. Tillier, Using coevolution to predict protein-protein interactions., *Methods Mol. Biol.* **781**, 237–256 (2011).

91. L. Salwinski, C. S. Miller, A. J. Smith, F. K. Pettit, J. U. Bowie, D. Eisenberg, The Database of Interacting Proteins: 2004 update., *Nucleic Acids Res.* **32**, D449-51 (2004).

92. W. R. Moyle, R. K. Campbell, R. V. Myers, M. P. Bernard, Y. Han, X. Wang, Co-evolution of ligand-receptor pairs., *Nature* **368**, 251–255 (1994).

93. N. Parameswaran, W. S. Spielman, RAMPs: The past, present and future., *Trends Biochem. Sci.* **31**, 631–638 (2006).

94. GTEx Consortium, Human genomics. The Genotype-Tissue Expression (GTEx) pilot analysis: multitissue gene regulation in humans., *Science* **348**, 648–660 (2015).

95. C. Evans, J. Hardin, D. M. Stoebel, Selecting between-sample RNA-Seq normalization methods from the perspective of their assumptions., *Brief. Bioinformatics* **19**, 776–792 (2018).

96. K. D. Hansen, R. A. Irizarry, Z. Wu, Removing technical variability in RNA-seq data using conditional quantile normalization., *Biostatistics* **13**, 204–216 (2012).

97. D. L. Hay, A. A. Pioszak, Receptor Activity-Modifying Proteins (RAMPs): New Insights and Roles., *Annu. Rev. Pharmacol. Toxicol.* **56**, 469–487 (2016).

98. S. Henikoff, J. G. Henikoff, Amino acid substitution matrices from protein blocks., *Proc. Natl. Acad. Sci. USA* **89**, 10915–10919 (1992).

99. T. H. Jukes, C. R. Cantor, in *Mammalian Protein Metabolism*, (Elsevier, 1969), pp. 21–132.

100. S. M. Foord, S. D. Topp, M. Abramo, J. D. Holbrook, New methods for researching accessory proteins., *J. Mol. Neurosci.* **26**, 265–276 (2005).

101. S. Fields, O. Song, A novel genetic system to detect protein-protein interactions., *Nature* **340**, 245–246 (1989).

102. A.-C. Gavin, M. Bösche, R. Krause, P. Grandi, M. Marzioch, A. Bauer, J. Schultz, J. M. Rick, A.-M. Michon, C.-M. Cruciat, M. Remor, C. Höfert, M. Schelder, M. Brajenovic, H. Ruffner, A. Merino, K. Klein, M. Hudak, D. Dickson, T. Rudi, V. Gnau, A. Bauch, S. Bastuck, B. Huhse, C. Leutwein, M.-A. Heurtier, R. R. Copley, A. Edelmann, E. Querfurth, V. Rybin, G. Drewes, M. Raida, T. Bouwmeester, P. Bork, B. Seraphin, B. Kuster, G. Neubauer, G. Superti-Furga, Functional organization of the yeast proteome by systematic analysis of protein complexes., *Nature* **415**, 141–147 (2002).

103. B. Ayoglu, E. Birgersson, A. Mezger, M. Nilsson, M. Uhlén, P. Nilsson, J. M. Schwenk, Multiplexed protein profiling by sequential affinity capture., *Proteomics* **16**, 1251–1256 (2016).

104. Y. A. Berchiche, T. P. Sakmar, CXC chemokine receptor 3 alternative splice variants selectively activate different signaling pathways., *Mol. Pharmacol.* **90**, 483–495 (2016).

105. A. Grunbeck, T. Huber, P. Sachdev, T. P. Sakmar, Mapping the ligand-binding site on a G protein-coupled receptor (GPCR) using genetically encoded photocrosslinkers., *Biochemistry* **50**, 3411–3413 (2011).

106. A. Grunbeck, T. P. Sakmar, Probing G protein-coupled receptor-ligand interactions with targeted photoactivatable cross-linkers., *Biochemistry* **52**, 8625–8632 (2013).

107. S. H. Park, C. Cheong, J. Idoyaga, J. Y. Kim, J.-H. Choi, Y. Do, H. Lee, J. H. Jo, Y.-S. Oh, W. Im, R. M. Steinman, C. G. Park, Generation and application of new rat monoclonal antibodies against synthetic FLAG and OLLAS tags for improved immunodetection., *J. Immunol. Methods* **331**, 27–38 (2008).

108. S. Barbash, E. Lorenzen, T. Persson, T. Huber, T. P. Sakmar, GPCRs globally coevolved with receptor activity-modifying proteins, RAMPs., *Proc. Natl. Acad. Sci. USA* **114**, 12015–12020 (2017).

109. M. Uhlén, E. Björling, C. Agaton, C. A.-K. Szigyarto, B. Amini, E. Andersen, A.-C. Andersson, P. Angelidou, A. Asplund, C. Asplund, L. Berglund, K. Bergström, H. Brumer, D. Cerjan, M. Ekström, A. Elobeid, C. Eriksson, L. Fagerberg, R. Falk, J. Fall, M. Forsberg, M. G. Björklund, K. Gumbel, A. Halimi, I. Hallin, C. Hamsten, M. Hansson, M. Hedhammar, G. Hercules, C. Kampf, K. Larsson, M. Lindskog, W. Lodewyckx, J. Lund, J. Lundeberg, K. Magnusson, E. Malm, P. Nilsson, J. Odling, P. Oksvold, I. Olsson, E. Oster, J. Ottosson, L. Paavilainen, A. Persson, R. Rimini, J. Rockberg, M. Runeson, A. Sivertsson, A. Sköllermo, J. Steen, M. Stenvall, F. Sterky, S. Strömberg, M. Sundberg, H. Tegel, S. Tourle, E. Wahlund, A.

Waldén, J. Wan, H. Wernérus, J. Westberg, K. Wester, U. Wrethagen, L. L. Xu, S. Hober, F. Pontén, A human protein atlas for normal and cancer tissues based on antibody proteomics., *Mol. Cell Proteomics* **4**, 1920–1932 (2005).

110. D. MacKenzie, A. Arendt, P. Hargrave, J. H. McDowell, R. S. Molday, Localization of binding sites for carboxyl terminal specific anti-rhodopsin monoclonal antibodies using synthetic peptides., *Biochemistry* **23**, 6544–6549 (1984).

111. D. R. Poyner, P. M. Sexton, I. Marshall, D. M. Smith, R. Quirion, W. Born, R. Muff, J. A. Fischer, S. M. Foord, International Union of Pharmacology. XXXII. The mammalian calcitonin gene-related peptides, adrenomedullin, amylin, and calcitonin receptors., *Pharmacol. Rev.* **54**, 233–246 (2002).

112. O. Söderberg, M. Gullberg, M. Jarvius, K. Ridderstråle, K.-J. Leuchowius, J. Jarvius, K. Wester, P. Hydbring, F. Bahram, L.-G. Larsson, U. Landegren, Direct observation of individual endogenous protein complexes in situ by proximity ligation., *Nat. Methods* **3**, 995–1000 (2006).

113. S. Mohammad, R. T. Patel, J. Bruno, M. S. Panhwar, J. Wen, T. E. McGraw, A naturally occurring GIP receptor variant undergoes enhanced agonist-induced desensitization, which impairs GIP control of adipose insulin sensitivity., *Mol. Cell. Biol.* **34**, 3618–3629 (2014).

114. S. J. Routledge, G. Ladds, D. R. Poyner, The effects of RAMPs upon cell signalling., *Mol. Cell. Endocrinol.* **449**, 12–20 (2017).

115. K.-S. Kim, J. Ren, Y. Jiang, Q. Ebrahem, R. Tipps, K. Cristina, Y. Xiao, J. Qiao, K. L. Taylor, H. Lum, B. Anand-Apte, Y. Xu, GPR4 plays a critical role in endothelial cell function and mediates the effects of sphingosylphosphorylcholine., *FASEB J.* **19**, 819–821 (2005).

116. S. Kapas, K. J. Catt, A. J. Clark, Cloning and expression of cDNA encoding a rat adrenomedullin receptor., *J. Biol. Chem.* **270**, 25344–25347 (1995).

117. S. P. Kennedy, D. Sun, J. J. Oleynek, C. F. Hoth, J. Kong, R. J. Hill, Expression of the rat adrenomedullin receptor or a putative human adrenomedullin receptor does not correlate with adrenomedullin binding or functional response., *Biochem. Biophys. Res. Commun.* **244**, 832–837 (1998).

118. S. Kapas, A. J. Clark, Identification of an orphan receptor gene as a type 1 calcitonin gene-related peptide receptor., *Biochem. Biophys. Res. Commun.* **217**, 832–838 (1995).

119. S. Andersson, M. Sundberg, N. Pristovsek, A. Ibrahim, P. Jonsson, B. Katona, C.-M. Clausson, A. Zieba, M. Ramström, O. Söderberg, C. Williams, A. Asplund, Insufficient antibody validation challenges oestrogen receptor beta research., *Nat. Commun.* **8**, 15840 (2017).

120. M. Uhlen, A. Bandrowski, S. Carr, A. Edwards, J. Ellenberg, E. Lundberg, D. L. Rimm, H. Rodriguez, T. Hiltke, M. Snyder, T. Yamamoto, A proposal for validation of antibodies., *Nat. Methods* **13**, 823–827 (2016).

121. I. Gomes, S. Sierra, L. A. Devi, Detection of receptor heteromerization using in situ proximity ligation assay., *Curr. Protoc. Pharmacol.* **75**, 2.16.1-2.16.31 (2016).

122. J. Zahiri, J. H. Bozorgmehr, A. Masoudi-Nejad, Computational Prediction of Protein-Protein Interaction Networks: Algo-rithms and Resources., *Curr. Genomics* **14**, 397–414 (2013).

123. P. S. Miller, J. Barwell, D. R. Poyner, M. J. Wigglesworth, S. L. Garland, D. Donnelly, Non-peptidic antagonists of the CGRP receptor, BIBN4096BS and MK-0974, interact with the calcitonin receptor-like receptor via methionine-42 and RAMP1 via tryptophan-74., *Biochem. Biophys. Res. Commun.* **391**, 437–442 (2010).

124. A. Gupta, A. S. Heimann, I. Gomes, L. A. Devi, Antibodies against G-protein coupled receptors: novel uses in screening and drug development., *Comb Chem High Throughput Screen* **11**, 463–467 (2008).

125. P. Maurice, J.-L. Guillaume, A. Benleulmi-Chaachoua, A. M. Daulat, M. Kamal, R. Jockers, GPCR-interacting proteins, major players of GPCR function., *Adv. Pharmacol.* **62**, 349–380 (2011).

126. J. Bockaert, L. Fagni, A. Dumuis, P. Marin, GPCR interacting proteins (GIP)., *Pharmacol. Ther.* **103**, 203–221 (2004).

127. R. Santos, O. Ursu, A. Gaulton, A. P. Bento, R. S. Donadi, C. G. Bologa, A. Karlsson, B. Al-Lazikani, A. Hersey, T. I. Oprea, J. P. Overington, A comprehensive map of molecular drug targets., *Nat. Rev. Drug Discov.* **16**, 19–34 (2017).

128. K. Nagata, Y. Katayama, T. Sato, Y. Kwon, T. Kawabata, Toward the next step in G protein-coupled receptor research: a knowledge-driven analysis for the next potential targets in drug discovery., *J. Struct. Funct. Genomics* **17**, 111–133 (2017).

129. D. O. Kechele, R. E. Blue, B. Zwarycz, S. T. Espenschied, A. T. Mah, M. B. Siegel, C. M. Perou, S. Ding, S. T. Magness, P. K. Lund, K. M. Caron, Orphan Gpr182 suppresses ERK-mediated intestinal proliferation during regeneration and adenoma formation., *J. Clin. Invest.* **127**, 593–607 (2017).

130. D. Scuteri, A. Adornetto, L. Rombolà, M. D. Naturale, L. A. Morrone, G. Bagetta, P. Tonin, M. T. Corasaniti, New Trends in Migraine Pharmacology: Targeting Calcitonin Gene-Related Peptide (CGRP) With Monoclonal Antibodies., *Front. Pharmacol.* **10**, 363 (2019).

131. I. Urits, M. R. Jones, K. Gress, K. Charipova, J. Fiocchi, A. D. Kaye, O. Viswanath, CGRP antagonists for the treatment of chronic migraines: a comprehensive review., *Curr Pain Headache Rep* **23**, 29 (2019).

132. Y.-L. Liang, M. Khoshouei, M. Radjainia, Y. Zhang, A. Glukhova, J. Tarrasch, D. M. Thal, S. G. B. Furness, G. Christopoulos, T. Coudrat, R. Danev, W. Baumeister, L. J. Miller, A. Christopoulos, B. K. Kobilka, D. Wootten, G. Skiniotis, P. M. Sexton, Phase-plate cryo-EM structure of a class B GPCR-G-protein complex., *Nature* **546**, 118–123 (2017).

133. J. R. Lane, P. M. Sexton, A. Christopoulos, Bridging the gap: bitopic ligands of G-protein-coupled receptors., *Trends Pharmacol. Sci.* **34**, 59–66 (2013).

134. L. M. Luttrell, S. Maudsley, L. M. Bohn, Fulfilling the Promise of "Biased" G Protein-Coupled Receptor Agonism., *Mol. Pharmacol.* **88**, 579–588 (2015).

135. D. Wacker, R. C. Stevens, B. L. Roth, How ligands illuminate GPCR molecular pharmacology., *Cell* **170**, 414–427 (2017).

136. S. E. Kuhmann, O. Hartley, Targeting chemokine receptors in HIV: a status report., *Annu. Rev. Pharmacol. Toxicol.* **48**, 425–461 (2008).

137. M. Samson, F. Libert, B. J. Doranz, J. Rucker, C. Liesnard, C. M. Farber, S. Saragosti, C. Lapoumeroulie, J. Cognaux, C. Forceille, G. Muyldermans, C. Verhofstede, G. Burtonboy, M. Georges, T. Imai, S. Rana, Y. Yi, R. J. Smyth, R. G. Collman, R. W. Doms, G. Vassart, M. Parmentier, Resistance to HIV-1 infection in caucasian individuals bearing mutant alleles of the CCR-5 chemokine receptor gene., *Nature* **382**, 722–725 (1996).

138. P. Colin, Y. Bénureau, I. Staropoli, Y. Wang, N. Gonzalez, J. Alcami, O. Hartley, A. Brelot, F. Arenzana-Seisdedos, B. Lagane, HIV-1 exploits CCR5 conformational heterogeneity to escape inhibition by chemokines., *Proc. Natl. Acad. Sci. USA* **110**, 9475–9480 (2013).

139. P. J. Klasse, R. J. Shattock, J. P. Moore, Which topical microbicides for blocking HIV-1 transmission will work in the real world?, *PLoS Med.* **3**, e351 (2006).

140. M. M. Lederman, A. Penn-Nicholson, M. Cho, D. Mosier, Biology of CCR5 and its role in HIV infection and treatment., *JAMA* **296**, 815–826 (2006).

141. H. Gaertner, F. Cerini, J.-M. Escola, G. Kuenzi, A. Melotti, R. Offord, I. Rossitto-Borlat, R. Nedellec, J. Salkowitz, G. Gorochov, D. Mosier, O. Hartley, Highly potent, fully recombinant anti-HIV chemokines: reengineering a low-cost microbicide., *Proc. Natl. Acad. Sci. USA* **105**, 17706–17711 (2008).

142. G. Simmons, P. R. Clapham, L. Picard, R. E. Offord, M. M. Rosenkilde, T. W. Schwartz, R.

Buser, T. N. Wells, A. E. Proudfoot, Potent inhibition of HIV-1 infectivity in macrophages and lymphocytes by a novel CCR5 antagonist., *Science* **276**, 276–279 (1997).

143. C. Pastore, G. R. Picchio, F. Galimi, R. Fish, O. Hartley, R. E. Offord, D. E. Mosier, Two mechanisms for human immunodeficiency virus type 1 inhibition by N-terminal modifications of RANTES., *Antimicrob. Agents Chemother.* **47**, 509–517 (2003).

144. O. Hartley, H. Gaertner, J. Wilken, D. Thompson, R. Fish, A. Ramos, C. Pastore, B. Dufour, F. Cerini, A. Melotti, N. Heveker, L. Picard, M. Alizon, D. Mosier, S. Kent, R. Offord, Medicinal chemistry applied to a synthetic protein: development of highly potent HIV entry inhibitors., *Proc. Natl. Acad. Sci. USA* **101**, 16460–16465 (2004).

145. C. A. Flanagan, Receptor conformation and constitutive activity in CCR5 chemokine receptor function and HIV infection., *Adv. Pharmacol.* **70**, 215–263 (2014).

146. C. Bönsch, M. Munteanu, I. Rossitto-Borlat, A. Fürstenberg, O. Hartley, Potent Anti-HIV Chemokine Analogs Direct Post-Endocytic Sorting of CCR5., *PLoS One* **10**, e0125396 (2015).

147. T. Asano, T. Katada, A. G. Gilman, E. M. Ross, Activation of the inhibitory GTP-binding protein of adenylate cyclase, Gi, by beta-adrenergic receptors in reconstituted phospholipid vesicles., *J. Biol. Chem.* **259**, 9351–9354 (1984).

148. B. Molon, G. Gri, M. Bettella, C. Gómez-Moutón, A. Lanzavecchia, C. Martínez-A, S. Mañes, A. Viola, T cell costimulation by chemokine receptors., *Nat. Immunol.* **6**, 465–471 (2005).

149. T. Kenakin, Ligand-selective receptor conformations revisited: the promise and the problem., *Trends Pharmacol. Sci.* **24**, 346–354 (2003).

150. J. Takasaki, T. Saito, M. Taniguchi, T. Kawasaki, Y. Moritani, K. Hayashi, M. Kobori, A novel Galphaq/11-selective inhibitor., *J. Biol. Chem.* **279**, 47438–47445 (2004).

151. R. Schrage, A.-L. Schmitz, E. Gaffal, S. Annala, S. Kehraus, D. Wenzel, K. M. Büllesbach, T. Bald, A. Inoue, Y. Shinjo, S. Galandrin, N. Shridhar, M. Hesse, M. Grundmann, N. Merten, T. H. Charpentier, M. Martz, A. J. Butcher, T. Slodczyk, S. Armando, M. Effern, Y. Namkung, L. Jenkins, V. Horn, A. Stößel, H. Dargatz, D. Tietze, D. Imhof, C. Galés, C. Drewke, C. E. Müller, M. Hölzel, G. Milligan, A. B. Tobin, J. Gomeza, H. G. Dohlman, J. Sondek, T. K. Harden, M. Bouvier, S. A. Laporte, J. Aoki, B. K. Fleischmann, K. Mohr, G. M. König, T. Tüting, E. Kostenis, The experimental power of FR900359 to study Gq-regulated biological processes., *Nat. Commun.* **6**, 10156 (2015).

152. B. R. Conklin, Z. Farfel, K. D. Lustig, D. Julius, H. R. Bourne, Substitution of three amino acids switches receptor specificity of Gq alpha to that of Gi alpha., *Nature* **363**, 274–276 (1993).

153. M. Thelen, Dancing to the tune of chemokines., *Nat. Immunol.* **2**, 129–134 (2001).

154. E. R. Neptune, H. R. Bourne, Receptors induce chemotaxis by releasing the betagamma subunit of Gi, not by activating Gq or Gs., *Proc. Natl. Acad. Sci. USA* **94**, 14489–14494 (1997).

155. J. R. Lane, L. T. May, R. G. Parton, P. M. Sexton, A. Christopoulos, A kinetic view of GPCR allostery and biased agonism., *Nat. Chem. Biol.* **13**, 929–937 (2017).

156. C. Klein Herenbrink, D. A. Sykes, P. Donthamsetti, M. Canals, T. Coudrat, J. Shonberg, P. J. Scammells, B. Capuano, P. M. Sexton, S. J. Charlton, J. A. Javitch, A. Christopoulos, J. R. Lane, The role of kinetic context in apparent biased agonism at GPCRs., *Nat. Commun.* **7**, 10842 (2016).

157. D. L. Burns, Subunit structure and enzymic activity of pertussis toxin., *Microbiol Sci* **5**, 285–287 (1988).

158. A. Nishimura, K. Kitano, J. Takasaki, M. Taniguchi, N. Mizuno, K. Tago, T. Hakoshima, H. Itoh, Structural basis for the specific inhibition of heterotrimeric Gq protein by a small molecule., *Proc. Natl. Acad. Sci. USA* **107**, 13666–13671 (2010).

159. K. Liu, S. Titus, N. Southall, P. Zhu, J. Inglese, C. P. Austin, W. Zheng, Comparison on functional assays for Gq-coupled GPCRs by measuring inositol monophospate-1 and intracellular calcium in 1536-well plate format., *Curr. Chem. Genomics* **1**, 70–78 (2008).

160. H. Gaertner, O. Lebeau, I. Borlat, F. Cerini, B. Dufour, G. Kuenzi, A. Melotti, R. J. Fish, R. Offord, J.-Y. Springael, M. Parmentier, O. Hartley, Highly potent HIV inhibition: engineering a key anti-HIV structure from PSC-RANTES into MIP-1 beta/CCL4., *Protein Eng Des Sel* **21**, 65–72 (2008).

161. Z. Truan, L. Tarancón Díez, C. Bönsch, S. Malkusch, U. Endesfelder, M. Munteanu, O. Hartley, M. Heilemann, A. Fürstenberg, Quantitative morphological analysis of arrestin2 clustering upon G protein-coupled receptor stimulation by super-resolution microscopy., *J. Struct. Biol.* **184**, 329–334 (2013).

162. L. Tarancón Díez, C. Bönsch, S. Malkusch, Z. Truan, M. Munteanu, M. Heilemann, O. Hartley, U. Endesfelder, A. Fürstenberg, Coordinate-based co-localization-mediated analysis of arrestin clustering upon stimulation of the C-C chemokine receptor 5 with RANTES/CCL5 analogues., *Histochem. Cell Biol.* **142**, 69–77 (2014).

163. J. Hanoune, N. Defer, Regulation and role of adenylyl cyclase isoforms., *Annu. Rev. Pharmacol. Toxicol.* **41**, 145–174 (2001).

164. S. G. F. Rasmussen, B. T. DeVree, Y. Zou, A. C. Kruse, K. Y. Chung, T. S. Kobilka, F. S.

Thian, P. S. Chae, E. Pardon, D. Calinski, J. M. Mathiesen, S. T. A. Shah, J. A. Lyons, M. Caffrey, S. H. Gellman, J. Steyaert, G. Skiniotis, W. I. Weis, R. K. Sunahara, B. K. Kobilka, Crystal structure of the β2 adrenergic receptor-Gs protein complex., *Nature* **477**, 549–555 (2011).

165. A. J. Flegler, G. C. Cianci, T. J. Hope, CCR5 conformations are dynamic and modulated by localization, trafficking and G protein association., *PLoS One* **9**, e89056 (2014).

166. M. Farzan, H. Choe, K. A. Martin, Y. Sun, M. Sidelko, C. R. Mackay, N. P. Gerard, J. Sodroski, C. Gerard, HIV-1 entry and macrophage inflammatory protein-1beta-mediated signaling are independent functions of the chemokine receptor CCR5., *J. Biol. Chem.* **272**, 6854–6857 (1997).

167. K. Leach, S. J. Charlton, P. G. Strange, Analysis of second messenger pathways stimulated by different chemokines acting at the chemokine receptor CCR5., *Biochem. Pharmacol.* **74**, 881–890 (2007).

168. M. Del Corno, Q. H. Liu, D. Schols, E. de Clercq, S. Gessani, B. D. Freedman, R. G. Collman, HIV-1 gp120 and chemokine activation of Pyk2 and mitogen-activated protein kinases in primary macrophages mediated by calcium-dependent, pertussis toxin-insensitive chemokine receptor signaling., *Blood* **98**, 2909–2916 (2001).

169. B. K. Atwood, J. Lopez, J. Wager-Miller, K. Mackie, A. Straiker, Expression of G protein-coupled receptors and related proteins in HEK293, AtT20, BV2, and N18 cell lines as revealed by microarray analysis., *BMC Genomics* **12**, 14 (2011).

170. H. Arai, I. F. Charo, Differential regulation of G-protein-mediated signaling by chemokine receptors., *J. Biol. Chem.* **271**, 21814–21819 (1996).

171. A. Mueller, P. G. Strange, CCL3, acting via the chemokine receptor CCR5, leads to independent activation of Janus kinase 2 (JAK2) and Gi proteins., *FEBS Lett.* **570**, 126–132 (2004).

172. J. Ngai, M. Inngjerdingen, T. Berge, K. Taskén, Interplay between the heterotrimeric G-protein subunits Galphaq and Galphai2 sets the threshold for chemotaxis and TCR activation., *BMC Immunol.* **10**, 27 (2009).

173. G. Shi, S. Partida-Sánchez, R. S. Misra, M. Tighe, M. T. Borchers, J. J. Lee, M. I. Simon, F. E. Lund, Identification of an alternative G{alpha}q-dependent chemokine receptor signal transduction pathway in dendritic cells and granulocytes., *J. Exp. Med.* **204**, 2705–2718 (2007).

174. T. Flock, A. S. Hauser, N. Lund, D. E. Gloriam, S. Balaji, M. M. Babu, Selectivity determinants of GPCR-G-protein binding., *Nature* **545**, 317–322 (2017).

175. J. Jin, P. Colin, I. Staropoli, E. Lima-Fernandes, C. Ferret, A. Demir, S. Rogée, O. Hartley, C. Randriamampita, M. G. H. Scott, S. Marullo, N. Sauvonnet, F. Arenzana-Seisdedos, B. Lagane, A. Brelot, Targeting spare CC chemokine receptor 5 (CCR5) as a principle to inhibit HIV-1 entry., *J. Biol. Chem.* **289**, 19042–19052 (2014).

176. R. Berro, P. J. Klasse, D. Lascano, A. Flegler, K. A. Nagashima, R. W. Sanders, T. P. Sakmar, T. J. Hope, J. P. Moore, Multiple CCR5 conformations on the cell surface are used differentially by human immunodeficiency viruses resistant or sensitive to CCR5 inhibitors., *J. Virol.* **85**, 8227–8240 (2011).

177. C. A. Rico, Y. A. Berchiche, M. Horioka, J. C. Peeler, E. Lorenzen, H. Tian, M. A. Kazmi, A. Fürstenberg, H. Gaertner, O. Hartley, T. P. Sakmar, T. Huber, High-Affinity Binding of Chemokine Analogs that Display Ligand Bias at the HIV-1 Coreceptor CCR5., *Biophys. J.* (2019), doi:10.1016/j.bpj.2019.07.043.

178. D. Spengler, C. Waeber, C. Pantaloni, F. Holsboer, J. Bockaert, P. H. Seeburg, L. Journot, Differential signal transduction by five splice variants of the PACAP receptor., *Nature* **365**, 170–175 (1993).

179. M. Hauge, M. A. Vestmar, A. S. Husted, J. P. Ekberg, M. J. Wright, J. Di Salvo, A. B. Weinglass, M. S. Engelstoft, A. N. Madsen, M. Lückmann, M. W. Miller, M. E. Trujillo, T. M. Frimurer, B. Holst, A. D. Howard, T. W. Schwartz, GPR40 (FFAR1) - Combined Gs and Gq signaling in vitro is associated with robust incretin secretagogue action ex vivo and in vivo., *Mol. Metab.* **4**, 3–14 (2015).

180. D. Bolognini, C. E. Moss, K. Nilsson, A. U. Petersson, I. Donnelly, E. Sergeev, G. M. König, E. Kostenis, M. Kurowska-Stolarska, A. Miller, N. Dekker, A. B. Tobin, G. Milligan, A Novel Allosteric Activator of Free Fatty Acid 2 Receptor Displays Unique Gi-functional Bias., *J. Biol. Chem.* **291**, 18915–18931 (2016).

181. Y. Zheng, G. W. Han, R. Abagyan, B. Wu, R. C. Stevens, V. Cherezov, I. Kufareva, T. M. Handel, Structure of CC Chemokine Receptor 5 with a Potent Chemokine Antagonist Reveals Mechanisms of Chemokine Recognition and Molecular Mimicry by HIV., *Immunity* **46**, 1005–1017.e5 (2017).

182. Q. Tan, Y. Zhu, J. Li, Z. Chen, G. W. Han, I. Kufareva, T. Li, L. Ma, G. Fenalti, J. Li, W. Zhang, X. Xie, H. Yang, H. Jiang, V. Cherezov, H. Liu, R. C. Stevens, Q. Zhao, B. Wu, Structure of the CCR5 chemokine receptor-HIV entry inhibitor maraviroc complex., *Science* **341**, 1387–1390 (2013).

183. N. Joseph, B. Reicher, M. Barda-Saad, The calcium feedback loop and T cell activation: how cytoskeleton networks control intracellular calcium flux., *Biochim. Biophys. Acta* **1838**, 557–568 (2014).

184. S. Barbash, T. Persson, E. Lorenzen, M. A. Kazmi, T. Huber, T. P. Sakmar, Detection of Concordance between Transcriptional Levels of GPCRs and Receptor-Activity-Modifying Proteins., *iScience* **11**, 366–374 (2019).

185. E. Lorenzen, T. Dodig-Crnković, I. B. Kotliar, E. Pin, E. Ceraudo, R. D. Vaughan, M. Uhlèn, T. Huber, J. M. Schwenk, T. P. Sakmar, Multiplexed analysis of the secretin-like GPCR-RAMP interactome, *Sci. Adv.* **5**, eaaw2778 (2019).

186. E. Lorenzen, T. P. Sakmar, Receptor structures for a caldron of cannabinoids., *Cell* **176**, 409–411 (2019).